ACCELEROMETRY:
THE KEY TO MEASURING SIZE-AT-AGE AND ACTIVITY IN FISH

by

Franziska Broell

Submitted in partial fulfilment of the requirements
for the degree of Doctor of Philosophy

at

Dalhousie University
Halifax, Nova Scotia
February 2016

Table of Contents

LIST OF TABLES

LIST OF FIGURES

ABSTRACT

Recent advancements in tracking technology have increased the ability to unravel key parameters affecting behaviour patterns among marine animals where direct observations are scarce. Within the suite of biologging techniques, tri-axial accelerometers are particularly promising for providing data that can link physiological and ecological processes in the context of movement. The objective of my thesis research was to determine how the analysis of accelerometer data can provide reliable and complex information on fish locomotion and behaviour that are relevant for advancing the informed management of commercially and recreationally valued fish. To reach this objective, a high-frequency accelerometer data logger was developed. Based on a series of controlled-environment and field experiments using this technology, a library of automated signal-processing algorithms was developed that relate acceleration signals to rates of activity, swimming speed, size-at-time and behavioural states in a variety of fish species. The algorithms are efficient in extracting behavioural states (feeding, escape, swimming) relevant to energy budgets as well as behaviour associated with spawning and courtship and parasite dislodging while being independent of animal size or tag placement. The most novel contribution is the development of a scaling relationship between tail beat frequency, speed and length in free-swimming fish that is based on accelerometer signal-processing techniques and early theoretical predictions. In the future, the technology and the models may provide valuable input for fish stock modelling by the *in situ* delivery of more reliable time series of length-at-age, and thus growth rate, in wild fish than that achieved using conventional techniques. Throughout this thesis, accelerometer data analyses challenge the assumption that movement data collected by accelerometer tags represent the normal behavioural repertoire of the tagged animal given low rates of tag sampling frequency currently employed as well as significant behavioural changes caused by tagging and handling stress as demonstrated by post-release fish behaviour modification observed in a field study. This thesis presents a significant contribution to the field through the development of an advanced accelerometer tag and processing algorithms that can be applied to many animal species to advance ecological and physiological theory.

LIST OF ABBREVIATIONS AND SYMBOLS USED

Symbol	Description	Units
a	Scaling parameter between A_{TBF} and length	
A_{TBF}	Tail beat amplitude	m
A_{fish}	Cross-sectional area of the fish	m²
A	Acceleration	g_o
A_{max}	Maximum acceleration	g_o
$A_{max,x}$, $A_{max,y}$, $A_{max,z}$	Maximum acceleration in x-axis; y-axis, z-axis	g_o
A_t	Acceleration at time, t	g_o
A_{tag}	Cross-sectional area of the tag, subscript indicates small (s) or large (l)	m²
$A_{tci,max}$	Instantaneous acceleration at time index where $\theta_{Ci,max}$	g_o
A_x, A_y, A_z	Absolute dynamic acceleration values measured with respect to the x, y, z-axes	
b	Proportionality constant for power model or intercept for linear model	
BL	Body length	m
C	Empirical weight associated with each parameter and event/activity class. Subscript identifies the related parameter and event or activity class	
C_i	Rotation segment	
c_d	Fish drag coefficient, subscript indicates tag (tag, or s-small, l-large) or fish (fish)	
$c_{d,S}$	Drag coefficient of small tag	
$c_{d,L}$	Drag coefficient of large tag	
CI	Confidence interval	
d	Mass displacement within MEMS sensor	cm

Symbol	Description	Units
D	Drag, subscript indicates tag (t) or fish (f)	kg m s^{-2}
E	Escape activity	
F	Feeding activity	
F_D	Drag force	kg m s^{-2}
FL	Fork length	m
FN	False negative	
FP	False positive	
FS	Fast-start event (F or E)	
g_o	Gravitational acceleration	9.81 m s^{-2}
I	Event correctly identified – subscript indicates event/activity class	
k_S	Constant factor characteristic of a spring	
l	Length	m
l_P	Model prediction of length	m
l_W	window length of zero-crossing algorithm	s
m	Mass	kg
MA	Acceleration magnitude, $\sqrt{x^2+ y^2 + z^2}$ not corrected for gravitational acceleration	g_o
MA_{max}	Maximum acceleration magnitude	g_o
n	Sample size; subscript indicates data subset), V = validation subset, T = training subset, D = whole dataset, s = small tag, l = large tag	
NR	Not observed (real) event – subscript indicates event/activity class (F – feeding, E – escape)	
OLS	Ordinary least squares linear regression	
P	Power	kg m^2 s^{-3}

Symbol	Description	Units
p	P-Value	
P(.|.)	Conditional probability	
P_S, P_{FS}, P_E, P_F	Identification probability, with subscript S = spontaneous, FS = fast-start, E = escape, F = feeding	
P_U	Prediction uncertainty; $P_U = 100\ t_{0.975,n-2}\ SE_{lp}/l_p$	
Q	Bit resolution of accelerometer chip	bit
R	Observed event (real) – subscript indicates event/activity class	
R_A	Range in acceleration values	g_o
r^2	Coefficient of determination	
RMS	Root-mean-square	
S	Spontaneous movement (haphazard turns, swimming etc.)	
SE_{lp}	Standard error for length prediction	
$_{sd}$	Standardized (e.g., by mean length)	
SD	Standard deviation	
$SQNR$	Signal to noise ratio due to quantization error	dB
St	Strouhal number	
t	Time step	
TBF	Dominant tail beat frequency	Hz
t_{ci}	Cross-over points from zero-crossing algorithm	
$tc_{i,1}$; $tc_{i,2}$.	Start and end index of rotation segment	
$t_{0.975,n-2}$	t-value from Student's t distribution	
Th	Stability threshold for zero-crossing algorithm, $Th = ThS^*((\Delta t_j - \Delta t_{j+1})_{max} - (\Delta t_j - \Delta t_{j+1})_{min})$	
ThS^*	Tuning parameters to determine TBF window stability	

Symbol	Description	Units
TL	Total length	m
TN	True negative	
TP	True positive	
u	Swimming speed	m s^{-1}
$VeDBA$	Vectorial sum of dynamic body acceleration, $\sqrt{{A_x}^2 + {A_y}^2 + {A_z}^2}$	g_o
υ_k	Cut-off value, i.e., parameter threshold for each of the k parameters	
W	Algorithm sliding window length	s
x	Lateral acceleration	g_o
y	Forward acceleration	g_o
z	Vertical acceleration	g_o
$\%TSS$	Percent time spent scouring	%
α	Proportional	
β	Model exponent or model slope	
Δt	Zero-crossing intervals, i.e., beat period	s
Δt_{max} ; Δt_{min}	Maximum zero-crossing interval within time series	s
θ_{Ci}, $\theta_{Ci\,max}$	(Maximum) angle between acceleration component and reference alignment in the xz-plane within C_i	°
θ_{Tag}	Initial tag orientation, angle calculated relative to the z-axis	°
θ_{Th}	Threshold angle	°
ρ	Correlation coefficient	
ρ_d	Density of seawater	kg m^{-3}
σ	Standard deviation	
τ	Autocorrelation coefficient	
ω_i	i'th identification parameter (in Ω)	
Φ	Detection parameter	
Ω	Identification parameter set	

Symbol	Description	Units
$\boldsymbol{a}$	Instantaneous acceleration at time t_i	g_o
$\overline{\boldsymbol{a}}$	Time averaged acceleration vector	g_o
$\overline{\boldsymbol{a}}'$	Projection of $\overline{\boldsymbol{a}}$ in the xz-plane	g_o
$\boldsymbol{a}'$	Projection of $\mathbf{a}$ in the xz-plane	g_o

ACKNOWLEDGEMENTS

First amongst the many people who deserve to be acknowledged is my advisor, Dr. Christopher Taggart, for his unfaltering support. I will never forget how on my first day, he welcomed me with a box full of circuit boards and wires with the words “Here, that’s your PhD project”. I am grateful for his ideas and belief not only in my abilities but also in our capacity to complete this project.

I thank my committee, Mike Dowd, Keith Thompson and Dale Webber (and through him, VEMCO), who provided valuable comments and guidance throughout my PhD studies.

This research would not have been possible without the work and commitment of Andre Benzanson. The technology he created was an integral part of this work and I thank him for his genuine interest in tackling all the engineering related issues. Many thanks go to Jean-Pierre Auclair for countless discussions of the intricacies of acceleration data and fish movement and help in MATLAB coding.

My project received pivotal support from the Ocean-Tracking Network and collaborations therein, first and foremost Dr. Matt Litvak and Andrew Taylor at Mount Allison University. I am grateful to Mark Merrimen for his help and the Aquatron staff and Dalhousie Veterinary, especially Jon Batt and Jim Eddington for their support in data collection and discussions. I thank Kendra Chisholm for her assistance with experiments. Finally, I want to thank my parents for helping me along this path and their unconditional support and encouragement.

“Advances are limited by imagination, not technology”

Hawkes (2011)

Chapter 1 INTRODUCTION

1.1 General

Quantifying activity patterns, energy budgets and the spatial-temporal distribution among animal species is essential to assess and identify basic life-history traits, habitat requirements and intra- and inter-specific interactions. Such information is also crucial for parameterising ecosystem models and for advancing the informed management of commercially and recreationally valued fish species. Traditionally, data on free-ranging animal distributions have been collected using simple physical tags (Petersen, 1896, Rounsefell and Lawrence, 1945; Eschmeyer, 1959; Ferreira and Russ, 1994). As a result of recent advancements in tracking technology a suite of electronic tags are now available to collect more detailed information on fish distribution in the wild (Cooke et al., 2004; Wilson et al., 2006; Bograd et al., 2010). Especially, the miniaturization of storage and processor technology over the past decade has facilitated the development of micro-storage tags that provide the means to remotely study the behaviour and environment of animals through a suite of sensors (e.g., temperature, pressure, light). Such data can be used to indirectly quantify variation in behaviour, energetics, and physiology, and therefore provide objective measurements of how animals interact with each other and their environment (Cooke et al., 2004). Acoustic telemetry or pop-up satellite tags (PSATs) can archive such information and (or) send the data to receivers moored on the ocean floor or to orbiting satellites, from where they can be accessed from anywhere in the world. Over the past decade, these tags have provided valuable insights on animal distribution, migration patterns and habitat use in time and space, and are now used for advancing habitat and ecosystem modeling and conservation management (e.g., Block et al., 2001; Bograd et al., 2010; Jensen et al., 2010).

1.2 Accelerometer Technology

Within the general suite of biologging techniques, tri-axial accelerometers are especially promising in providing data that can link physiological and ecological

processes in the movement context (Wilson et al., 2006; Nathan et al., 2012). The use of accelerometers for studying the movement of organisms stems from epidemiological studies, originating in the 1950s, aimed at assessing changes in human health status in relation to physical activity (e.g., Smidt et al., 1977; Chen and Bassett, 2005). Accelerometer data collected from animals can be used to quantify behavioural states and rates and to estimate energy expenditure in the field (Kawabe et al., 2003a,b; Tsuda et al., 2006, Wilson et al., 2006; Sato et al., 2007; Shepard et al., 2008b; Whitney et al., 2010; Carroll et al., 2014) and in mesocosm environments (Gleiss et al., 2010; Noda et al., 2013; Noda et al., 2014; Wright et al., 2014). In fish, acceleration metrics have been linked to heart rate and energy expenditure (Clark et al., 2010), spawning behaviour (Tsuda et al., 2006; Gleiss et al., 2010), activity (Kawabe et al. 2003a,b) and more recently, feeding behaviour (Føre et al., 2011; Noda et al., 2013; Noda et al., 2014).

Generally, accelerometer tags continuously record data at some defined frequency, or time-averaged data thereof, that are either digitally stored or transmitted for subsequent post-processing. Post-processing is typically based on a broad categorization of the acceleration data (signal) using the average and extreme values of the acceleration (e.g., Murchie et al., 2010; O'Toole et al., 2010), or various frequency components thereof (e.g., fast Fourier transform, FFT, and wavelets; Sato et al., 2007; Sakamoto et al., 2009), and often this is done subsequent to data transformation to various components of dynamic and static acceleration (Tanaka et al., 2001; Wilson et al., 2006; Gleiss et al., 2010). These signals and their variation (e.g., rates of change) are then combined to estimate activity and energy budgets or to classify various behaviours such as resting, swimming, etc. For example, during body or caudal fin propulsion, fish contract their muscles on either side of their body to generate waves of flexion that travel the length of the body from head to tail (Videler, 1993). The vector forces exerted on the water by this motion generate a net force backwards, which in turn pushes the fish forward through the water. The acceleration in the lateral plane during these body oscillations represents a sinusoidal wave at a frequency that corresponds to the frequency of the oscillation. This is referred to as the *tail beat frequency* and each zero-crossing in the oscillation corresponds to the lateral excursion of the tail and is easily measured with an

accelerometer (Kawabe et al., 2003a,b). In contrast, the extraction of more complex behaviours such as predator-prey interactions, require species-specific accelerometer measurements that are calibrated and validated by observations from tagged animals in the field or laboratory (Nathan et al., 2012). The development of automated methods that relate the accelerometer signal pattern to a range of activities and behaviours of a given species at accelerometer sampling frequencies capable of resolving such patterns remains challenging (Nathan et al., 2012).

While the use of accelerometer tags in the field and laboratory has increased due to their data-storage capabilities, decreasing size (Ropert-Coudert and Wilson, 2005; Rutz and Hays, 2009) and commercial availability, the technology remains costly ($1000 - $4000/unit), provides little customisation and often with limited functionality in hardware (storage capability, size, duration) and software (sensor programmability), and thus presents challenges for many applications.

1.3 Objectives

The goal of my research is to determine how the analysis of accelerometer sensor data can provide more reliable and more complex information on fish locomotion and behaviour that is relevant to advance habitat and ecosystem modeling for sustainable management. Given the challenges surrounding the hardware and data-processing techniques, I aim to improve the current tag technology to make it more suitable for fish-specific applications and then demonstrate how these tags can be used to measure a suite of behaviours and activities in the context of locomotion.

I set out to develop a library of automated signal-processing methods that relate accelerometer signal patterns to a suite of fish behaviours and movements. To achieve these goals, I first focus on the development of a reusable micro-accelerometer tag relevant to fish applications that records and stores tri-axial acceleration at high (up to 1 kHz) sampling frequencies. I then use this tag to obtain laboratory and field measurements of acceleration in free-swimming fish of various species (sturgeon, sculpin, cod, saithe) in controlled-environment experiments. The data collected in the controlled-environment experiments are used to advance the

signal processing of acceleration records to identify fish behaviour, activity (e.g., time-varying tail beat frequency) and size-at-age (over time, growth). I then seek to apply the developed tag technology and computational algorithms to extract information on fish movement and behaviour routines in relation to the ambient environment in a field study. This provides a proof-of-concept for the tag design along with insights into the efficiency of the analytical techniques in differentiating behaviour and activity based on data that are not validated through visual observations.

With this thesis I further aim to challenge the assumption that movement data collected by the current generation of accelerometer tags represent the normal behavioural repertoire of the tagged animal given 1) the sampling frequency constraints of the current technology and how that may lead to aliasing of the signal and thus compromised behaviour classification and 2) the effect of tagging procedures and the tag load of externally attached tags and how they can lead to reduced swimming performance through added drag as well as behavioural adjustments due to tag load. This is especially relevant in biologging studies where typically, data from a few (<10) individuals are collected to make inferences about entire populations (Cooke et al., 2004).

Therefore, my thesis focuses on two main themes. 1) How can data from high-frequency accelerometer sensors be analyzed to measure a variety of fish behaviours and movements in the framework of locomotion and 2) how such information may be compromised based on technological limitations and behaviour.
To realize the overall objective and using the new accelerometer technology, I will address the following specific questions:

- Can high-frequency (> 50 Hz) accelerometers be used to measure fast-start movements (feeding, escape response) in fish?

- Can accelerometers be used to measure size-at-time in fish across species and could this method provide an alternative to traditional methods that estimate size-at-age in the wild?

- How are accelerometer data and extracted estimates on fish behaviour compromised by technological limitations (e.g., sampling frequency)?

- Can accelerometer data be compromised due to tagging effects such as tag weight, or behavioural effects resulting from tag load, tagging and handling in the lab and in the wild?

- How can the established signal processing techniques be used to determine how fish change their behaviour and activity in response to variation in their surrounding environment (temperature, light, depth)?

1.4 Outline And Structure of Thesis

This thesis is divided into seven chapters (including this general introduction). Chapters 2 through 7 address the above objectives. Apart from **Chapter 2**, each chapter has been designed as a stand-alone manuscript for primary publication. Hence, the reader is forewarned that parts of this introduction and subsequent chapters contain some repetition. **Chapter 2** outlines the electronic and mechanical design considerations for a low-cost, rechargeable miniature high-frequency accelerometer data logger that I developed in collaboration with A. Bezanson (Dalhousie University). A Bezanson was responsible for the majority of the implementation of the tag design and some proprietary information is not disclosed herein. **Chapter 3** introduces a novel algorithm that links different behaviours to acceleration signals in a model fish species and investigates the effect of sampling frequency on algorithm performance. The chapter emphasizes the importance of sufficient sampling frequency to record behaviour and associated energy expenditure in fish. **Chapter 4** introduces a new scaling relationship between tail beat frequency, speed and length in free-swimming fish based on accelerometer signal-processing techniques and theoretical predictions and provides a discussion on the implications of measuring size-at-age, and ultimately growth rate in the wild based on the scaling relationship. **Chapter 5** introduces an algorithm to extract behavioural response to tag and parasite load in fish and discusses how this may be used in extracting parasite load in aquaculture settings. It further considers the implications for data

collected from external tags in the wild and how such data may be compromised. **Chapter 6** determines post-release behaviour and the behavioural response to environmental variability in shortnose sturgeon in the wild. Finally, in **Chapter 7**, I present the summary and conclusions, provide a discussion of my overall research and attempt to predict future directions in acceleration biologging.

At the time of submission, several parts of this thesis have been published, submitted for publication in the primary literature and presented at conferences. Parts of **Chapter 3** are published in the University of Washington Library as Broell *et al* (2011)[1] and the majority of **Chapter 3** is published in the *Journal of Experimental Biology* as Broell *et al.* (2013)[2]. I was responsible for designing and implementing the data analysis (with insights from JP Auclair), interpretations and implications of results for this manuscript. T Noda and S Wright contributed to data collection and along with P Domenici and JF Steffensen contributed to the design and execution of the experimental design. As primary author I was also responsible for drafting and editing the final manuscript and all other co-authors provided critiques on the research and the manuscript.

The majority of **Chapter 4** is published in *PLoS ONE* as Broell and Taggart[3]. CT Taggart conceived of the research and I was responsible for experimental design and data collection. I helped design the instruments used in the study, developed the theoretical framework and conducted the analyses and prepared the manuscript with help and advice on writing and interpretations from CT Taggart.

---

[1] **Broell, F., Noda, T., and Wright, S.** (2011). Analysis of fast-start movements using accelerometer and video tracking in the Great Sculpin (*Myoxocephalus polyacanthoceaphalus*). University of Washington Library

[2] **Broell, F., Noda, T., Wright, S., Domenici, P., Steffensen, J. F., Auclair, J.-P. and Taggart, C. T.** (2013). Accelerometer tags: detecting and identifying activities in fish and the effect of sampling frequency. *J. Exp. Biol.* **216**, 1255-1264.

[3] **Broell, F. and Taggart, C.T.** (2015) Scaling in free-swimming fish and implications for measuring size-at-time in the wild. *PLoS ONE* **10(12)**, e0144875.

Chapter 5 is in press as Broell et al.[4] in the *Journal of Experimental Biology*. CT Taggart conceived of and secured funding for the research. I developed the experimental design with ideas from CT Taggart and executed the experimental studies. I helped design the accelerometers and conducted the analyses with input from C Burnell and prepared the manuscript with help and advice on writing and interpretation of the results from CT Taggart and C Burnell.

Parts of **Chapter 6** is under review in *Animal Biotelemetry* as Broell et al[5]. As lead author was I was responsible for the experimental design with insights from MK Litvak and CT Taggart. Data collection was achieved in collaboration with MK Litvak, AD Taylor and CT Taggart. I was responsible for data analysis and manuscript preparation with insights and interpretation from CT Taggart and all authors contributed to the manuscript.

Chapter 2 will not be published but as a result of the technological advancements, in 2014, A Bezanson and I have founded *Maritime bioLoggers*, a start-up company to commercialize the tag technology and we are currently in the process of obtaining a patent surrounding the technology.

---

[4] **Broell, F., Burnelle, C.T., and Taggart, C.T.** (*in press*). Measuring abnormal rotational movements in free-swimming fish with accelerometers: implications for quantifying tag- and parasite-load. Submitted to *J. Exp. Biol.* doi: 10.1242/jeb.133033

[5] **Broell, F., Taylor, A. D., Litvak, M. K., and Taggart, C. T.** (*under review*). Post-release behaviour and habitat use in shortnose sturgeon measured with high-frequency accelerometer and PSATs. *Anim. Biotel.*

Chapter 2 DEVELOPMENT OF A LIGHT-WEIGHT, OPEN-SCOURCE, REUSABLE ACCELERATION DATA-LOGGER FOR MONITORING ANIMAL MOVEMENT

2.1 Introduction

Recent advancements in tracking technology have increased our capacity to unravel key parameters affecting behaviour patterns in the context of movement among animal species. Such tracking technology is especially promising for collecting data in marine animals due to a paucity of direct observations and the need for parameterising ecosystem models and to advance the informed management of commercially and recreationally valued fish species (Lowe & Goldman, 2001; Lowe, 2002; Schindler et al., 2002). Micro-accelerometer tags are the most promising technology in providing data that can link physiological and ecological processes in the context of movement (Wilson et al., 2006; Nathan et al., 2012). In fish research such tags have been used to identify and/or measure behavioural and energetic states/rates and thus provide critical information for advancing ecosystem and fisheries management (e.g., Kawabe et al., 2003a, Tsuda et al., 2006; Gleiss et al., 2010; Gleiss et al., 2011). Accelerometers provide measurements of two types of acceleration: static and dynamic acceleration. Static acceleration is due to the force of the gravitational field of the earth, whereas dynamic acceleration is due to animal movement (Shepard et al., 2008a).

Generally, accelerometer tags continuously record data at some defined frequency, or time-averaged data thereof, that are either digitally stored or transmitted (acoustic or satellite telemetry) for subsequent post-processing. Unlike other electronic sensor output (e.g., temperature, pressure and location) that has been the focus over the past decades for integrating movement and environmental data (e.g., Block et al., 2001), acceleration data are not suited for intuitive interpretation, and often require validation via visual observation. While some routine movements in fish such as steady-swimming can be readily extracted from acceleration signals since the rate of change of velocity during swimming describes a well-defined acceleration signal

(Videler, 1993; Kawabe et al., 2003a), the linkage between acceleration and behaviour, for example, requires a more sophisticated analytical approach.

The general method for obtaining acceleration-based behavioural classification is characterized by a two-step protocol (e.g., Nathan et al., 2012), which is especially important where no prior knowledge on animal behaviour is known (Figure 2.1). The first step serves to obtain accelerometer data along with visual observations (e.g., through video recordings) in controlled laboratory of field conditions using a high-frequency recording accelerometer tag (5 to 10 times that of the expected signal frequency, Ogata, 1970). Validated acceleration measurements can then be used to train machine-learning algorithms that can subsequently be used to classify unobserved behaviours from non-validated acceleration data derived from field deployments (Step 3, Figure 2.1, and e.g., Nathan et al., 2012; Noda et al., 2013; Noda et al., 2014). Additionally, validated accelerometry data provide the opportunity to determine a minimum sampling frequency required to resolve for the classification. After the validation step, an intermediary step can serve to optimize the tag technology (battery and storage) by incorporating either a variable sampling frequency and (or) duty cycling, or by the on-board data processing of classification algorithms burned into the tag microcontroller (Step 2, Figure 2.1). This not only ensures sufficient sampling frequency to capture behaviours and movement of interest, but by determining the minimum required sampling frequency, storage and battery power can be maximized for field applications. Since both are a function of sampling frequency and directly relate to recording duration and tag size, this can significantly contribute to minimizing tag load and tag effects (Jepsen et al., 2005). This can be especially relevant for fish where information on activity patterns can inform sleep-mode for the tag during periods of low activity (e.g., diurnal activity).

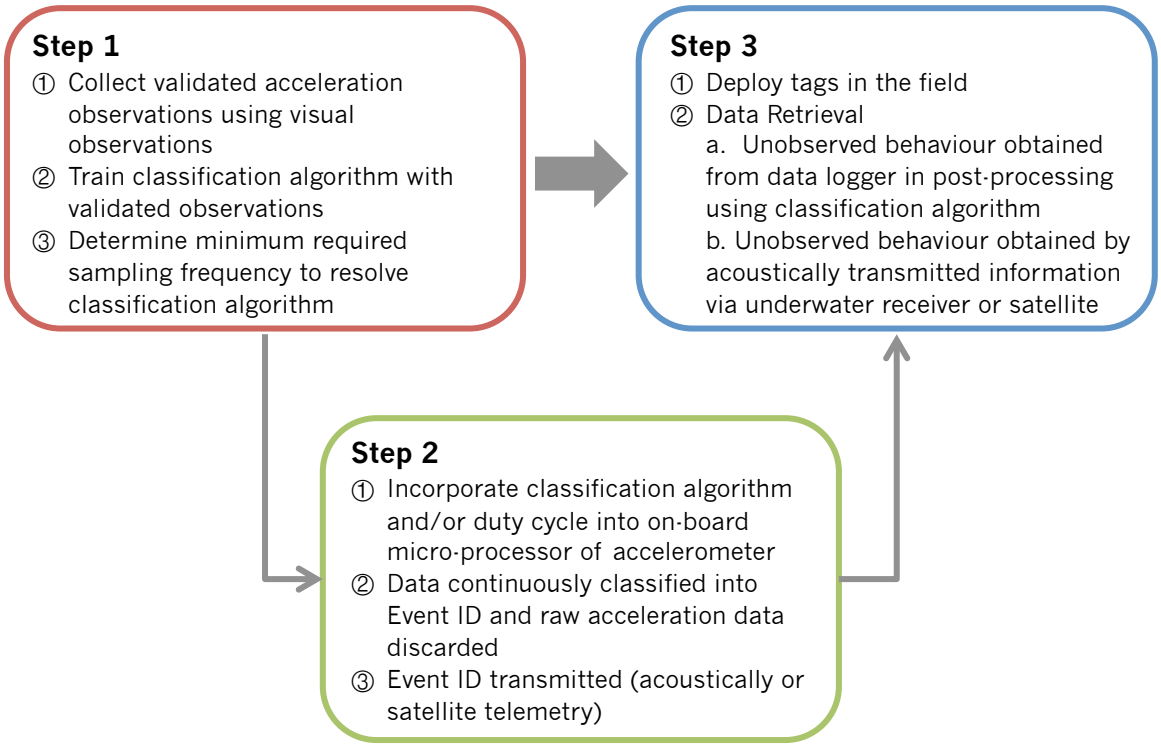

Figure 2.1 A conceptual outline for a two or three-step protocol for accelerometer research. Step 2 is optional but desirable to optimize tag logging duration and size.

Step 1 typically requires the use of a (low-cost), lightweight, short-duration, high frequency micro-accelerometer data logger with simple deployment and data retrieval for controlled environment (lab or mesocosm) experiments. Commercially available accelerometer tags are generally expensive (from $1000 to $4000/tag available from various animal tag manufacture companies) or have limited functionality due to low sampling frequencies (≤ 32 Hz). Although, recent trends in the development of low-cost yet sophisticated integrated circuits have revolutionized such industries as telecommunications and portable computing (Sastry and Sreenu 2012, Kaur 2013), many other applications have yet to implement these technological advances.

The accelerometer tag outlined here uses such low-cost accelerometer circuit boards and associated open-source coding that is readily available through Arduino (Kushner, 2011). The acceleration data-logger, *MBLog mini* is specifically designed for applications in fish to collect acceleration data on the three Cartesian axes at high (~550 Hz) sampling frequency. The *MBLog mini* is packaged in a cylindrical

pressure casing optimized for internal or external attachment. Data are saved on-board a MicroSD card and can be uploaded to a computer via a standard MicroSD card reader after the tag is retrieved. To control the device, the open-sourced Arduino microcontroller, Arduino Pro Mini 3.3 V (SparkFun Electronics, Boulder, USA), is utilized. The board is powered by a 3.3 V supply that makes it ideal for battery powered applications and facilitates small size, functionality and low-cost. The board provides an 8 MHz processor clock speed allowing for high frequency data collection. The open source nature of the Arduino microcontroller simplifies the development of the data-logger since it supplies pre-existing software thus reducing development time and allows for direct customization with respect to tag size, logging duration, sampling frequency, and sensor resolution. The data-logger design is a significant contribution to the field given its customization ability to capture high frequency data.

2.2 Development Considerations

2.2.1 Accelerometer Chip Selection

The selection of an appropriate accelerometer chip for the data logging device requires the consideration of several factors including sampling rate, measurement range, sampling resolution, communication protocol, and battery type. In the design process for the *MBLog mini* these factors were considered in the context of laboratory applications in fish research.

Sensor type. Ultimately, the choice of sensor package is governed by a balance between miniaturization and the desire for multi-sensor sampling (Muramoto et al., 2004). Typically, the addition of sensor packages directly relates to the size of the resulting tag, not only because these sensors need to be fitted on the circuit board, but increased sensor capability generally results in higher power consumption and storage requirements and therefore battery size and tag size needs to increase accordingly (Muramoto et al., 2004). The number of parameters that can be recorded is often limited for smaller devices. For motion recording tags, the choice lies between accelerometer sensors (tri-axial acceleration), gyroscope (tri-axial vector velocity) and magnetometer (tri-axial compass). Given the context of

measuring movement in fish in the laboratory, I chose the accelerometer sensor without gyro or magnetometer given the advantage of the lowest power consumption. For example, a sensor chip commonly used in biologging tags (InveSense MPU-9250, InveSense, 2015) with a typical operating circuit in the 3-axis gyro mode requires a supply of 3.2 mA, while in the 3-axis accelerometer mode requires 0.45 mA – nearly 7-fold less at the same operating supply voltage.

Sampling frequency. Digital systems can only store data at specific intervals governed by the sampling frequency. As the sampling frequency is increased a more accurate representation of the underlying signal is obtained (Figure 2.2), however, this occurs at the cost of increased memory usage and file size and power consumption. Appropriate sampling frequency depends on the underlying signal, the purpose of the experiment and the range of frequencies of interest. If the data of interest were to be a sine wave (e.g., lateral acceleration in a swimming fish as shown in Figure 2.3 as a solid waveform) then aliasing will occur if the sampling frequency drops below twice that frequency, i.e., the Nyquist frequency (Oppenheim and Schafer, 1989, Sabin, 2008). For example, when data are sampled at regular intervals less than twice the frequency of interest (e.g., 80 Hz), then the frequency of interest (100 Hz) appears as a lower frequency signal at 20 Hz. If the signal of interest is not a sine wave or has a spectral peak and/or there is noise that can be aliased, then the signal needs to be sampled at much higher rates and the standard practice to avoid the effects of aliasing is to select a sampling frequency greater than 10 times the frequencies of interest in the signal (Ogata, 1970).

A sampling frequency that is significantly lower than the frequency content of the acceleration signal of interest, may lead to movements occurring over short time scales either to be missed or misidentified. Given that short-burst acceleration events associated with high energy expenditure during predator-prey interactions typically span a range of 200-700 ms in fish (Domenici and Blake, 1997), high sampling rates (> 50 Hz) are likely required to adequately capture these events in the accelerometer record. It is especially important to quantify such events in the context of activity and energy budgets since they are energy intensive (Goolish, 1991), and thus make critical contributions to energy expenditure. In contrast, if the purpose of the

experiment is to observe a lower-frequency signal such as steady-swimming, which is typically between 1 - 10 Hz depending on fish species and size (Bainbridge, 1958; Videler, 1993) a lower sampling frequency may be sufficient (Videler and Wardle, 1991; Kawabe et al., 2003a,b).

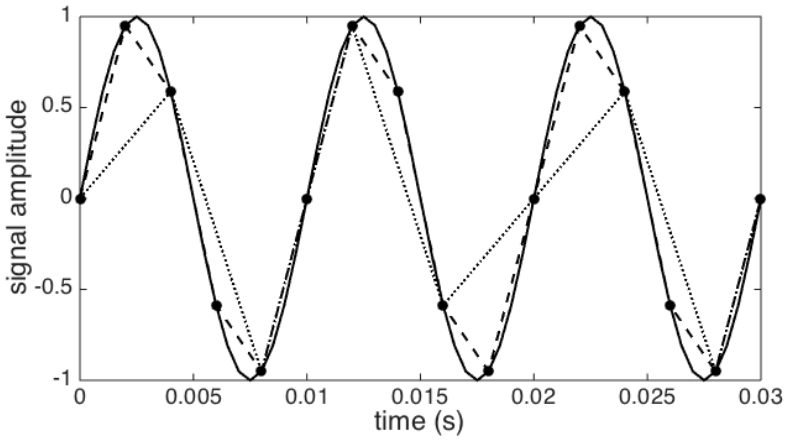

Figure 2.2 The effect of discretization in the time domain where the solid line indicates the waveform of interest at (100Hz), solid circles indicate the times at which the system can sample and record the sensor output, the dashed line indicates the recorded waveform sampled at 500 Hz, and the dotted line when sampled at 250 Hz.

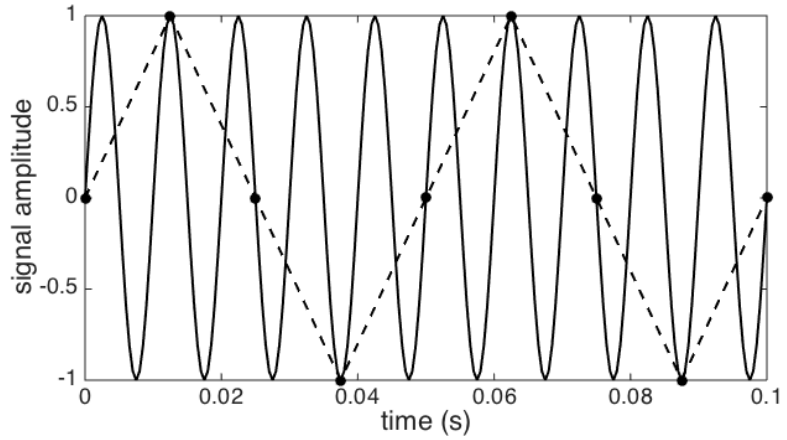

Figure 2.3 The effect of aliasing when the sampling frequency is less than twice the highest frequency of interest results in a significant distortion known as aliasing. The distortion causes signals near the sampling frequency to be detected at a lower frequency. The solid line is the true waveform at 100 Hz, the solid circles indicate the times at which the system can sample and record the sensor output, and the dashed line indicates the sampled signal at 80 Hz appearing as a 20 Hz signal.

Given these considerations, the *MBLog mini* was designed to provide the option of being adjusted to a sampling frequency up to 1 kHz. This not only allows the capture of short-time-scale events such as those that occur during burst acceleration (~100

ms) and associated with swimming, escape, or feeding in fish (Domenici and Blake 1997), but also for the detection of higher frequency components not previously accounted for without very high sampling frequency (> 500 Hz, Ogata, 1970; Pflug et al., 1993; Schreier, 2005). If the purpose of the experiment is the recording of a lower-frequency signal (e.g., steady-swimming) a lower sampling frequency (e.g., in the 10 to 100 Hz range) can then be selected to maximize battery power.

Accelerometer Resolution. The range of acceleration values that a chip can record has an impact on the maximum acceleration values that can be captured as well as the resolution of the accelerometer. In fish, maximum acceleration can vary across species, size, maturity and animal health (Webb, 1978). Experimental studies (Webb, 1978; Harper and Blake, 1990) have shown that across various species and sizes, maximum acceleration rates can range from 2 to 4 g_o with average rates from 0.6 to 1.2 g_o, and with the highest rates of acceleration reaching 12 g_o to 25 g_o in rare cases (e.g., Northern Pike, *Esox Lucius*, Harper and Blake, 1990). Therefore, a sensor chip capable of capturing a wide range of acceleration values is necessary.

The resolution of an accelerometer is the minimum change in acceleration that can be detected and it is directly related to the range of acceleration. A N-bit accelerometer with a binary output has a resolution corresponding to the range of acceleration values that can be measured, divided by 2^N.

To compute an acceleration value at time t, A_t, from a digital value with B_{in} representing the value output by the accelerometer, the following formula is used:

$$A_t = (A_{\max} - A_{\min})\frac{B_{in}}{2^N - 1} \qquad \text{Eq 2.1}$$

Therefore, increasing the bit count will increase the resolution of the device by decreasing the amount of change in the signal that can be measured. The choice in acceleration range requires a thoughtful approach in weighing the need to capture maximum acceleration and the degree of resolution required. In most cases, the output from the sensors is digitized using an analog-to-digital (A/D) converter with 12-bit resolution, after being amplified and filtered with an analog circuit. Although

A/D converters with > 14-bit resolution are commercially available, it is not normally required because of the comparatively low signal-to-noise ratio of measurements made on wild animals (Muramoto et al., 2004, see section 2.2.5).

Based on considerations of sensor type, sampling frequency, accelerometer range and resolution, the ADXL345 accelerometer chip was selected due to its variable range (from $\pm$ 2 g_o to $\pm$ 16 g_o) combined with its small footprint (< 0.5 cm^2), customizable sampling rate (as high as 3.2 kHz), I2C Inter-Integrated circuit digital communication, and 10-bit resolution. Currently, the ADXL354 chip costs less than US$17.90 (Digikey, Thief River Falls, United States), making it ideal for low-cost applications. The I2C communication protocol is advantageous as it requires only two communication lines, one data transmission line and one clock line, while still providing a peak data transmission rate as high as 25 kilobytes per second (kBps).

The ADXL345 is an integrated 3D MEMS accelerometer, with the basic principle of a simple mass spring system. The ADXL345 consists of a proof mass-spring system, a capacitive sensor to measure displacement, and the appropriate signal conditioning circuitry. The proof mass is a freestanding beam of silicone, and tethers, which attach to each corner of the mass and implement the spring system. When acceleration occurs, the mass, m, moves with respect to the anchored ends of the tethers. This displacement, d, is captured by differential parallel-plate capacitance where the motion of a central movable plate is measured by a capacitance change. The displacement can then be used to deduce acceleration, a, based on Hooke's and Newton's law ($k_S\, d = ma$), where k_S is the constant factor characteristic of the spring.

2.2.2 Memory Storage

The rate of data generation is a function of the sampling frequency, the resolution and the number of channels. Each sample consists of 10-bit data for each of the three channels (corresponding to the three axis, x-lateral, y-forward and z-vertical), which is padded out to 16 bits (2 bytes) to simplify memory addressing by allowing the data to fit within standard sizes of memory block. This equates to 8 bytes per sample as the 6 data bytes are followed by 2 bytes to mark the end of the sample. Given a sampling frequency of 500 Hz the data transfer speed is subsequently 4 kBps (500

Hz•8 bytes/sample). This means, 14.4 MB of data are generated per hour. Since the device is intended for applications across several days, a storage capacity of ≥ 1 GB is required. Given this memory storage requirement, several storage solutions are available such as on-board flash memory or external memory devices; such as USB flash drives or MicroSD cards. MicroSD cards provide advantages due to their small size (12 mm x 16 mm x 1.5 mm), simple interface and large memory capacity (up to 64 GB). Furthermore, in contrast to other memory storage solutions that require the direct interfacing of the device with a host PC, data retrieval is simplified since the MicroSD card can be removed from the storage tag and inserted into a standard memory card reader.

To further simplify data retrieval the data can be saved to the MicroSD card as a standard text file. While this involves the conversion from binary values to ASCII characters, and thus increases the size of each data file, the large data storage capabilities of the MicroSD card can easily accommodate this conversion. For example, at a sampling frequency of 1 kHz during a three-day recording, around 2 GB of data would be collected. In the case of *MBLog mini*, the battery constraint (e.g., 72 hours) will outweigh the data storage constraint for any possible sampling rate.

2.2.3 Circuit Design

The circuitry has three sections (Figure 2.4): the battery, the peripherals (used for data capture and storage) and the Arduino microcontroller. The behavioural layout of the data-logger circuit illustrates the data flow from the ADXL345 accelerometer to the Arduino Pro Mini microcontroller (Figure 2.4).

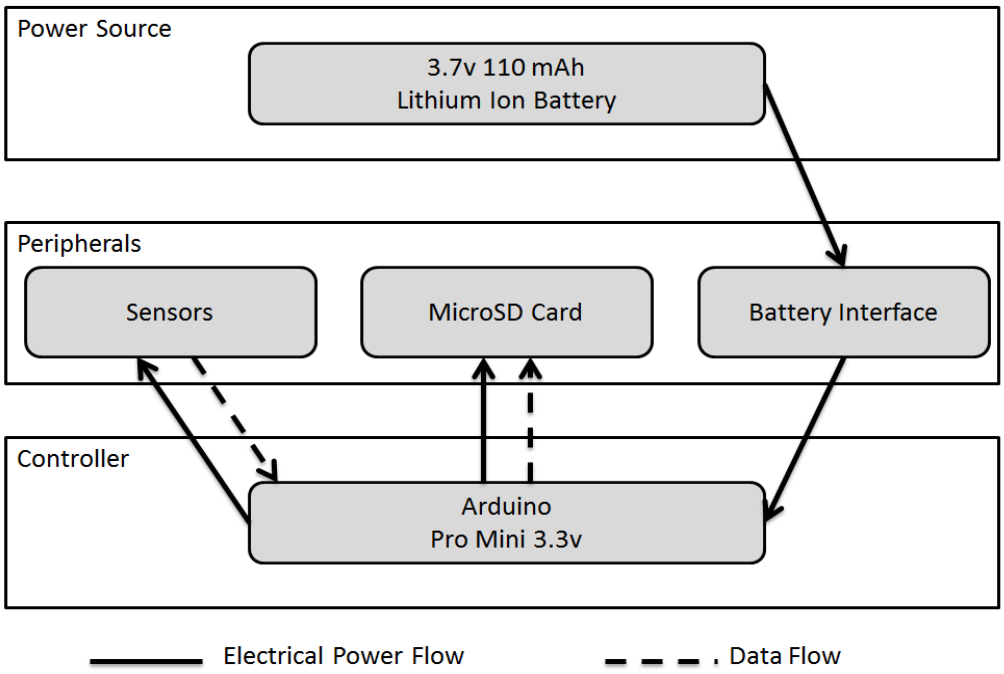

Figure 2.4 *MBLog mini* behavioural circuit. The design utilizes a three level (stack) layout composed of a battery, the sensory/storage peripherals, and the microcontroller.

The Arduino microcontroller then writes the data to a MicroSD card where it is stored for later upload. A rechargeable 3.7 V, 110 mAh lithium-ion battery provides power to the microcontroller, the ADXL345 accelerometer and the MicroSD card. To further reduce power consumption, LED current limiting resistors of 10 kΩ are used. The current consumption of the entire circuit is approximately 4 mAh and in this configuration the device can run for 24 hours on a single 3.7 V, 100 mAh battery. If a longer recording duration is desired, multiple battery packs can be connected in parallel increasing the logging duration in a linear manner (i.e., 2 packs 48 hours etc.).

Both the rechargeable battery and MicroSD card are removable allowing for charging and data retrieval. A 10 µF capacitor is placed next to the power supply pin to the ADXL345 accelerometer to reduce power supply noise. As MicroSD cards generate significant levels of electrical noise, the power supply is connected to the power supply of the MicroSD card via a 10 Ω resistor with a 47 µF capacitor; this decouples the power supply from the MicroSD card.

The Arduino controller and battery can be purchased directly, however, the various peripherals require a customized printed circuit board. Cadsoft – Eagle circuit layout software (CadSoft Inc., Pembroke Pines, United States) was used for the layout of the circuit and the circuit boards were fabricated by SEEEDStudio (Seeed Technology Inc., Shenzhen, China). Components were purchased from Digikey Corporation (Digikey Corporation, Thief River Falls, USA) and manually soldered onto the circuit.

To minimize the complexity of the circuit and to reduce the overall package size, the Arduino microcontroller is programmed prior to installation in the circuit. This reduces the packaging size of the sensors by removing headers and components necessary for the programming of the circuit. However, as the sampling frequency and acceleration ranges may need to be tailored to the specific application, the device is programmed such that a configuration file can be uploaded to the MicroSD card, which allows for control of these parameters by the user. The microcontroller then reads the file and automatically adjusts the sampling rate and range to the desired input parameters.

2.2.4 Packaging

As salt water is electrically conductive, it is essential to protect the electronics in the device from exposure. Since the protection may be subject to a high-pressure environment, a pressure casing was designed to be water tight and robust to > 100 m with a cylindrical shape, which is optimal due to its high strength to weight ratio. The case was manufactured from polyoxymethylene (Delrin™) with Buna-N O-rings for the sealing surfaces (Parker Hannifin Corp, Mayfield Heights, United States).

The inside diameter of the cylinder is a function of the size of the electrical components (circuit board and battery pack(s)) and the outside diameter was determined based on an analysis of the diameter required to withstand the pressure stresses (>100 m) the package would likely experience. For a 24-hour application (1 battery pack) the inside diameter is 14.2 mm and the outside diameter is 16 mm. The length of the electronics and the length of the two end caps to seal the cylinder determine the length of the pressure casing making the total length 52 mm (Figure 2.5, Figure 2.6). To accommodate additional battery packs that extend the sampling

duration, a longer (or wider) case can easily be implemented based on this basic design.

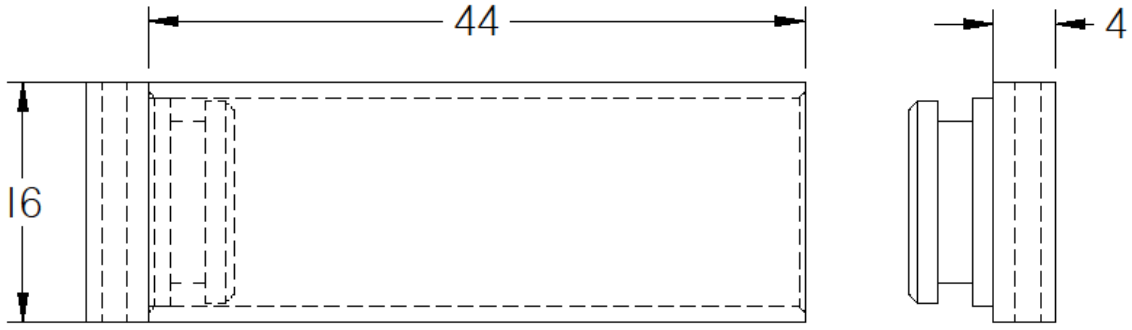

Figure 2.5 Cylindrical Pressure case diagram (units in mm) where the right side shows the end cap with internal features. This design can accommodate the sensor board and one 3.7 V, 110 mAh lithium-ion battery and can be modified to accommodate more batteries.

Each end cap uses one 2-017 Buna-N O-ring to seal the pressure case. The dimensions for the O-ring grooves were determined from the Parker O-ring Handbook (Parker Hannifin GmBH & Co. KG, Bietigheim-Bissingen, Germany) under static O-ring applications. For O-ring lubrication TriboGel, Medium Gel Structure (Aerospace Lubricants, Inc. Columbus, USA) is used. In its current design the packaged device is within -1 g of being neutrally buoyant and with a total weight of 13.2 g in air. To achieve neutral buoyancy of the packaged device, the end cap material can be substituted with a denser material (resulting in a reduction of buoyancy) or the length of the cylindrical section can be elongated (resulting in an increase of buoyancy). The pressure case has been tested to 120 m depth.

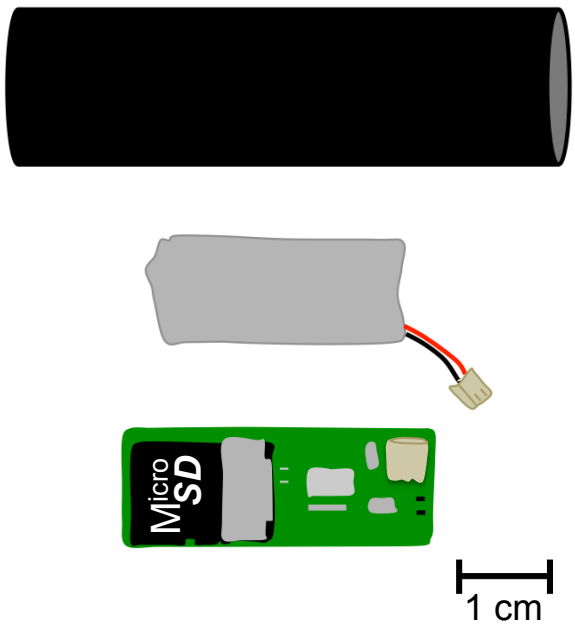

Figure 2.6 *MBLog mini* schematic showing the pressure case for a 24 h duration configuration (top), a 24-h lithium-ion battery (middle) and the accelerometer sensor board (bottom). For deployment, the battery is connected to the sensor board and then sealed in the pressure case.

2.2.5 Signal To Noise Ratio

The primary concern in the design of an acceleration data-logger is to construct a device capable of obtaining the acceleration data required to determine behavioural events reliably. While the sampling rate of the digital signal is crucial (see above), another important degradation of the signal is the signal to noise ratio. Though data related to the required signal to noise ratio are not currently available, it is important to outline how the conversion from analogue signals to digital data affects the signal to noise ratio due to quantization error, *SQNR*, which is given by:

$$SQNR = 20\log_{10}(2^{Q}) \qquad \text{Eq 2.2}$$

where the *SQNR* is in decibels (dB) and *Q* represents the bit resolution of the device. The ADXL345 chip has a noise level of 1.1 bits (Analogue Devices, Norwood, United States). The *SQNR* of the ADXL345 can be determined where 2^{Q} = *Signal Amplitude/Noise Level Amplitude*. The *Signal Amplitude* is equal to (2^{10} - 1) bits and the *Noise Level Amplitude* is equivalent to the value of 1.1 bits amounting to a *SQNR* of 59.4 dB.

Though more research is needed to determine the *SQNR* 's necessary to accurately resolve behavioural events, a *SQNR* of approximately 60 dB should provide an appropriate level as high quality electronic equipment used for medical imaging typically operate within a *SQNR* of 60 dB (Bushberg, 2012). As such this *SQNR* should represent strong signal integrity. Another option is to sample at a much higher frequency than required (e.g., 2 kHz) and then subsample or average the raw acceleration series for data processing after low-pass filtering to remove high-frequency noise.

A second source of noise stems from animal-related factors such as tag movements on the animal that are independent of body movements. When a tag is not securely attached to the animal it may independently move or vibrate even when the animal is immobile. This is especially problematic in aquatic environments where ambient currents can cause such vibrations. To minimize such movements a secure and two-pointed tag attachment (internal or external) is necessary. For that purpose, the pressure case caps can be furnished such that they allow for a two-point anchor either internal or external, via sutures.

Data collected by the acceleration sensor has three major components: the translational or dynamic acceleration, gravitational or static acceleration (Shepard et al., 2008a) and the external noise. Static acceleration is due to the force of the earth's gravitational field and the orientation of the accelerometer with respect to that field while the dynamic acceleration relates to the animal movement (Shepard et al., 2008). Isolating static from dynamic acceleration allows separating the changes in animal attitude from changes in animal movement. Analytical methods for separating static and dynamic acceleration typically rely on the assumption that the gravity-based acceleration component is characterized by low-frequency changes in the acceleration signal. Conventional methods include the running-mean smoothing method (e.g., Wilson et al., 2006; Shepard et al., 2008) or the frequency-based filtering method (e.g., Tanaka et al., 2001). Yet, recently, Noda et al. (2013) suggest that it is difficult to precisely estimate attitude and dynamic acceleration using only an accelerometer, because gravity-based acceleration and dynamic acceleration cannot be fully separated using only these sensors and can only be achieved by

combining information from inertial sensors (gyro, magnetometer, accelerometer). This is suggested to be especially problematic for fast-moving animals during unsteady locomotion such as fast-start movement in fish (e.g., Domenici and Blake, 1997) where the error of estimating true dynamic acceleration and attitude by the conventional method will become larger because the attitude change is much faster than during steady locomotion (Noda et al., 2013). Therefore, additional to external noise sources, the effect of gravitational acceleration on the accelerometer signal requires consideration in the development of analysis methods.

2.3 Discussion

The *MBLog mini* is a customizable, high-frequency tri-axial accelerometer data logger that is light-weight, low-cost (< US$100 in production) and reusable. Design considerations included appropriate sensor chip selection, sampling frequency, chip resolution, data storage and device packaging. The tag is now commercially available through Maritime bioLoggers, a start-up company founded by A. Bezanson, who was responsible for the technology development of the sensors, and myself.

Due to the customization ability of the sensor and the low-cost, this technology opens up research areas where data on many (>10) individuals are required simultaneously. The reusability of the tags allows for a more economical application than comparable units and an increased number of replicas (animals, time, space) in laboratory studies. The *MBLog mini* is most suitable for laboratory-based studies where tag retrieval is possible and to establish appropriate sampling frequencies and validate accelerometer signals to train classification algorithms (Figure 2.1). The current design and battery duration constraints do not yet allow for recording a duration exceeding 72 hours in a tag size configuration that minimizes impact on smaller fish. Furthermore, the tag does not include a real time clock, which is essential for time referencing the collected data as well as for synchronizing data from different instruments (e.g., video observations). Another disadvantage is that the tag does not have an ON/OFF switch and is turned on when the battery is connected, which is inconvenient and given the short battery duration requires direct access to the animal and prohibits internal attachment.

Currently, Maritime bioLoggers is in the process of developing a novel rechargeable long-duration inertial biologging tag that addresses the issues outlined above. By implementing the more advanced micro-processor ARM and sophisticated ARM architecture, the data-logging capacity has been increased significantly to 1 month given the tag dimensions outlined above. The tag is cased in epoxy and able to withstand > 1000 m pressure, turned on with a magnetic switch and a micro USB connector serves for data download and battery recharging. Further features include a real-time-clock and programmable duty cycle to increase tag logging duration, as well as an advanced sensor suite (inertial sensor chip, pressure, temperature). The first prototype of this tag has been successfully tested in a 1-month field deployment on Pacific Halibut in Alaska, USA and long-term tests (> 6 months) are currently underway on a large group (> 15 individuals) of grey seals on Sable Island, Canada.

Future Design Considerations The main drawback in the current and other commercially available inertial and accelerometer tags is the logging duration at small sizes. In the near future, revisions of the data-logger will center on minimizing the overall size of the package, reducing power consumption and developing signal-processing techniques for the extraction of critical data on board. Investigations into additional battery storage solutions for increasing the runtime of the device will be conducted. For example, an ideal application would be piezoelectric energy harvesting power supplies that have been developed for other applications (e.g., Aktakka et al., 2011; Shafer et al., 2015a). To further reduce power consumption a sleep-mode could be implemented that constantly collects data without saving to the SD card (which consumes most of the power on the tag) and if the acceleration exceeds a certain pre-determined threshold (e.g., 1.5 g_o) it triggers a transfer into the operational mode when the tag records data and/or turns on other channels (e.g., gyro and magnetometer) that consume significantly more power than the accelerometer sensor. Implementing on-board micro processing of *a priori* determined classification algorithms could further increase tag capability. While this would likely not reduce power consumption, it would allow for data to be compressed and then transmitted acoustically to underwater receivers or via

satellite-telemetry, thus allowing for more wide-range applications that do not require a physical retrieval of the data logger, as this is challenging in the marine environment.

Chapter 3 ACCELEROMETER TAGS: DETECTING AND IDENTIFYING ACTIVITIES IN FISH AND THE EFFECT OF SAMPLING FREQUENCY

The majority of this chapter has been published as:

Broell, F., Noda, T., Wright, S., Domenici, P., Steffensen, J. F., Auclair, J. -P. and Taggart, C. T. (2013). Accelerometer tags: detecting and identifying activities in fish and the effect of sampling frequency. *J. Exp. Biol.* **216**, 1255-1264.

3.1 Introduction

Quantifying activity patterns and energy budgets among animal species is essential to assess and identify basic life-history traits, habitat requirements and intra- and inter-specific interactions. Such information is also essential for parameterising ecosystem models and for advancing the informed management of commercially and recreationally valued fish species. Field observations of the behaviour and locomotion of aquatic animals in the wild are typically challenging, though micro-accelerometer (archival or acoustic and satellite telemetry) tags now provide the means to remotely monitor animals in the wild.

Accelerometer data can be used to quantify behavioural states and rates and to estimate energy expenditure in the field (Tsuda et al., 2006; Sato et al., 2007; Murchie et al., 2010; Payne et al., 2011; Whitney et al., 2010). In fish, acceleration metrics have been linked to heart rate and energy expenditure (Clark et al., 2010), spawning behaviour (Tsuda et al., 2006), activity (Kawabe et al., 2003a,b) and more recently feeding behaviour (Føre et al., 2011). Generally, accelerometer tags continuously record data at some defined frequency, or time-averaged data thereof, that are either digitally stored or transmitted for subsequent post-processing. Post-processing is typically based on a broad categorization of the acceleration data

(signal) using the average, extreme values of the acceleration signal (e.g., Murchie et al., 2010; O'Toole et al., 2010), or various frequency components thereof (e.g., fast Fourier transform, FFT, and wavelets; Sato et al. 2007, Sakamoto et al. 2009), and often this is done subsequent to data transformation to various components of dynamic and static acceleration (Tanaka et al., 2001; Wilson et al., 2006; Shepard et al., 2008a,b; Gleiss et al., 2010). These signals and their variation (e.g., rates of change) are then combined to estimate activity and energy budgets or to classify various behaviours such as resting, swimming, etc.

Many accelerometer studies involving fish (Kawabe et al., 2003a,b; Tsuda et al., 2006; Murchie et al., 2010; O'Toole et al., 2010) employ sampling frequencies ≤32 Hz due to battery, data-storage and size constraints associated with commercially available tags. Observations obtained at such frequencies may allow for the identification of relatively simple behaviours such as resting and swimming or some complex behaviours such as spawning in large salmon (Tsuda et al., 2006) or mating in large sharks (Whitney et al., 2010). However, few studies address behaviours that in some fish species occur over short time-scales of the order 100 milliseconds; e.g., feeding strikes or escape responses (Webb, 1978). These kinds of short-duration high-amplitude accelerations are essential components when estimating activity and energy expenditure.

A link between accelerometer data and the movements associated with swimming bouts such as haphazard turns, predator-prey escape response, or feeding strikes in fish has yet to be established. Video analyses, based on kinematic experiments focusing on such 'fast-start' behaviours in controlled laboratory conditions have demonstrated relations among acceleration metrics and high-resolution video records of movement (Harper and Blake, 1989; Harper and Blake, 1990; Domenici and Blake, 1997; Domenici et al., 2004). The above studies suggest that accelerometer data can be used to qualify and quantify more detailed variations in locomotion and behaviour, provided that the sampling frequency is sufficiently high (Harper and Blake, 1989). If the sampling frequency is too low, aliasing of the acceleration signal will occur (e.g., Oppenheim and Schafer, 1989; Sabin, 2008). Thus, behaviours associated with swimming, predator-prey escape response or

feeding strikes may either be missed or misidentified. Since such short bursts of activity may result in anaerobic metabolic pathways being used and thus increased energetic demand (Goolish, 1991), the estimates of activity and energy budgets will at best be biased. To obtain estimates of state- and rate-inferred behaviours, and for confident estimation of activity patterns in any fish species, quantifying the species-specific effect of sampling frequency on the detection of locomotion associated with such behaviours is essential – especially if the activities occur over short time-scales.

Given the above concerns, this study focused on two questions. 1) How can I statistically differentiate among various locomotion behaviours such as spontaneous movement, escape response and feeding strikes in fish? 2) What is the effect of accelerometer sampling frequency on the detection and identification of these event classes; i.e., when does sampling frequency compromise detection and identification? I used a readily available and hardy species, the great sculpin (*Myoxocephalus polyacanthocephalus*), as a model fish to collect acceleration data and associated statistical parameters from a suite of activity trials to address the two questions. I then considered how appropriate sampling frequencies could be used in field studies to remotely monitor complex fish behaviour in a manner not previously possible.

3.2 Materials

Study animal

Seven great sculpin (*Myoxocephalus polyacanthocephalus*, Pallas 1814) ranging in size from 29.0 to 35.0 cm fork length (average ± SD, 31.8 cm ± 2.0) weighing between 560 – 940 g (average ± SD, 668.7 g ± 142.9) were collected using a beach seine at two locations on the southeast side of San Juan Island, Washington, USA, and were used in the activity trials conducted at the Friday Harbor Laboratories. The fish were held in a 1.70 m diameter outdoor tank with flow-through seawater maintained at 11±1 °C (average ± SD) and 1 m depth. Fish were acclimatized to the tank for at least one week prior to the tagging and the activity trials that took place over a 14-day period. After tagging, food was withheld to ensure a feeding response to the presence of live, wild-caught sandlance (*Ammodytes* spp.); a preferred prey-

type for sculpin based on preliminary food selection trials using multiple natural prey-types. The use of dead prey was also tested, but it elicited unnatural feeding behaviour from the animals.

Accelerometer

An ORI-380D3GT micro-accelerometer (Little Leonardo Ltd., Tokyo, Japan) was used to record tri-axial acceleration. The accelerometer (±4 g_o) sampling frequency was set at 100 Hz using a 12-bit resolution and 10 h data-storage capacity. The accelerometer tag was 12 mm in diameter and 45 mm length with a weight of 10 g (≤2% of fish fresh-weight).

Activity trials

Fish anaesthetized with MS222 (80 mg l^{-1}) were measured for length and weight and tagged using Petersen Disk tags (Floy Tag & Mfg. Inc, Washington, USA) one week prior to the feeding and escape activity trials. Two disk-tags, one forward and one aft of the centre of the 1st dorsal fin were attached ~0.5 cm below the insertion point of the fin; a location assumed to be the least invasive and located at an attachment point closest to the centre of gravity, estimated (post-mortem, point balance) at 0.35 body lengths from the tip of the snout (Figure 3.1). The temporary (for trials) attachment of the accelerometer tag to the disk-pair was accomplished using Velcro®. No complications were experienced during the tagging procedure.

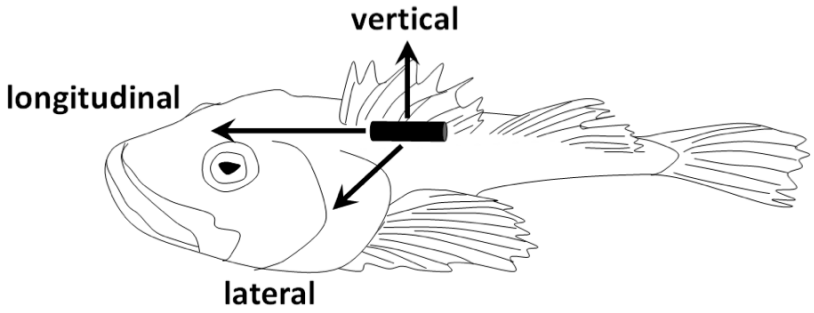

Figure 3.1 Schematic representation of a sculpin with a Petersen Disc tag mounted with a tri-axial accelerometer showing the orientation of the lateral (x), longitudinal (y) and vertical (z) axes.

For each activity trial an individual fish was tagged with the accelerometer during transfer from the holding tank to an identical and adjacent trial tank where the water level was maintained at 0.5 m depth to ensure reliable video (see below). The transfer and tagging time ranged between 2 and 3 min after which none of the animals showed signs of stress and settled quickly in the trial tank. Fish were acclimated to the trial tank for 30 min prior to the start of the activity trials. For escape trials, an escape response was triggered at ~30-min intervals using the method of Domenici et al. (2004). Between 9 and 15 escape responses were elicited and recorded for each fish. For feeding trials, 5 live sandlance were introduced to the tank to allow the fish to feed *ad libitum*. Depending on the responsiveness of the fish, between 12 and 22 feeding strikes (successful or not) were recorded per fish. Additionally, 10 spontaneous swimming events (haphazard turns, swimming, minor body movements when at rest) were recorded for each fish during the suite of trials. Activities were noted manually when visually observed, recorded using the accelerometer, and video-recorded using a 30 Hz standard USB webcam (Microsoft LifeCam, VX-1000 and H264 Webcam 3.83 software) located 2.6 m above the tank bottom. Manual notation (computer clock), accelerometer, and video recording were synchronized prior to a set of activity trials. The data used for analyses were based on a total of 160 h of accelerometer recordings among the activity trials.

The care and sampling protocol for the tagging surgery and live predator-prey experiments in this study was approved by the University of Washington in accordance with Institutional Animal Care and Use Committee (IACUC) standards (permit number 4238-04).

3.3 Methods

3.3.1 Acceleration Data Extraction

The timestamps on the accelerometer and the video recording were used to localize acceleration events. Using visual observations of locomotion, the events were assigned a class, either spontaneous, S, or 'fast-start', FS, (Domenici and Blake, 1997), where the latter was further divided into feeding, F, and escape, E, activity classes. For each observed fast-start event and 10 randomly selected spontaneous

events, a 1-s period of the acceleration record was extracted, and centred on the maximum acceleration. This 1-s interval is hereafter referred to as 'event'. The length of the event period was chosen after video observations revealed that all observed fast-start events occurred within that period.

The acceleration data were processed as 3-dimensional acceleration (lateral, longitudinal and vertical) here referred to as the *x*-, *y*-, and *z*-axes, and the magnitude of acceleration (*MA*) which is the vector norm, not corrected for gravitational acceleration (cf. Chapter 2):

$$MA = \sqrt{x^2 + y^2 + z^2} \qquad \text{Eq 3.1}$$

To avoid unnecessary complications due to the directionality of events in the lateral *x*-axis (left- or right-lateral), the events were standardized such that the maximum acceleration amplitude in the *x*-axis was always positive. Event data (n_{Ds} = 70, n_{De} = 82, n_{Df} = 105) were randomly divided into two subsets, the training subset (n_{Ts} = 40, n_{Te} = 51, n_{Tf} = 53), which served to establish parameter threshold values, and the validation subset (n_{Vs} = 30, n_{Ve} = 31, n_{Vf} = 52) that was treated as a independent data set with the purpose of testing parameter efficiency and the effect of sampling frequency. Statistical analyses and algorithm computations were performed using 'R' Statistical Computing Software (version 2.13.0, R Foundation for Statistical Computing, Vienna, Austria, 2011), and MATLAB 7.12 (Natick, Massachusetts: The MathWorks Inc., 2011).

3.3.2 Discrete Parameter Analysis

My goal was to establish a parameter or a parameter set capable of detecting events and identifying the activities with minimal variation within and amongst individuals, and independent of values that depend on the accelerometer mounting position and the size of the fish (e.g., maximum acceleration). Parameters from the frequency domain, using spectral and wavelet analysis, the probability domain using the probability density function, population parameters such as mean, maximum, and variation in acceleration, and the time domain using autocorrelation and pattern descriptive parameters (integral, derivative) were examined for their utility in detecting and identifying activity in the acceleration records. While there are more

formal systematic ways to determine suitable parameters and parameter combinations (e.g., Linear Discriminant Analysis), I chose to implement a more pragmatic approach. A systematic signal processing approach, as conceptualized in Figure 3.2, was developed to: 1) detect fast-start events using an event detection parameter (Φ), and 2) to identify fast-start events as being either feeding or escape activity by using a parameter set, $\Omega = [\omega_1, \omega_2, ..., \omega_i]$, where ω_i is the i'th identification parameter in the Ω set. Suitable parameters were established using the entire event data set [I]. Threshold values for significant parameters were then determined using an optimization routine based on the training subset [II]. Finally, the efficiency of the established parameters and the effect of sampling frequency were determined using the validation subset [III].

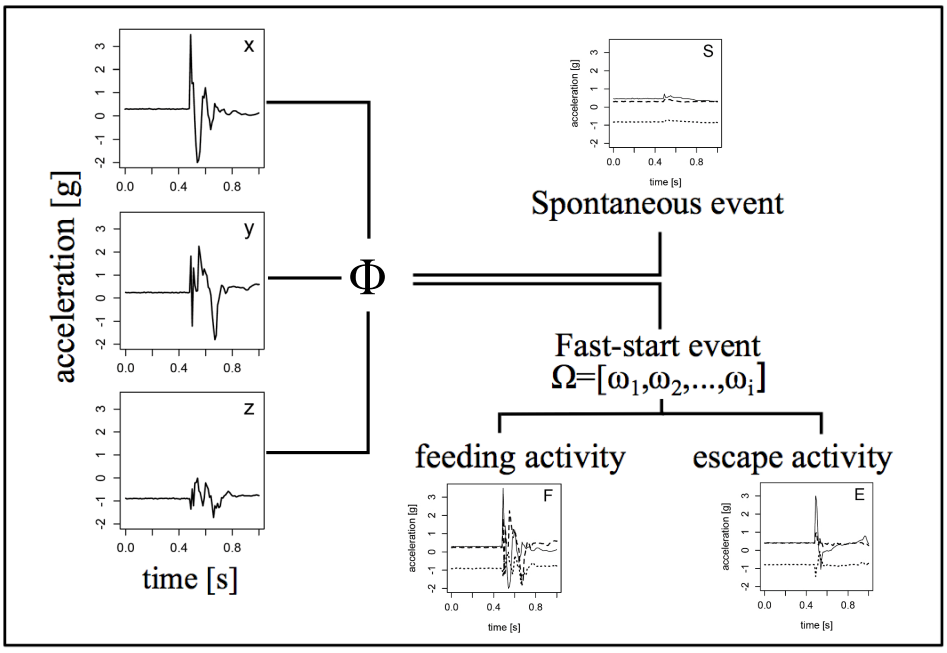

Figure 3.2 Schematic representation of using tri-axial (x-lateral, y-longitudinal, and z-vertical) acceleration (g_o) time (s) series to first detect (Φ parameter) and then identify (Ω parameter set) spontaneous (S) events, and feeding (F) and escapes (E) activities in sculpin with representative event acceleration series for illustration.

I. Establishing suitable parameters

Procedure – All parameters identified as being potentially useful were tested for average differences (Student's t-test after testing for normality, Wilcox-Sign Rank test otherwise) between spontaneous and fast-start events and between activity classes for all fish in the aggregated and the disaggregated (individual fish) data.

Parameters were rejected if differences between event or activity classes were insignificant for either the aggregated or disaggregated data. Parameters derived from the frequency and probability domains suffered from low data density. For example, escape activity, typically occurring over an average of 250 ms, contain ~25 data values when sampled at 100 Hz. Thus, these domains were suboptimal and were dismissed. Parameters describing the 'shape' of the event, such as the acceleration integral or the acceleration derivative, were tested and dismissed because no difference between activity classes was determined. Furthermore, average acceleration values for *MA* (the vector norm), or individual components thereof, were not different between activities.

Detection Parameter Φ – The most robust and efficient detection parameter for the fast-start movements was the standard deviation of the vector norm of acceleration, σ_{MA}. The standard deviation was significantly smaller for spontaneous than for fast-start events (Figure 3.3, Table 3.1). Maximum acceleration of the vector norm was also greater among the fast-start events; however it was dismissed because of its dependency on fish size and the attachment location of the accelerometer.

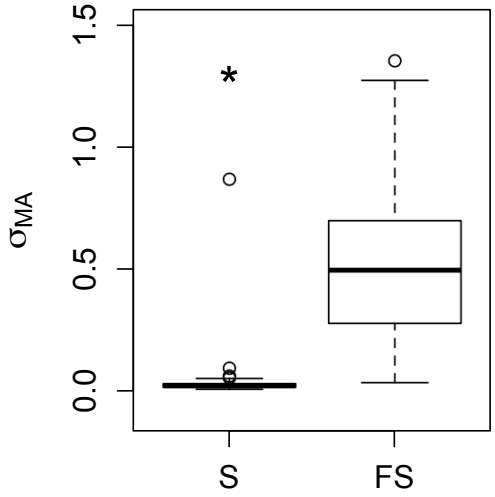

Figure 3.3 Box and whisker plots of standard deviation of the magnitude of acceleration (σ_{MA}) for 7 different great sculpin from spontaneous (S, n_s = 71) and fast-start events (F_S, n_{FS} = 187) using aggregate fish based on the entire dataset where the box illustrates the inter-quartile range (IQR), the bar the median, the whiskers are ±1.5 IQR, the open circles represent outliers and the asterisk (*) indicates that spontaneous events population mean is lower than that of fast-start events (see Table 3.1) for details

Identification parameters Ω – Six significant parameters [ω_1, ..., ω_6] that were different between fast-start event activity classes were determined following the procedure outlined above and as summarized in Figure 3.4 and in Table 3.1. For parameters [ω_1, ..., ω_4], a statistical property of acceleration in the x-axis differed from that in the y-axis for escape activity, but not for feeding activity. For example, ω_1 was based on the standard deviation, i.e., $\sigma_x - \sigma_y > 0$ for escape events and $\sigma_x - \sigma_y = 0$ for feeding events. The other parameters were based on the maximum acceleration (ω_2), the range of the acceleration data (ω_3) and the root mean square (ω_4). Parameter ω_5 was based on the sum of the autocorrelation coefficient τ at lags 1 to 3 in *MA*, which was significantly greater in escape events than in feeding events. Parameter ω_6 was based on the Spearman correlation coefficient, ρ, between the x- and y-axis which was greater in feeding than escape events.

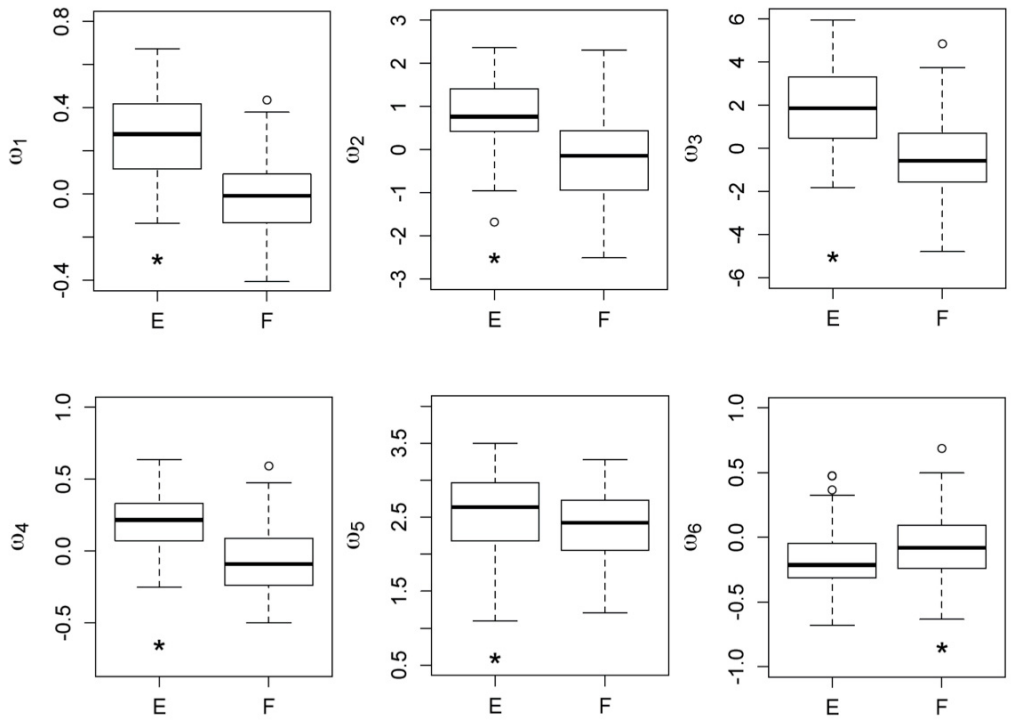

Figure 3.4 Box and whisker plots illustrating differences between escape (E) and feeding (F) activities for each ω_i parameter values, where the box illustrates the inter-quartiles range (IQR), the bar the median, the whiskers are ±1.5 IQR, the open circles represent outliers and the asterisk (*) indicates that parameter values are higher ($p < 0.05$) in E than F for all except the ω_6 parameter where the reverse is the case, see Table 3.1 for details).

Table 3.1 Summary of differences (p) in the Φ parameter in detecting spontaneous (S) and fast-start (FS) events, and in the ω_1 through ω_6 parameters in detecting feeding (F) and escape (E) activities, all based on the number (n) of events and activities in the entire event data. Student's t-test statistic (t) with degrees of freedom (df) was used if the data were normal based on the Anderson-Darling (AD) test statistic (A) and the Wilcox Sign-Rank (WSR) test statistic (V) if otherwise.

Parameter	AD test statistic (A) n_{Ds} = 70, n_{De}= 82, n_{Df} = 105	WSR (V) and Student's (t) test statistics
Φ	$p_{FS} < 0.05$ (A=1.5) $p_S < 0.05$ (A=2.5)	V = 108 $p < 0.001$
ω_1	p_E = 0.11 (A=0.62) p_F = 0.83 (A=0.22)	$p < 0.001$ (df = 159, t = 10.3)
ω_2	p_E = 0.2 (A=0.51) p_F = 0.4 (A=0.38)	$p < 0.001$ (df = 183, t = 8.13)
ω_3	p_E = 0.09 (A=0.64) p_F = 0.14 (A=0.57)	$p < 0.001$ (df = 177, t =9.21)
ω_4	p_E = 0.56 (A=0.31) p_F = 0.07 (A=0.70)	$p < 0.001$ (df =185, t = 9.02)
ω_5	$p_E < 0.05$ (A=1.5) p_F = 0.22 (A = 0.48)	V = 3526 $p < 0.05$
ω_6	$p_E < 0.05$ (A=1.3) p_F = 0.01 (A=0.97)	V = 3795 $p < 0.001$

II. Establishing parameters thresholds values

For the Φ and each of ω_1, ..., ω_6, parameters a threshold value and parameter weights were empirically determined using an optimization routine based on the test data subset. This routine was designed to find cut-off values, v_k (k = 1, ...,7), which maximize both the percentile of the observed parameter values of one event/activity class falling below v_k, and the percentile of the observed values falling above v_k of the other event/activity class (Table 3.2). For example, the detection parameter, σ_{MA} was greater than the optimized threshold value, v_1, of 0.2, for fast-start events and <0.2 for spontaneous events. Hence the threshold of 0.2 was of significance in correctly detecting a fast-start event. This example applied for each of the ω parameters accordingly (Table 3.2). The optimized percentiles represent the empirical weight (C_Φ, $C\omega_{i,E}$, $C\omega_{i,F}$; Table 3.2) of each parameter for a given threshold, which can be interpreted as a confidence in each parameter for each event class. For example, the

detection parameter, σ_{MA} had a weight of 0.989 for fast-start events, which means that 98.9% of all fast-start events exhibited a standard deviation that was greater than the optimized threshold.

Table 3.2 Summary of the threshold values from optimization routine results for spontaneous (S) and fast-start (FS) events and feeding (F) and escape (E) activities all based on the number of events and activities in the training subset data. The parameters include the standard deviation of the acceleration vector norm, σ_{MA} (Φ), and the parameter set Ω including the standard deviation, σ, in the x or y acceleration axes (ω_1), the maximum acceleration amplitude A_{max} in the x or y axes (ω_2), the range in acceleration, R_A, in the x or y axes (ω_3), the root mean square, RMS, in the x or y axis (ω_4), the sum of autocorrelation coefficients, τ, for lags 1, 2, 3 in the vector norm (ω_5), and the correlation coefficient, ρ, between the x and y axis (ω_6). The subscripted parameter weights, C, are the number of events where the parameter threshold applies, expressed as a proportion.

Parameter	Event/ activity class	Optimization Result	Weight, C
Φ	FS	$\sigma_{MA} > 0.2$	$C_{FS} = 0.989$
	S	$\sigma_{MA} < 0.2$	$C_S = 0.949$
ω_1	E	$\sigma_x - \sigma_y > 0.08$	$C_E = 0.714$
	F	$\sigma_x - \sigma_y < 0.08$	$C_F = 0.700$
ω_2	E	$A_{max,x} - A_{max,y} > 0.31$	$C_E = 0.755$
	F	$A_{max,x} - A_{max,y} < 0.31$	$C_F = 0.750$
ω_3	E	$R_{A,x} - R_{A,y} > 0.54$	$C_E = 0.673$
	F	$R_{A,x} - R_{A,y} < 0.54$	$C_F = 0.670$
ω_4	E	$RMS_x - RMS_y > -0.01$	$C_E = 0.642$
	F	$RMS_x - RMS_y < -0.01$	$C_F = 0.652$
ω_5	E	$\sum_{m=1}^{3} \tau_m > 2.7$	$C_E = 0.611$
	F	$\sum_{m=1}^{3} \tau_m < 2.7$	$C_F = 0.625$
ω_6	E	$\rho_{xy} < -0.14$	$C_E = 0.653$
	F	$\rho_{xy} > -0.14$	$C_F = 0.648$

III. Testing parameters

Procedure – Parameter efficiency was tested using the validation data subset. These data stem from 50 h of continuous acceleration records (1.8×10^7 data values) spanning numerous spontaneous and 83 observationally verified fast-start events. I used these data to determine the detection probability (fast-start events), the identification probability (feeding or escape activity) of detected events, and the performance of the individual parameters. I also examined the effect of accelerometer sampling frequency on detection and identification probability (see 3.3.3 below).

Detection probability – The fast-start detection probability was established using a fast-start detection algorithm. This is a sliding window algorithm that calculated the standard deviation for each 1-s window of the *MA* time series and, based on that value (compared to the threshold v_1, Table 3.2), allocated an event ID ('fast-start event', 'spontaneous event') to the acceleration window. The detection P(D|R) and false detection P(D|NR) probabilities were then established by comparing the fast-start events detected by the algorithm with the observed ('real') events, where D = event detected, R = real event, NR = not real event.

Identification probability – For each 1-s (detected and real) event from the fast-start detection algorithm, the parameter set Ω was calculated. The identification (F, E) was obtained from a sum of diagnostic indicators ('feeding' or 'escape') for every parameter weighted by their confidence (Table 3.2). To determine the identification probability (number of correctly identified events/number of real events), the identification (F, E) was compared to the real event identity (F, E). I then estimated the probability of correctly identifying a detected and real event, and the equivalent probability for escape (E) given detection and for feeding events (F) given detection. These probabilities determined the performance of the algorithm (detection and identification). Given detection, the probability of correct identification, P(E|E) and P(F|F), and misidentification, P(F|E) or P(E|F), was also determined for each activity class and parameter, and was used to assess the performance of the identification parameters.

3.3.3 Sampling Frequency

Various sampling frequencies were considered to assess their effect on the ability of the algorithm to correctly detect events and identify activities. The lower frequency time series were obtained from the 100 Hz data by subsampling the original acceleration record to generate an array of every possible sub-sampled series. For example, four different 25 Hz series were generated by starting from each of the first through fourth data point and keeping every fourth subsequent data point. Multiple lower frequency sets of series from 50 Hz to 3.33 Hz were generated similarly, by starting with the 2nd trough 30th data point in the original series. To avoid additional biasing in the lower frequency analyses, parameters, thresholds values and weights (as detailed in *I – Establishing parameters* and *II – Establishing thresholds* above) were re-assessed for each sampling frequency. Consequently, 'dynamic' threshold values for spontaneous and fast-start events and feeding and escape activities and their associated 'dynamic' weights were generated as a function of frequency.

The detection parameter, Φ, remained significant in differentiating fast-start and spontaneous events for all sampling frequencies considered. The previously determined threshold also applied across all the decreasing sampling frequencies, with a slight decrease in weights (ranging from 0.95 to 0.85).

For the set of identification parameters, Ω, only [ω_1, …, ω_4] remained applicable for differentiating between escape and feeding events across the decreasing sampling frequencies (Figure 3.5). Parameters [ω_5, ω_6] did not provide sufficient confidence (≤0.5) and were therefore removed from the analysis. For significant parameters, a dynamic threshold and dynamic weights were established (Figure 3.6). The dynamic weights for the identification parameters also decreased with decreasing frequencies. Using the recalculated thresholds and weights, detection and identification probabilities for each sampling frequency were established, as above. Since the subsampling procedure provided multiples series at each simulated frequency, the detection/identification probability was described by the average detection probability and one standard deviation for all sampling frequencies < 100 Hz.

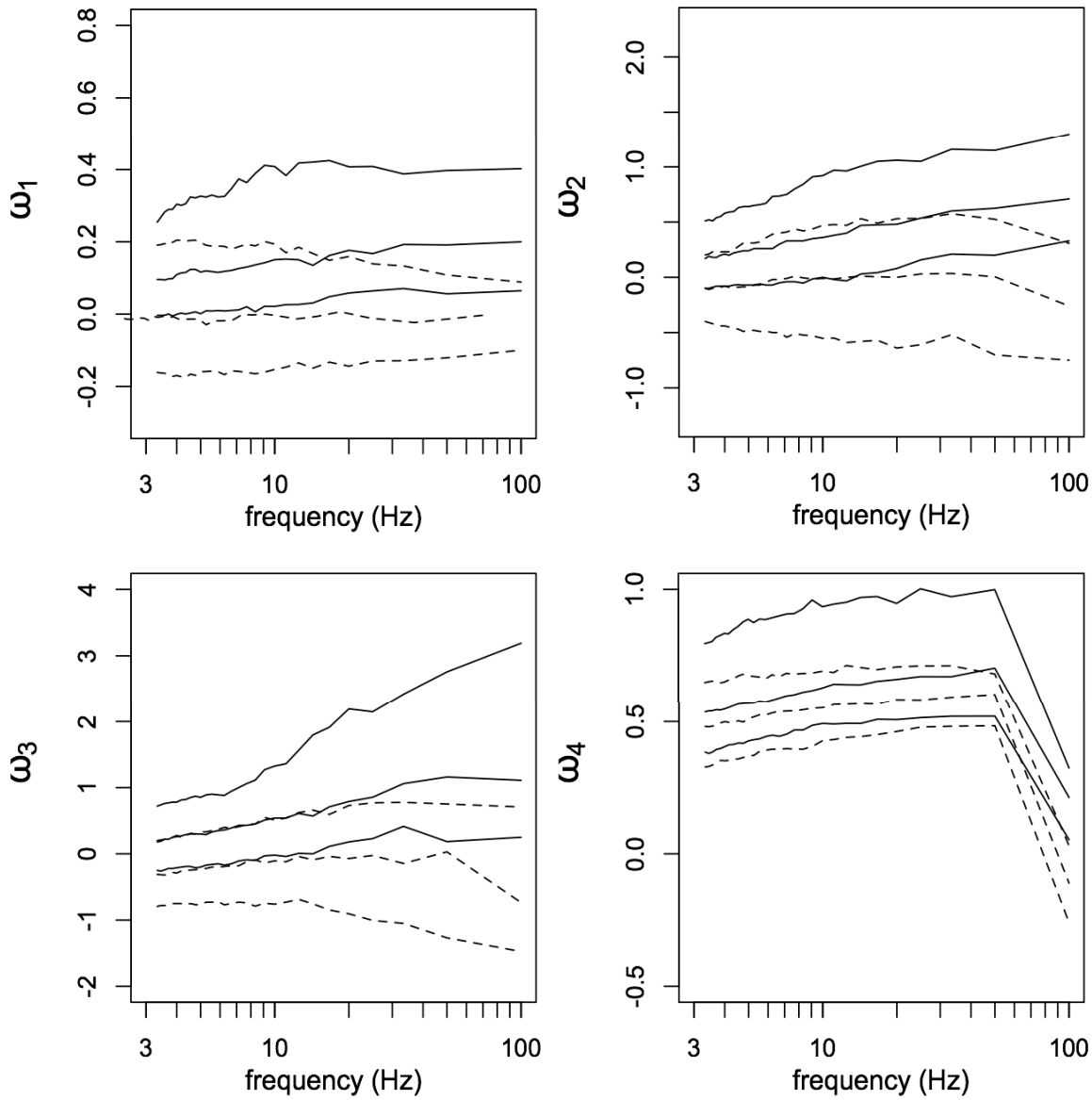

Figure 3.5 Median values with upper and lower quartiles for parameters [$\omega_1, \omega_2, \omega_3, \omega_4$] as a function of sampling frequency calculated using the entire event dataset for escape (solid line) and feeding (dashed line) activities (see Table 3.2) on a semi-log scale.

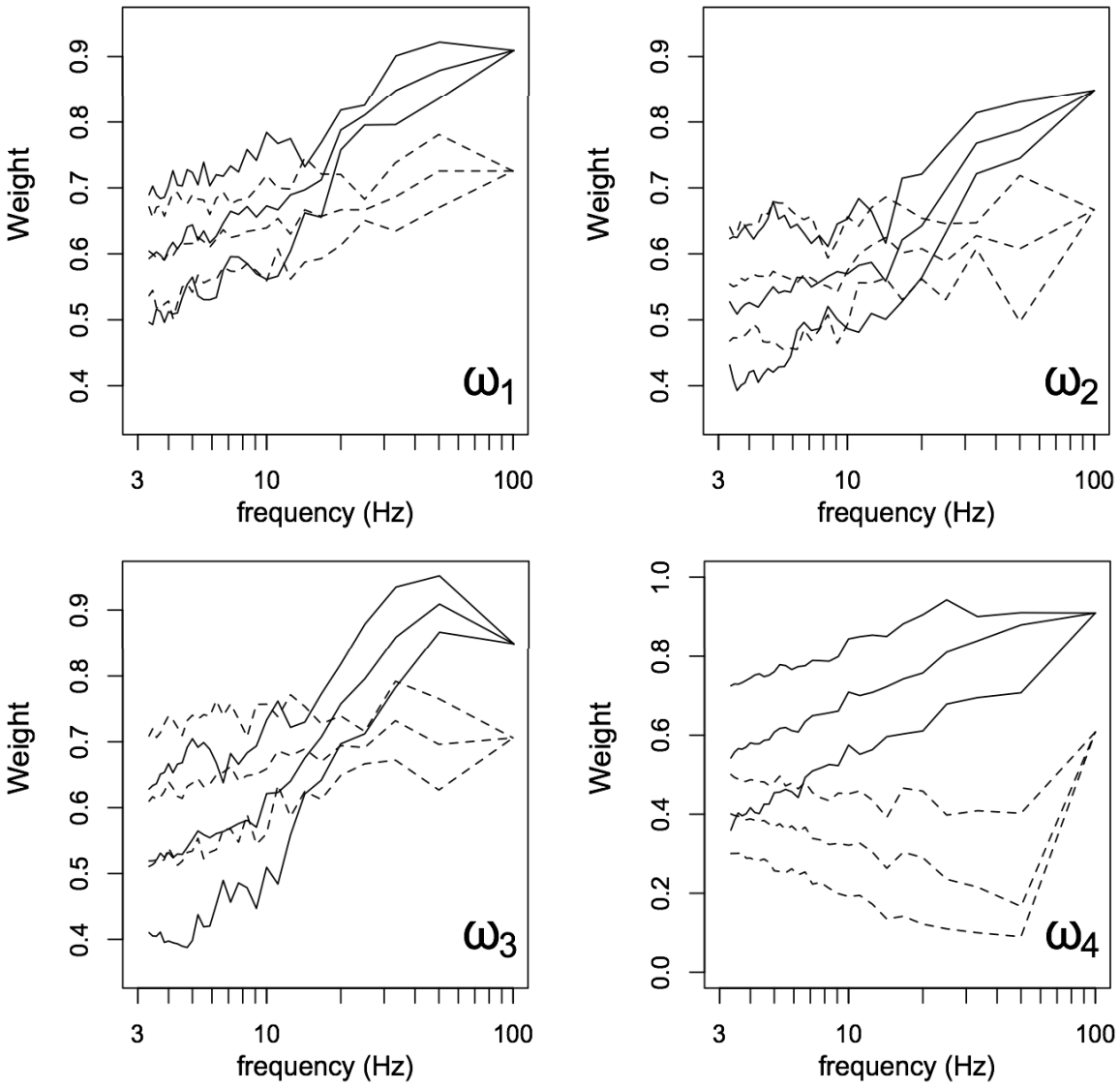

Figure 3.6 Median values ±1 SD of weights for parameters [ω_1, ω_2, ω_3, ω_4] calculated using the entire event dataset for escape (dashed) and feeding (solid) activities as a function of sampling frequency (see Table 3.2) on a semi-log scale.

3.4 Results

3.4.1 Parameter Performance

The detection parameter Φ was highly efficient, with a detection probability of 0.89 and a miss-detection probability of 0, specifically 0.94 for escape and 0.85 for feeding (Table 3.3). The identification parameter set, Ω, was also efficient with a cumulative identification rate of 0.77. 91% of escape events and 69% of feeding events were detected and correctly classified. The efficiencies of each parameter in identifying escape or feeding, given detection, were variable, as illustrated in Figure 3.7.

Table 3.3 Summary of detection and classification results for feeding events (F) and escape events (E) based on 83 verified behavioural events.

Detection	Event ID		Classification	Event ID	
	E	F		E	F
Detected	0.94	0.85	Escape	0.97	0.2
Not Detected	0.06	0.15	Feeding	0.03	0.8
Total	1	1	Total	1	1

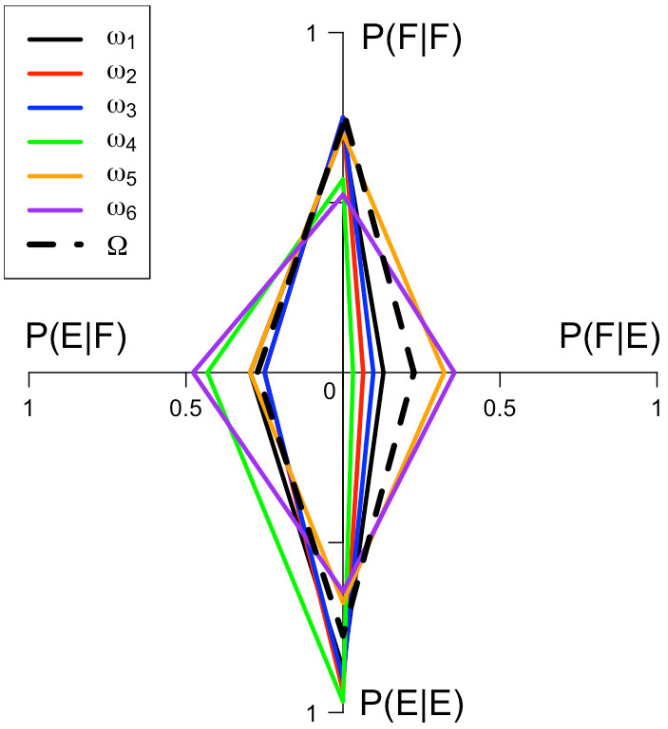

Figure 3.7 Colour coded quadrangle representation of the parameter efficiency space showing the probabilities of activity identification for each of the parameters in Ω (solid colour) and the Ω parameter set (dashed black) where correct identifications are represented by the vertical between P(E|E) and P(F|F) and misidentifications are represented by the horizontal between P(E|F) and P(F|E).

The quadrangle in this figure allows a relative comparison of efficiencies among parameters and the entire parameter set, where perfect event identification is represented by a line from -1 to 1 on the vertical; i.e., 100% probability of properly identifying both escape (-1) and feeding (1) events. The horizontal axis corresponds to the probability of misidentifications P(E|F) on the negative side and P(F|E) on the positive side. While the full parameter set, Ω, was very efficient in the identification of escape events with P(E|E) = 0.97, it was less efficient in identifying feeding events with P(F|F) = 0.79 (Figure 3.7). This asymmetry in performance was also evident for most individual parameters [ω_1, ω_2, ω_3, ω_4], where P(E|E) > P(F|F). In turn, ω_5 performed poorly for escape event identification while being efficient in identifying feeding events and ω_6 seemed generally poor. However, neglecting ω_6 led to a noticeable decrease in the identification efficiency. This shows that less accurate

parameters can compensate for diagnostic errors introduced by other parameters when there was low agreement among the high confidence parameters.

3.4.2 Identification And Detection Rates

The average detection and identification probabilities and their standard deviations, over the range of sampling frequencies examined, are provided in Figure 3.8. The detection and identification rates are the probabilities of detection and identification (i.e., correct classification) given detection, as a function of sampling frequency. I considered this to be the most appropriate tool for assessing the total effect of sampling frequency because it incorporated the cumulative effect of sampling frequency on both detection and identification. The detection rate decreased hyperbolically while identification rates decreased logarithmically (Figure 3.8a) with decreasing frequency. At 100 Hz, 89% of all fast-start events were detected and 77% were properly identified. The class-specific identification probability was 69% for feeding and 91% for escape (Figure 3.8b). Detection decreased to 50% near 4 Hz and identification near 14 Hz for all fast-start events combined, or near 16 Hz for feeding and 7 Hz for escape separately. At 30 Hz, the maximum frequency typically used in the field, 85% of the events were detected and 67% were properly identified. Class-specific identification rates decreased to 62% for feeding and 74% for escapes at this frequency.

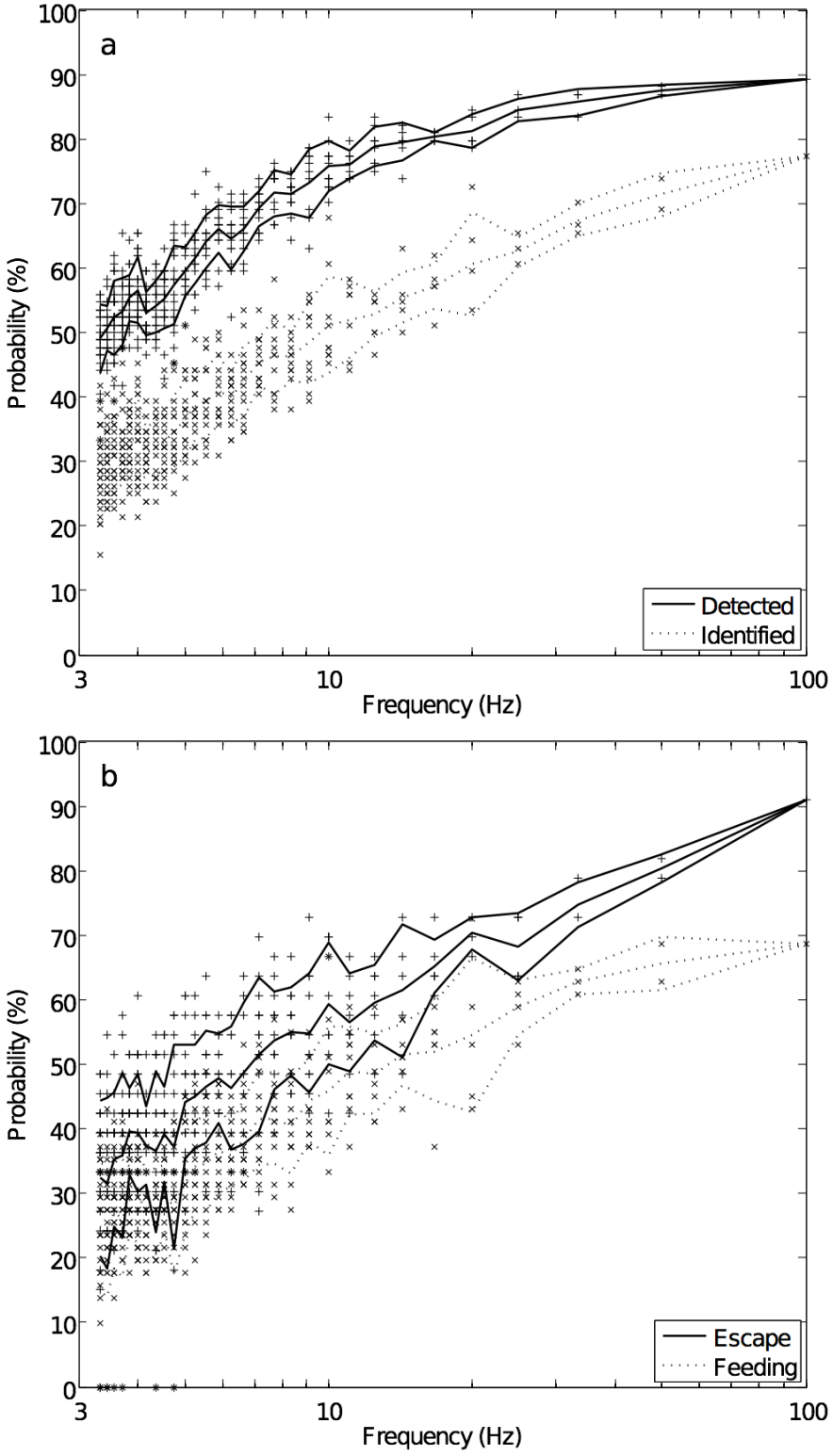

Figure 3.8 Cumulative detection and identification algorithm efficiency expressed as a probability (%) as a function of sampling frequency on a semi-log scale for (a) event detection ('+') and identification ('x'), and (b) identification of feeding ('x') and escape ('+') activity (b) given detection.

3.5 Discussion

As best as I can determine, this is the first study that uses a high-frequency (> 50 Hz) accelerometer tag to detect and identify different types of behavioural events in fish with relatively high efficiencies of ~90% for event detection, ~80% for event identification, and between ~70% and ~90% for feeding and escape activities given detection respectively. I have shown that these efficiencies can be achieved using a relatively simple set of statistical parameters drawn from the time and probability domains of the acceleration record without the need to pre-process (filter) or remove gravitational acceleration from the acceleration signal. Apart from the generally descriptive, and cautionary work of Ropert-Coudert and Wilson (2004) and the metabolic studies of Halsey et al. (2009), this also appears to be the first study that quantitatively demonstrates that achieving the above efficiencies is a function of the accelerometer sampling frequency; i.e., decreased sampling frequency results in decreased event detection and identification probability.

Accelerometers are often used in studies where the sampling frequency of the device depends on the technology (power, storage, etc.) and the size of the animal. Securing high-frequency data generally implies a larger battery requirement and a larger storage capability, each of which increase the tag dimensions. They are typically attached to animals in the field, retrieved at some later time and the data are analysed. In fish, simple parameters such as tail beat frequency and general activity is readily available, yet constrained sampling frequencies will alias the signal and thus compromise the ability to detect movements that occur over short time scales.

Parameters

The suite of parameters I established were selected by statistical significance with some biological underpinnings. For the giant sculpin, acceleration variation in the *y*- and *z*-axes provided a smaller contribution to the vector norm in spontaneous movements of any type investigated. For example, steady swimming was dominated by sinusoidal lateral acceleration (tail beat) with little acceleration in the longitudinal and vertical axes. As shown above, fast-start movements resulted in accelerations and decelerations over milliseconds in all three axes. Not surprisingly, these

movements exhibited greater variation in the vector norm (*MA*) and became manifest in the detection parameter σ_{MA}. To identify the fast-start events, I used 6 parameters, 4 of which were generally robust and of use at sampling frequencies <100 Hz (Figure 3.5). While the detection parameter, Φ, and only one identification parameter (ω_5) were based on the vector norm (comparable to overall dynamic body acceleration, *ODBA*, see Wilson et al. (2006) and Halsey et al. (2009) without a correction for gravity), these other 4 identification parameters were related to inter-axial (*x*- and *y*-axes) comparisons. When based on the vector norm, they failed in event identification. This indicates that *MA* may be suitable for some applications, though my results demonstrate that valuable information is lost when the 3 axes are combined into one metric, especially when investigating short time-scale movement. Interestingly, parameters for *MA* or axis-specific metrics such as the acceleration integral or derivative, or average acceleration, have been used for physiological classification purposes (Clark et al., 2010), for both physiological and activity classification (Murchie et al., 2010, O'Toole et al., 2010) and for metabolic studies (Payne et al., 2011). However, these parameters were incapable of detecting or identifying events and/or activities in my study due, in part, to large intra-individual variation – too large to establish a significant difference between events or activities. Perhaps more importantly, relatively infrequent events associated with substantial changes in acceleration over short time scales, if averaged, may become undetectable and unidentifiable, and increasingly so with the width of the averaging window exacerbated with decreasing sampling frequency. This implies that physiological and (or) metabolic estimates based on data manipulations, such as averaging, may be compromised, especially if fast-start activities comprise a substantial proportion of the behavioural repertoire; e.g., ambush predators.

Limitations on Parameters

The family of identification parameters achieved high rates of event detection (89%) and identification (77%) for a sampling rate of 100 Hz. While powerful in the correct identification of escape events (> 90%), 20% of detected feeding events were misidentified as escape events. This is likely explained by feeding events being more variable than escape events because they are influenced by prey direction and distance, as well as by strike success. This would also be consistent with the variation

in most parameters being greater among feeding events than among escapes. Preliminary examinations of parameter interactions (not presented here) did not improve the efficiency of the parameter set. Additionally, the activity identification of feeding events was more limited by feeding event detection (85%), which was lower than that for escape events (94%).

Many studies address the effect of size on fast-start acceleration in fish, especially A_{max} (Webb, 1976b, 1978; Domenici and Blake, 1997; Domenici unpublished); therefore, in my study I kept the size of the animals relatively constant. The detection parameter was specifically designed to exclude values such as A_{max} (although significantly different between spontaneous and fast-start events) to avoid the influence of size, and fortuitously the attachment location and (or) angle (Tsuda et al., 2006). The [ω_1, ..., ω_4] parameters were based on inter-axial differences (0 or ≠ 0) and I assumed that if acceleration values (±) or magnitude changed with size, the relative differences of axes within the animal would be near constant. Correlation parameters [ω_5, ω_6], which were not based on inter-axial comparisons but on inter-event comparisons, may have been subject to changes in threshold values accordingly to animal size.

Compared to most other fish, the sculpin is limited in terms of movement, especially vertical, and this most likely explains the negligible contribution of the vertical axis to the full parameter set, Ω. If a fish species that moves more in the vertical domain had been used, such as a cruise predator, I would expect vertical acceleration to make a greater contribution to the parameter set (e.g., Kawabe et al. 2003a). Fast-start event detection may be more complex if the vertical acceleration contribution to spontaneous movement increased, which could decrease the power of the standard deviation as a stand-alone detection parameter and thus other parameters may be required to detect fast-start events.

Sampling Frequency

The issues associated with aliasing are well known in the time series analysis and signal processing literature (Oppenheim and Schafer, 1989). However, in the field of animal accelerometry, the question of sampling frequency has received

comparatively little attention. Given that fast-start events typically span a range of 200-700 ms in animals of comparable size (Domenici and Blake, 1997), high sampling rates are required to adequately capture these events in the accelerometer record. I have shown that detection and identification rates of these events significantly decrease with decreasing sampling frequency; i.e., the signals of interest are increasingly aliased at lower frequencies.

There are only few accelerometer studies on aquatic organisms that employ accelerometer tags sampling at frequencies greater than 32 Hz (Noda et al., 2013; Noda et al., 2014). Sampling at such low frequencies may be justified for large animals such as whales and large sharks where observable behaviour occurring over milliseconds is unlikely (Whitney et al., 2007; Gleiss et al., 2009; Whitney et al., 2010; Gleiss et al., 2011; Goldbogen et al., 2011), but for smaller species such as trout, salmon, flatfish etc. (Kawabe et al., 2003a,b; Tsuda et al., 2006) higher accelerometer sampling frequency will likely prove informative, as shown above. The decrease in event detection probability at low sampling frequencies may be acceptable (a sampling frequency of 20 Hz results in detection probability of ~ 60% of fast-start events), yet the identification of the event type decreases rapidly – especially for feeding events, where only 60% of events are properly identified at 30 Hz. Coincidentally, <30 Hz is a typical sampling frequency for archival or acoustic transmitter tags used in most experiments cited above and thus some information may be compromised. While the foci of such studies are on large time-scale movements (e.g., tail beat frequency) and the quantification of general activities (resting vs. swimming), short-burst acceleration events such as feeding and escape are energy intensive and thus make critical contributions to activity and (or) energy expenditure. It is therefore necessary and essential to be able to detect the events to avoid compromised activity budgets and related physiological estimates. This will apply in the laboratory and perhaps more so in the wild where there is virtually no knowledge of how often fast-start events occur. Further, activity detection and identification in the wild, particularly with the differentiation of successful and unsuccessful feeding events, could be especially useful in estimating energy budgets, especially the temporal (day vs. night) and spatial variation (e.g., depth-structured temperature gradients) in energy expenditure and gain (feeding), for which we also

know little. For example, methodologies similar to those developed here, used in combination with depth or location sensors could allow the determination of feeding grounds with important implications for various habitat management strategies (Cartamil and Lowe, 2004).

Technological constraints do not, as yet, easily allow for conventional accelerometer tags to sample at high frequencies for durations greater than several days. However, I argue that continuing advances in micro-technology should result in decreased size and more efficient accelerometer units (battery, storage, micro-processors) that will allow for increasing sampling frequencies, onboard processing, greater storage and longer duration. Until such time, I recommend that accelerometer field studies focusing on behaviour, activity, physiological costs, kinematics etc., include phases of laboratory experiments with high-resolution, short-duration accelerometer tags as shown here to quantify: a) the parameters of interest, and b) the essential sampling frequencies (see Chapter 2). While many studies have demonstrated the use of accelerometers to link some behavioural traits and animal locomotion to acceleration in field applications, for short time-scale events it will be necessary to *a priori* establish the link between the behaviour or physiology and acceleration and to do so at the appropriate sampling frequency.

Future in tag micro-processing

On-board micro-processing, such as already used in some accelerometer tags, decreases the amount of storage of high-resolution data to be archived or transmitted. Based on this study, micro-processing technology could be advanced to the point where algorithms determined *a priori* (e.g., activity detection and identification) constantly calculate the key parameters, allocate event IDs as they occur, and store or transmit the data (see Føre et al., 2011); thus the *in situ* delivery of activities and behaviour over time. This would only be possible if micro-processing uses little power. While this study cannot solve the technological issues around high-resolution accelerometers, it does address the consequences of aliasing when using low sampling frequencies. Although not all studies will require high-resolution accelerometers, I stress the importance of aliasing when embarking on field-tagging studies.

Chapter 4 SCALING IN FREE-SWIMMING FISH AND IMPLICATIONS FOR MEASURING SIZE-AT-TIME IN THE WILD

The majority of this chapter has been published as:

Broell, F., and Taggart, C. T. (2015). Scaling in free-swimming fish and implications for measuring size-at-time in the wild. *PLoS ONE* **10(12)**, e0144875.

4.1 Introduction

In 2007, Neuheimer and Taggart postulated that it might be possible to collect length-at-age time series (and thus growth rate) among fishes in the wild by using archival accelerometer tags. The underlying principles for such a postulate can be found in A.V. Hill's (1950) isometric scaling model that predicts geometrically similar animals should move their limbs at a similar velocity and run or swim at the same velocity with a stride frequency that is proportional to $mass^{-1/3}$ or $length^{-1}$. This scaling model relies on basic physics where the work produced by a muscle during locomotion is a function of its mass and thus the resultant kinetic energy will depend on the mass and the velocity squared. Consistent with this model, observations on a range of free-swimming seabirds and mammals, presumed to be swimming 'efficiently' (Sato et al., 2007), suggested that the animals adopted cruising speeds that are independent of body size and that the associated dominant stroke cycle frequencies scaled with $mass^{-0.29}$ (Sato et al., 2007) For geometrically similar soaring seabirds (Sato et al., 2009) and penguins (Sato et al., 2010) the dominant stroke cycle frequency was shown to be proportional to $mass^{-0.30}$ and $mass^{-0.28}$ respectively, and in each the scaling exponent was not significantly different from -1/3 (Sato et al., 2007, 2009, 2010). Most recently, Gazzola et al. (2014) proposed that for a turbulent flow regime, at a given speed *u,* tail beat frequency is inversely proportional to tail beat amplitude. Given the experiments by Bainbridge (1958) that indicate tail beat

amplitude is proportional to length at any given speed, tail beat frequency therefore is inversely proportional to length, which provides a new theoretical justification for such observations (Sato et al., 2007, 2009, 2010). Such scaling relationships are expected to hold for large (adult) swimmers in the inertial flow regime or as long as swimmers are not trading efficiency for another performance parameter such as speed, with a likely nonlinear relationship in laminar and intermediate flow regimes (e.g., van Leeuwen et al., 2015).

Notably, the above multi-species studies (Sato et al., 2007) included only two species of fish and each with a small sample size: Japanese flounder (*Paralichthys olivaceus*), $n = 5$, and chum salmon (*Oncorhynchus keta*), $n = 2$. Not only does the limited sample size not allow me to firmly conclude that the scaling law does apply for fish species, for the flounder the dominant stroke frequency (tail beat frequency, *TBF*) was anomalously low relative to the fitted inter-specific scaling model. This was attributed to the estimates being derived from potentially 'inefficient' swimming, and thus contradicts the assumption of 'efficient' locomotion (Hill, 1950; Sato et al., 2007, 2010) although there is no clear definition of efficient swimming for fishes.

Efficiency can be defined at several organizational levels such as mechanical efficiency (propeller efficiency) or metabolic efficiency (entire organism). In swimming and locomotion research, studies define efficiency as the ratio of useful to total work or power. To assess propulsive performance, studies often calculate hydrodynamic or mechanic efficiency as the ratio of useful over total work done by the propeller (e.g., Chattopadhyay et al., 2006, Kern and Koumoutsakos, 2006); swimming or metabolic efficiency include muscle and respiratory processes to calculate efficiency (e.g., van Ginneken et al., 2005) or measure oxygen consumption (energy expenditure) in closed respirometer experiments during steady-swimming (e.g., Steinhausen et al., 2005). Efficient swimming is also assumed to occur during high-energy-cost movements, e.g., during migration or feeding bouts (Sato et al., 2007). Some of these efficiencies are only applicable in a narrow range of behaviours, e.g., steady-swimming. For example, efficiency during steady-swimming has also been measured using the Strouhal number, which relates tail beat amplitude and frequency to swimming speed (Sato et al., 2007; Gazzola et al., 2014). According to

Sato et al. (2007), unlike breath-holding mammals, reptiles and birds, fish do not necessarily swim efficiently, at least at top speed, and thus Hill's isometric scaling may not hold. Furthermore, the deviation of the studied fish species from the interspecific scaling relation should not be unexpected since interspecific scaling relations are known to differ from intraspecific relations (e.g., Toro et al., 2003; Glazier, 2005) given ontogenic constraints (Toro et al., 2003) as well as the complications that arise from fitting a bivariate relation to a multivariate problem (Taylor and Thomas, 2014).

To my knowledge, there is a very limited literature examining the above scaling relations among sizes and/or species of (adult) fish, and this is likely due to the inherent difficulty of obtaining such data on free-swimming fish. The few studies that have been published do not include sufficient data or information to allow the conversion of measurements to a common size-related parameter. The consequence is that most analyses of the relations between fish size and locomotion remain theoretical (Hill, 1950; Bainbridge, 1961; Gray, 1968; Webb, 1976a). However, advances in digital accelerometer tags now provide a method of obtaining the necessary swimming data in the laboratory (Noda et al., 2013; Noda et al., 2014), and in the field (Kawabe et al., 2003a,b; Tsuda et al., 2006), and such data have been used to quantify behavioural states and rates and to estimate such things as energy expenditure and swimming activity (Kawabe et al., 2003a,b; Wright et al., 2014) through the extraction of tail beat frequency estimates (Sato et al., 2007; Kawabe et al., 2003a,b; Tsuda et al., 2006).

Quantifying relationships between size and movement may help reconcile co-evolutionary mechanisms (Sato et al., 2009) and help address the ecological implications of size-dependent locomotion (Peters, 1983). It will also have practical applications in fisheries science because fish size influences metabolic rate, physiology, and ingestion rate, and thus growth, maturity and fecundity and ultimately abundance (Peters, 1983). Size-at-age measures are also essential in fisheries science because virtually all population and assessment models involve some component of growth-rate-dependent demography that varies among cohorts and age-classes. Measuring size-at-time and inferring growth rate in wild fish is

inherently difficult, and to date can only be achieved over relatively long time scales using mark and recapture techniques or by using post-mortem morphometrics such as otolith microstructure that have their own inherent uncertainties (Pannella, 1971; Campana, 1990).

Here, I suggest a new method of measuring size-at-time in fish, and potentially growth rate, based on Hill's isometric scaling. I hypothesise that if it is possible to establish a within- or among-species allometric relationship (model) that relates fish size to tail beat frequency from acceleration data, then such a model could be used to estimate size-at-time, and thus growth rate over time in the wild. I therefore collected acceleration data and the derived tail beat frequency estimates among a size range of free-swimming saithe (*Pollachius virens*), a species widely studied in kinematic experiments (Videler and Hess, 1984; Hess and Videler, 1984; Steinhausen et al., 2005) and analytical models (Cheng et al., 1998; Kohannim and Iwasaki, 2014), and shortnose sturgeon (*Acipenser brevirostrum*) (Webb, 1986; Long, 1995; Deslauriers and Kieffer, 2012).

4.2 Materials

4.2.1 Study Animals

Saithe (n = 18) of fork length (l; m) ranging from 0.26 to 0.56 m (average ± SD, 0.41 m ± 0.089) with mass (m; kg) between 0.18 and 1.6 kg (0.93 kg ± 0.48) were collected near Nova Scotia, Canada. Accelerometry data were collected from the fish swimming freely in the Aquatron pool tank (Dalhousie University), a large mesocosm with a diameter of 15.24 m, a depth of 3.54 m at the perimeter and 3.91 m at the centre, and a volume of 684 m^3 natural seawater held at 9 °C ± 2. Swim trials were conducted over 9 trial-days spanning a month. Each individual fish swim trial lasted between 24 and 29 h with a recovery period of two to five days.

Shortnose sturgeon (n = 22) with l ranging from 0.56 to 1.2 m (0.79 m ± 0.18) were used for free-swimming trials. Individual mass, which could not be measured, was estimated using a mass-at-length relationship for adult fish (Figure 7 in Dadswell, 1979) based on average age (collected in 1998-1999 in the Saint John River, NB,

Canada and held in captivity at the nearby Mactaquac Biodiversity Facility). Accelerometry data were collected over a one-week period in two 11 x 11 m-wide, 1 m-depth, outdoor flow-through tanks held at an ambient river-water temperature of 15.5 °C ± 0.5.

4.2.2 Accelerometers

I used three tri-axial accelerometer tag models (Maritime bioLoggers, Halifax, Canada). For saithe, I recorded tri-axial acceleration at 50 Hz (10-bit resolution) at ± 4 g_o. Saithe exceeding 40 cm were tagged with the MBL PT-1 (50 mm length, 23 mm diameter, 18.8 g in air). Smaller fish were tagged with the MBL PT-2 (25 mm length, 17 mm width, 11 mm height, 6.1 g in air). Shortnose sturgeon were tagged with the MBL PT-0 (53 mm length, 35 mm width, 15 mm height, 14.6 g in air) sampling at 550 Hz (10-bit resolution) at ± 3 g_o.

4.2.3 Swim Trials

Saithe were anaesthetized with MS222 (40 mg l^{-1}), measured for l and m and tagged using Petersen Disc tags (see Chapter 3 for tag attachment details) and before each swim trial an accelerometer was attached (in a removable manner) to the disc. Fish swam *ad libitum* for 48 hours with no external stimulus save a natural daylight cycle. Following each trial the accelerometer was detached and the animals recovered in a holding tank (2 x 2 m). At least 4 h of free-swimming accelerometer data were collected for each individual fish for a total of 845 h of data.

Sturgeon were measured for l and tagged using a spandex belt (housing the accelerometer) wrapped around the caudal peduncle, anterior to the dorsal fin. Fish were randomly assigned to the swim-trial tank (isolated) or the holding tank (communal) where they were allowed to swim *ad libitum* in a continuous but spatially variable current (0.0 to 0.3 ms^{-1}) in natural daylight conditions. At least 0.5 h of free-swimming data were collected for each individual for a total of 18 h of data.

4.3 Methods

4.3.1 Estimating Dominant Tail Beat Frequency

Tail beat is a non-stationary periodic oscillation in the acceleration time series (Kawabe et al., 2003a,b; Sato et al., 2007). Thus, to extract continuous, steady swimming data from accelerometer records, I defined steady swimming segments as intervals during which *TBF* (Hz) did not statistically vary. I then developed a *TBF* extraction algorithm that was based on zero-crossings (Figure 4.1; see also Kedem, 1986; Stein, 2000) with adaptive window lengths. The algorithm was applied to an acceleration time series after removing the high-frequency noise (IIR Butterworth filter with a 15 Hz cut-off). An initial window length was chosen to resolve the lowest, expected, species-specific *TBF* (Videler and Hess, 1984; Long, 1995), e.g., 2 seconds for saithe given their minimum observed tail beat frequencies at ~0.5 Hz (Steinhaussen et al., 2005). Steady swimming segments were those where the period between zero-crossings was 'stable'; established by comparing the variability in the time between zero-crossings (i.e., beat periods, Δt's) to a stability threshold, *Th* that was based on the range of differenced Δt's in the entire series $(\Delta t_j - \Delta t_{j+1})_{\max}$ - $(\Delta t_j - \Delta t_{j+1})_{min}$) multiplied by a scaling parameter (*ThS**). Segment length was then established by statistically comparing consecutive windows of *TBF* estimates based on nonparametric mean comparisons. Each series of consecutive windows of relatively invariant *TBF* was assumed to represent a steady swimming segment. To estimate the dominant *TBF*, I combined segments from the same individual among multiple swim trials. The algorithm above was used to extract a list of frequencies and corresponding segment lengths. Stable *TBF* segments within the longest 10 % by duration, were used for analyses, assuming they represented preferred steady swimming modes. These segments were then used to establish weighted histograms, means, medians and standard deviations, where the weights corresponded to the length of each segment with a stable *TBF*. The evaluation of the zero-crossing algorithm can be found in Appendix A.

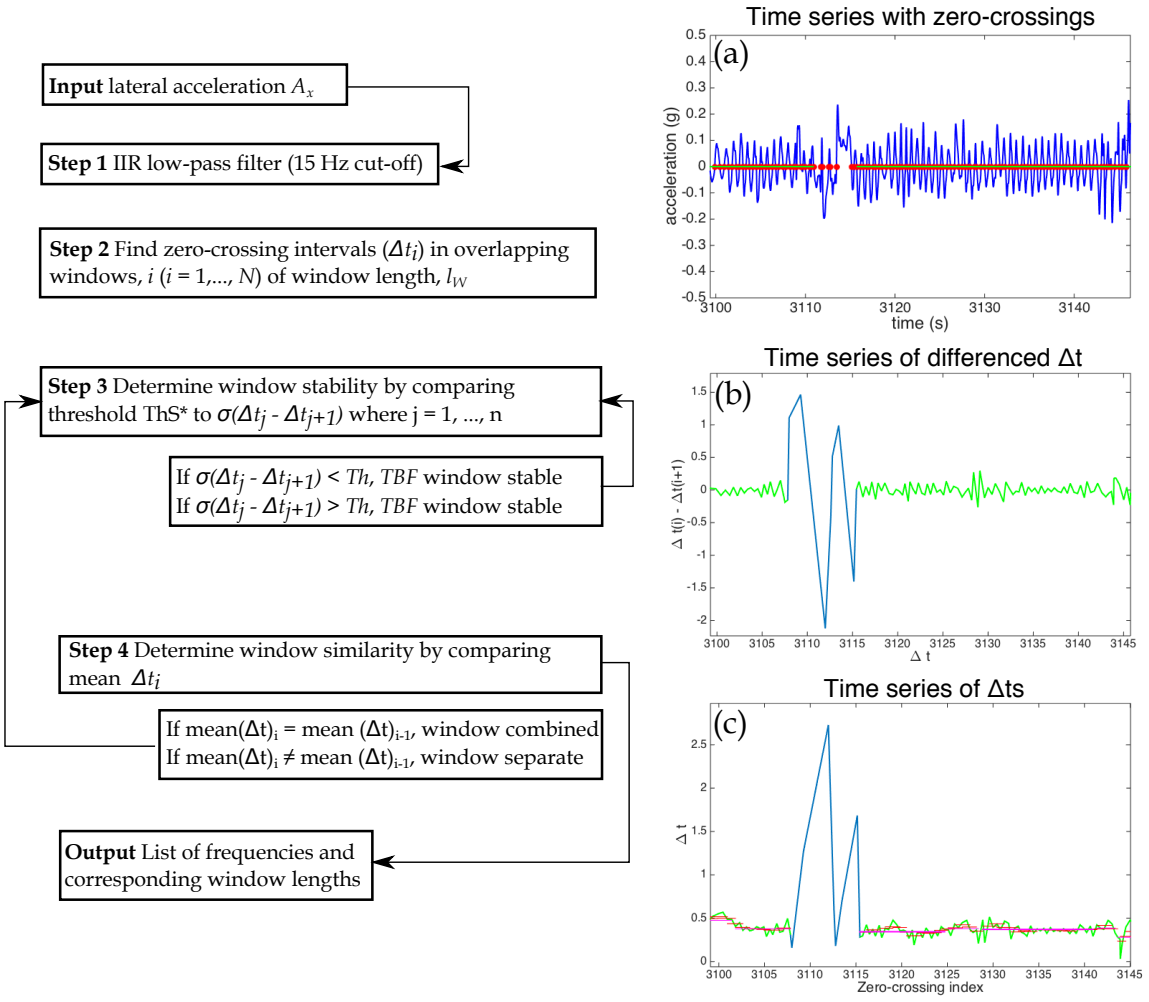

Figure 4.1 Flow-chart of the zero-crossing algorithm used to extract time-varying tail beat frequency (*TBF*) where Δt is the beat half period, σ is the standard deviation, mean$(\Delta t)_i$ is the average beat half period within window i and Th is a function of the range of all differenced periods in the times series and the tuning parameter ThS^* (i.e., $Th = ThS^*((\Delta t_j - \Delta t_{j+1})_{max} - (\Delta t_j - \Delta t_{j+1})_{min})$). Finding zero-crossings is based on Kedem, 1986. A typical species-specific initial window length, l_W for e.g., saithe is 2 seconds. (a) shows time series of lateral acceleration (blue) and zero-crossings (red). (b) green line indicates differenced Δt's for a stable period, turquoise line indicates unstable periods. (c) time series of Δt's (green) with unstable segments (turquoise) and individual windows (pink lines)

4.3.2 Species-Specific Scaling Analyses

I calculated weighted log-log regressions for each species using the moments of the *TBF* distribution. The response variable was $\log_e$ of the median *TBF* obtained from the weighted *TBF* distributions for each individual, and the predictor variable was $\log_e$ of l or m. The regression weights were determined using the variance of the *TBF* (Aitken, 1935; Burnham and White, 2002).

Absolute average swimming speed, u (ms^{-1}), was estimated as a function of dominant *TBF* and l based on literature models. For saithe I used the empirical relation provided by Videler and Hess (1984) where $u = l\ 0.977\ TBF^{0.883}$. For shortnose sturgeon I used the relation from Long (1995) where $u = l\ (0.005 + 0.138\ TBF)$.

Algorithm computations and statistical analyses were performed using R (version 0.98.977, R Foundation for Statistical Computing, Vienna, Austria), and MATLAB R2014b (The MathWorks, Natick, MA, USA). Unless otherwise noted, all estimates are provided as the average estimate plus or minus one standard deviation. Subscripts indicate species (*P,* saithe and *S,* sturgeon).

Fish care and protocols for fish holding, surgery, tagging, and swim trials were approved by Dalhousie University (saithe, Permit 12-049) and Mount Allison University (sturgeon, Permit 10-16) in accordance with the Canadian Council for Animal Care standards.

4.4 Results

4.4.1 Tail Beat Frequency

Distributions - *TBF* estimates for saithe were log-normally distributed (Figure 4.2) with medians ranging from 0.6 to 2 Hz (1 Hz ± 0.3) across all sizes. Estimates for sturgeon were near log-normal (Figure 4.2) with medians ranging from 1.1 to 2.4 Hz (1.5 Hz ± 0.3). For each species no significant deviation from normality for $\log_e l$ was determined.

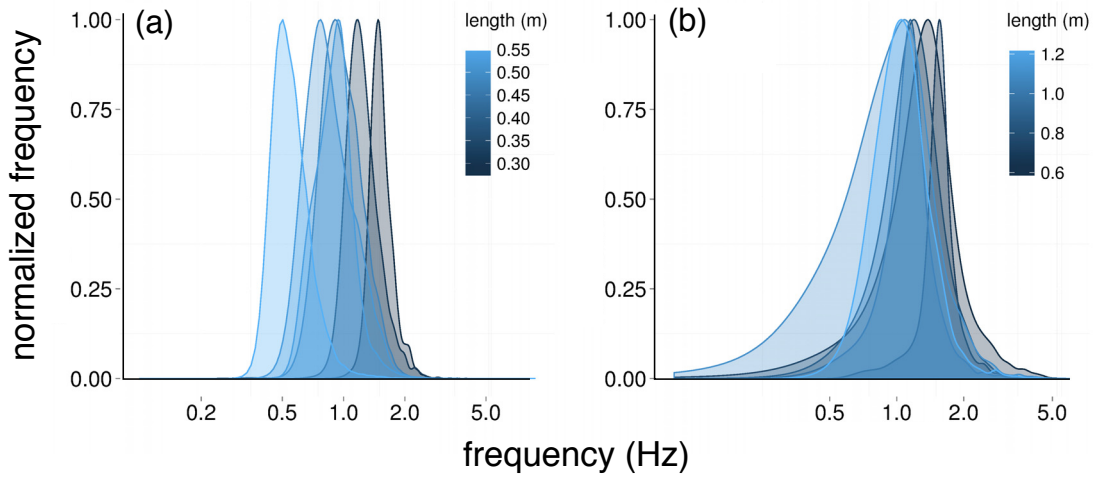

Figure 4.2 Examples of normalized tail beat frequency (*TBF*, Hz) distributions from accelerometer records of free-swimming (a) saithe (n=6) and (b) sturgeon (n=6) based on weighted histograms of *TBF* extracted using the zero-crossing algorithm

***TBF* as a function of length** - In general, fish length and mass tend to be strongly correlated (for saithe from my data r^2 = 0.93 and for sturgeon from Dadswell (1979), r^2 = 0.99). As shown in Figure 4.3 and Table 4.1 the dominant (median) *TBF* was a strong function of l for each species:

for saithe

$$TBF_P = 0.43\, l^{-0.99} \ (n = 18, r^2 = 0.73) \qquad \text{Eq 4.1}$$

for sturgeon

$$TBF_S = 1.1\, l^{-0.89} \ (n = 22, r^2 = 0.82) \qquad \text{Eq 4.2}$$

The above length exponents were not different (p = 0.64) between species and the 95% confidence intervals (CIs) for the slopes each bracketed a slope of -1.0 (Table 4.1) as predicted (Hill 1950; Sato et al., 2007, 2009, 2010).

The species-specific relations could not be combined for phylogenetic analyses (Sato et al., 2007, 2009, 2010) because average *TBF* and length among the sturgeon were each greater than among the saithe (Student's t-test, p < 0.05) and thus the difference between their respective proportionality constants. When *TBF* estimates

and lengths were scaled by the species-specific average *TBF* and average length, the *TBF* for the combined species was again a strong function of l (Table 4.1, Figure 4.3);

$$TBF = 0.94\, l^{-1.0} \quad (n = 40,\ r^2 = 0.73) \qquad \text{Eq 4.3}$$

Table 4.1 Summary of allometric relations among swimming parameters based on dominant tail beat frequency (*TBF*, Hz), estimated swimming speed (u, ms^{-1}), and fork length (l, m) in two fish species. Subscript, *sd*, indicates standardized by the species-specific average, where the 95% confidence interval (CI), coefficient of determination (r^2) and sample size (n) are provided. [a]Predicted value based on Hill (1950); *from log-log ordinary least square slope, using u and *TBF* model from †Videler and Hess (1984); and ‡Long (1995)

Species	Relation	Exponent (β)*(±SE)	95% CI for β	Pred. β [a]	r^2	n
P. virens	$TBF \ \alpha \ l^{\beta}$	-0.99 (±0.15)	-1.3; -0.68	-1	0.73	18
	$u \ \alpha \ l^{\beta}$	0.12† (±0.13)	-0.16; 0.40	0	0.01	18
A. brevirostrum	$TBF \ \alpha \ l^{\beta}$	-0.89 (±0.094)	-1.09; -0.69	-1	0.82	22
	$u \ \alpha \ l^{\beta}$	0.12‡ (±0.092)	-0.067; 0.32	0	0.01	22
Combined	$TBF_{sd} \ \alpha \ l^{\beta}_{sd}$	-1.0 (±0.097)	-1.2; -0.80	-1	0.73	40
	$u_{sd} \ \alpha \ l^{\beta}_{sd}$	0.12†‡ (±0.086)	-0.054; 0.29	0	0.05	40

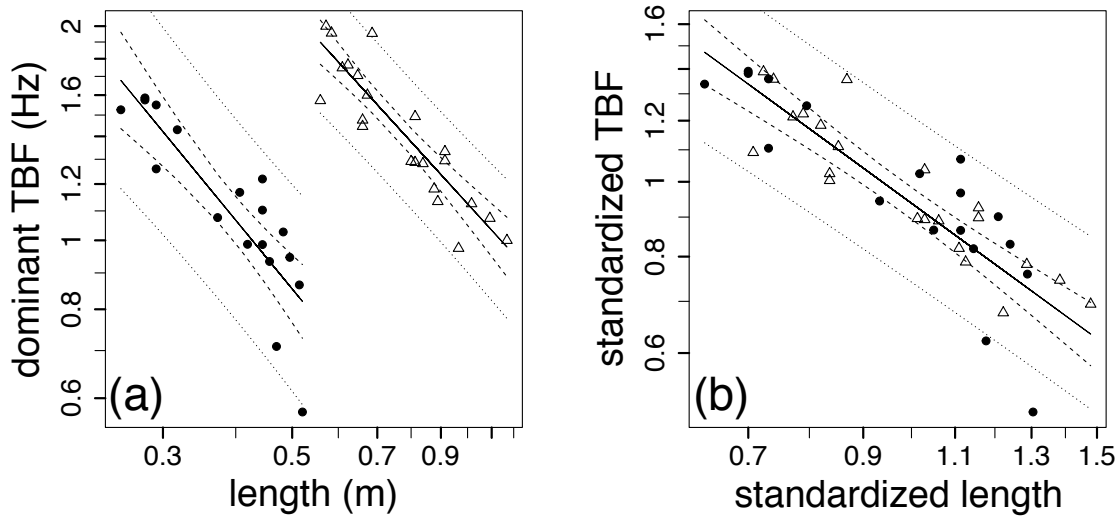

Figure 4.3 Log-log relations between (a) dominant tail beat frequency (*TBF*, Hz) and length (m) and (b) standardized *TBF* in relation to standardized length for saithe (solid circles, n=18) and sturgeon (open triangles, n=22). Weighted ordinary least square regressions (solid line) are bracketed by the 95% confidence intervals (CIs) around the regression (dashed line) and the unweighted 95% CIs around the predictions (dotted lines).

***TBF* as a function of mass** - Tail beat frequency was a function of mass (Figure 4.4, Table 4.2) for saithe $TBF_P = 0.99m^{-0.29}$ (n = 18, r^2 = 0.63) and for sturgeon $TBF_S = 2.22m^{-0.29}$ (n = 22, r^2 = 0.82). The model exponents were not different (p = 0.99). The 95% confidence intervals for the species-specific slopes bracket a slope of -1/3 as predicted (Table 4.2). When beat frequencies and mass were scaled by the species-specific average *TBF* and average mass, the best-fit model for mass (Figure 4.4, Table 4.2) was $TBF = 0.90m^{-0.29}$ (n = 40, r^2 = 0.63).

Table 4.2 Summary of allometric relations among swimming parameters based on dominant tail beat frequency (*TBF*, Hz), estimated swimming speed (u, ms^{-1}), and body mass (m, kg) in two fish species. Subscript, *sd*, indicates standardized by the species-specific average, where the 95% confidence interval (CI), coefficient of determination (r^2) and sample size (n) are provided. [a]Predicted value based on Hill (1950); *from log-log ordinary least square slope, using u and *TBF* model from †Videler and Hess (1984); and ‡Long (1995)

Species	Relation	Exponent (β)*(±SE)	95% CI for β	Pred. β^a	r^2	n
P. virens	$TBF \propto m^{\beta}$	-0.29 (±0.055)	-0.41; -0.17	$-1/3^a$ -0.28^b	0.63	18
	$u^{\dagger} \propto m^{\beta}$	$0.052^{\dagger}$ (±0.040)	-0.034; 0.14	0^a 0.05^b	0.11	18
A. brevirostrum	$TBF \propto m^{\beta}$	-0.29 (±0.030)	-0.35; -0.22	$-1/3^a$ -0.28^b	0.82	22
	$u^{\ddagger} \propto m^{\beta}$	$0.039^{\ddagger}$ (±0.029)	-0.021; 0.10	0^a 0.05^b	0.01	22
Combined	$TBF_{sd} \propto m^{\beta}{}_{sd}$	-0.29 (±0.057)	-0.36; -0.22	$-1/3^a$ -0.28^b	0.63	40
	$u_{sd} \propto m^{\beta}{}_{sd}$	$0.052^{\dagger\ddagger}$ (±0.026)	-0.001; 0.11	0^a 0.05^b	0.11	40

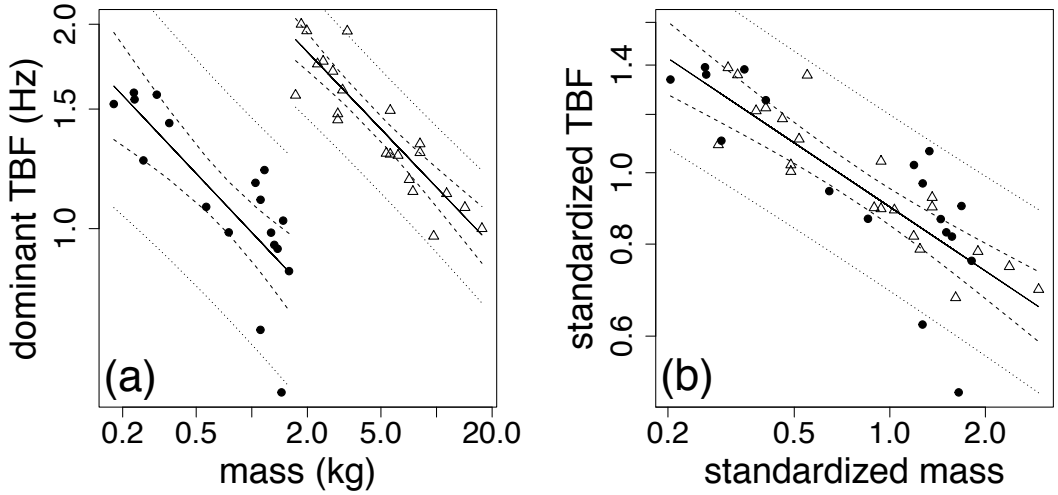

Figure 4.4 Log-log relations between (a) dominant tail beat frequency (*TBF*, Hz) and mass (kg) and (b) standardized *TBF* in relation to standardized mass for saithe (solid circles, n=18) and sturgeon (open triangles, n=22). Weighted ordinary least square regressions (solid line) are bracketed by the 95% confidence (dashed line) and prediction (dotted lines) intervals.

4.4.2 Swimming Speed

Speed as a function of length - The derived absolute swimming speed estimates, which were estimated from the literature (Videler and Hess, 1984; Long, 1995), were normally distributed (Anderson Darling, $p > 0.5$, Figure 4.5) with average speeds of 0.41 ms^{-1} ± 0.05 for saithe, and 0.15 ms^{-1}± 0.01 for sturgeon. The predictor variable, l, was log transformed to stabilize the variance. Within species, average swimming speed was independent of l ($p > 0.01$, Table 4.1, Figure 4.5). While the length exponents for each species were not different (Table 4.1), the proportionality constants were (Figure 4.5) again preventing inter-species comparison. When standardizing the response and predictor variables by the species-specific averages, the standardized average swimming estimates were independent of l (weighted ordinary least squares, $p = 0.17$, Table 4.1, Figure 4.5)

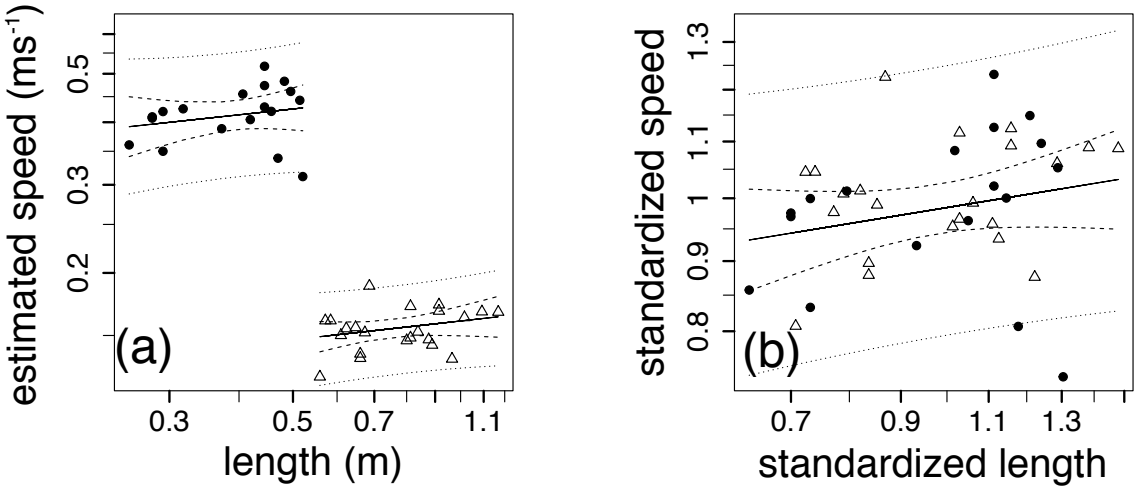

Figure 4.5 Log-log relations between (a) swimming speed and length and (b) standardized swimming speed and standardized length for saithe (solid circles, n=18) and sturgeon (open triangles, n=22) where weighted ordinary least square regressions (solid line) are bracketed by the 95% confidence intervals (CI) around the regression (dashed lines) and unweighted 95% CI around the predictions (dotted lines).

Speed as a function of mass - Within species, average swimming speed was independent of m (p > 0.05, Table 4.2, Figure 4.6) However, when speed and mass were standardized by the species-specific averages, the relationship was marginally significant (weighted ordinary least square regression, p < 0.03, Table 4.2, Figure 4.6).

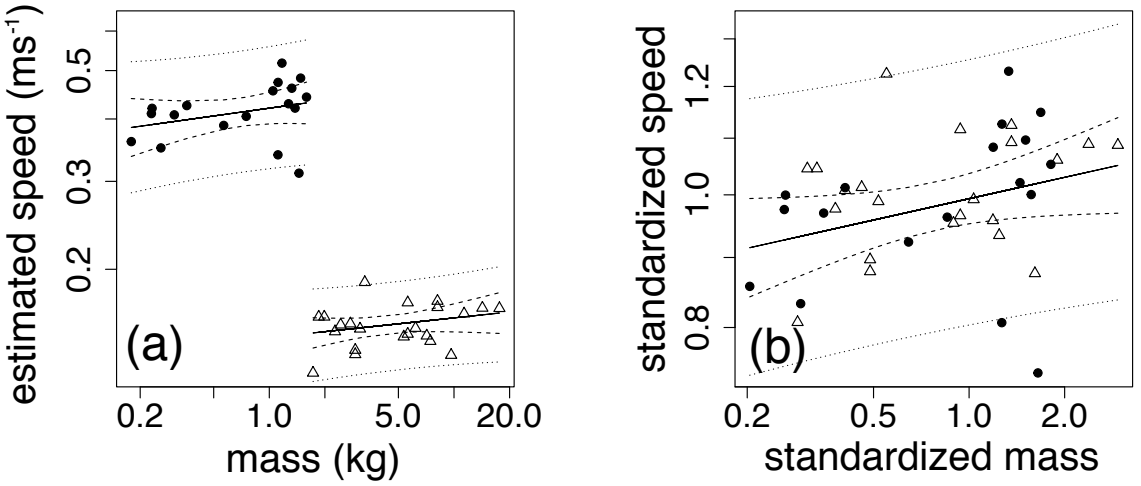

Figure 4.6 Log-log relations between (a) swimming speed (ms^{-1}) and mass (kg) and (b) standardized swimming speed and standardized mass for saithe (solid circles, n=18) and sturgeon (open triangles, n=22) where weighted ordinary least square regressions (solid line) are bracketed by the 95% confidence intervals (CI) around the regression (dashed lines) and unweighted 95% CI around the predictions (dotted lines).

4.4.3 Prediction Of Length

Given Eq 4.1 and Eq 4.2 above, it was not surprising that, from a prediction perspective, length was a function of dominant *TBF* (Figure 4.7, Table 4.3) where l = 0.47 $TBF^{-0.74}$ (r^2 = 0.73), and also for sturgeon (Figure 4.7, Table 4.3) where l = 1.1 $TBF^{-0.91}$ (r^2 = 0.81). The species-specific exponents were different (p = 0.003) and the exponent for sturgeon was not different from -1 (p = 0.4), and for saithe it was marginally different from -1 (p = 0.03). Figure 4.7 illustrates the uncertainty in size predictions for each species based on the maximum sizes (~1.2 m) typically observed in nature (Dadswell, 1979; Cargnelli et al., 1999). For each species, the 95% prediction uncertainty was expressed as $P_U = t_{0.975,n-2}\, SE_{lp}/l_p$, where l_p is the model predicted size and *SE* the associated standard error. Due to the fish lengths available for the study, the greatest confidence for prediction was at intermediate sizes (> 0.2

and < 0.6 m for saithe and > 0.4 m for sturgeon). The least uncertainty for saithe was at 0.4 m (~25%) and for the sturgeon at 0.7 m (~18%), while the largest uncertainty for saithe was at 1.2 m (~36%) and for sturgeon at 0.2 m (~30%). For each species *m* was also related to dominant *TBF*. For saithe, mass was proportional to $TBF^{-2.2}$, for sturgeon to $TBF^{-2.9}$ (Table 4.3). The exponents were not statistically different (p = 0.27) between species. When *TBF* estimates collected from a comparable sturgeon species in the wild (Chinese sturgeon, *Acipenser sinensis*, Watanabe et al., 2008) are used as model input (1.08 Hz, 0.77 Hz, 0.91 Hz) length predictions (1.03 m, 1.39 m, 1.19 m) are between 4 – 14 % when compared to the measured length (0.95 m, 1.22 m, 1.15 m, respectively), which provides more confidence in my results.

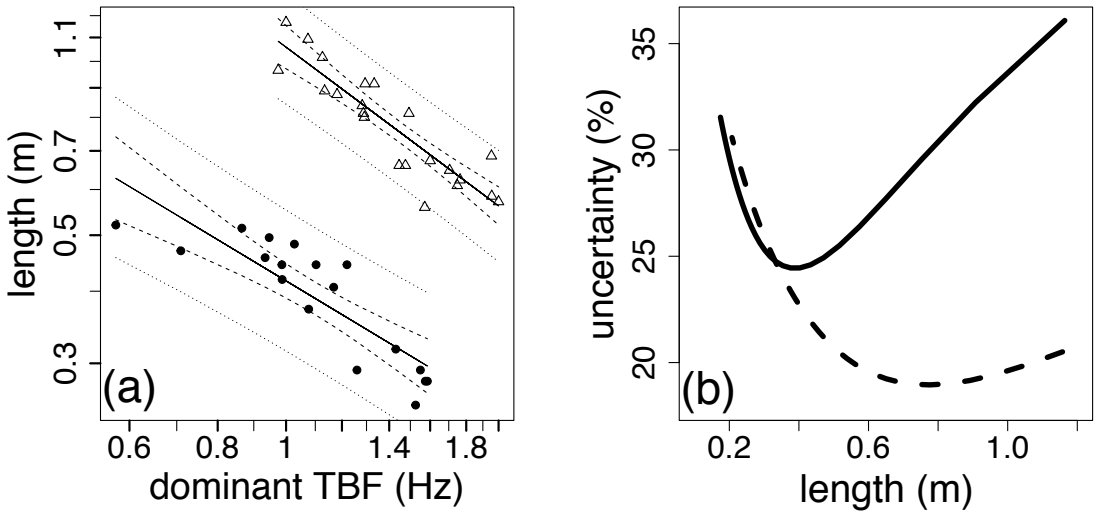

Figure 4.7 (a) Log-log relations between dominant tail beat frequency (*TBF*, Hz) as predictor and length (m) for saithe (solid circles, n=18) and sturgeon (open triangles, n=22) showing ordinary least square regressions (solid line) bracketed by the 95% confidence intervals around the regression (dashed lines) and predictions (dotted lines), and (b) prediction uncertainties, P_U as a function of length (m) for saithe (sold line) and sturgeon (dashed line) expressed as $P_U = 100\ t_{0.975,n-2}\ SE_{lp}/l_p$ where lp is the model prediction and SE_{lp} is the standard error for the prediction.

Table 4.3 Summary of regression models for predicting fork length (l, m) as a function of dominant tail beat frequency (*TBF*, Hz) for saithe (*P. virens*) and sturgeon (*A. brevirostrum*) where the proportionality constant with the 95% confidence interval (CI), exponent (β) with standard error (SE) and 95% CI, coefficient of determination (r^2) and sample size (n) are provided. * from log-log ordinary least square intercept and slope

Species	Relation	Proportionality constant, b* [95% CI]	Exponent, β* (±SE) [95% CI]	r^2	n
P. virens	$l \ \alpha \ b\ TBF^{\beta}$	0.47 [0.39; 0.45]	-0.74 (±0.11) [-0.97; -0.50]	0.73	18
	$m \ \alpha \ b\ TBF^{\beta}$	0.85 [0.66; 1.1]	-2.2 (±0.42) [-3.0; -1.3]	0.63	18
A. brevirostrum	$l \ \alpha \ b\ TBF^{\beta}$	1.1 [0.97; 1.1]	-0.91 (±0.10) [-1.1; -0.70]	0.81	22
	$m \ \alpha \ b\ TBF^{\beta}$	13 [9.8; 16]	-2.9 (±0.31) [-3.5; -2.2]	0.81	22

4.4.4 Maximum Tail Beat Frequency

Maximum *TBF* was estimated based on a relationship obtained from observations provided in the literature (Bainbridge, 1958, Videler and Hess, 1984) (Table 4.4, Figure 4.8). Maximum *TBF*, TBF_{max} was a function of length (n = 44, r^2 = 0.41, Figure 4.8) and dominant *TBF* was a predictor of TBF_{max} for saithe (n = 18, r^2 = 0.79, Table 4.4, Figure 4.8) and sturgeon (n = 22, r^2 = 0.78) respectively, with different relationships (slope and intercept) for each species.

Table 4.4 Summary of log-log regression models for predicting tail beat frequency (*TBF*, Hz) as a function of maximum tail beat frequency (TBF_{max}) for saithe (*P. virens*) and sturgeon (*A. brevirostrum*), and fork length (l, m) a function of TBF_{max} for various fish species†, where the proportionality constant/intercept and exponent/slope (β) with standard errors (SE) and 95% confidence intervals (CI), coefficient of determination (r^2) and sample size (n) are provided. †data from Bainbridge, 1958; Videler and Hess, 1984 * from log-log ordinary least square intercept and slope

Species	Relation	Intercept or proportionality constant, b* (±SE) [95% CI]	Slope or exponent, β* (±SE) [95% CI]	r^2	n
P. virens	$TBF \ \alpha \ b + \beta\ TBF_{max}$	3.9 (±0.38) [3.0; 4.7]	2.6 (±0.32) [1.9; 3.3]	0.79	18
A. brevirostrum	$TBF \ \alpha \ b + \beta\ TBF_{max}$	2.6 (±0.26) [2.1; 3.2]	1.5 (±0.18) [1.1; 1.9]	0.78	22
Various species†	$l \ \alpha \ b\ TBF^{\beta}{}_{max}$	4.18 (±0.21) [2.76; 6.36]	-0.51 (± 0.09) [-0.71; -0.32]	0.41	44

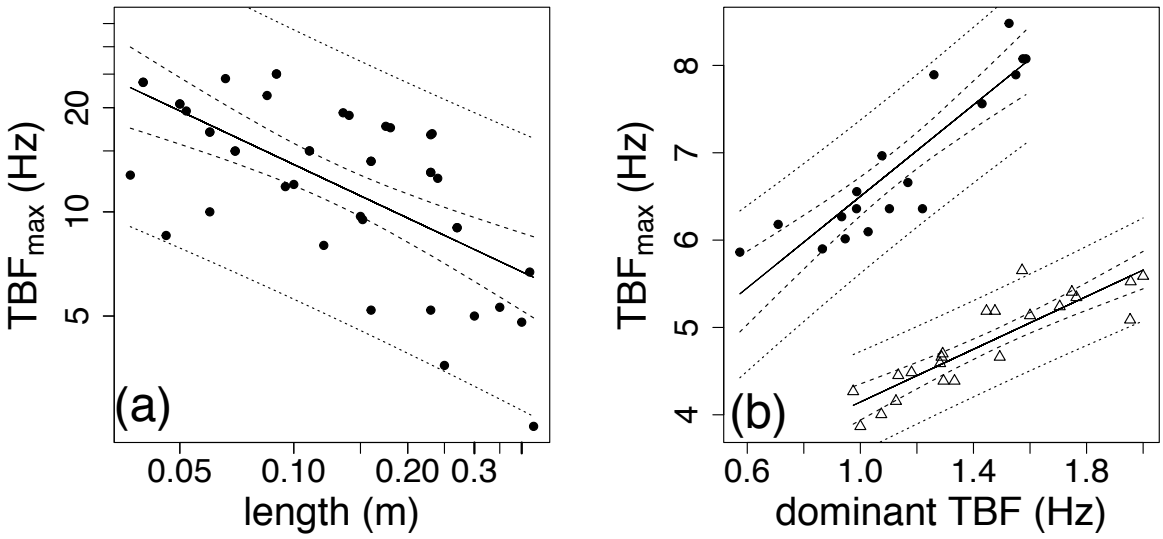

Figure 4.8 (a) Log-log relation between maximum tail beat frequency (*TBF*, Hz) in relation to length based on 11 species (n = 44) from the literature (Bainbridge, 1958; Videler and Hess, 1984) and (b) linear relation between maximum tail beat frequency (TBF_{max}, Hz) and dominant *TBF* (Hz) for saithe (filled circles, n=18) and sturgeon (open triangles, n=22) with ordinary least square regressions (solid line) bracketed by 95% confidence intervals around the regression (dashed line) and the predictions (dotted lines).

4.5 Discussion

It has been historically difficult to examine allometric scaling relationships between swimming speed, tail beat frequency and size in fish beyond the theoretical (Hill, 1950; Bainbridge, 1961; Gray, 1968; Webb, 1976a), largely due to the difficulty of obtaining data on free-swimming fish across a suitable size range (Robinson and Motta, 2002). Here, I quantified and validated theoretical allometric scaling relationships for two different free-swimming fish species of relatively large but different size ranges by using accelerometer tags. Using the acceleration records from the free-swimming saithe and sturgeon, I developed a signal-processing algorithm that extracts, from a non-stationary signal, the dominant tail beat frequency (*TBF*) for steady swimming and demonstrated that *TBF* is a function of size for each species; scaling with length^{-1} and mass$^{-0.29}$. These exponents are not statistically different from Hill's isometric prediction that *TBF* scales with length^{-1} and mass$^{-1/3}$ (Hill, 1950) and results from the species-specific independence between average swimming speed and each of length and mass (Sato et al., 2007). These

results subsequently allowed me to demonstrate that dominant *TBF* can be used to predict species-specific length-at-age with prediction uncertainties as low as 18%, thus providing a novel method for estimating length-at-age in the wild.

Similar to my results, Sato et al. (2007) provided a unifying scaling model that predicts that similarly sized animals, among many large and widely disparate species (0.5 to 1600 kg), should display the same dominant stroke cycle frequency at a given mass (or length). In contrast, I found species-specific differences manifested as different model proportionality constants, despite the presumed geometric similarities. Such differences may be masked in Sato et al. (2007) by the large species-size range they analyzed and when their data were reanalyzed from a species-specific perspective, the differences emerged. My results above predict that the dominant *TBF* for sturgeon is twice that of saithe at the same size (and the observed was as much as three fold higher), and I estimated that the swimming speed for saithe, while necessarily taken with caution, was lower in sturgeon of the same size. Since my results also indicate that swimming speed and size are independent for each species (Sato et al., 2007), this difference may be due to differences in pressure load (Gazzola et al., 2014). Morphological limitations, such as high drag resulting from body form and external bony scutes, exacerbated by low thrust from a heterocercal tail (Webb, 1986), may further account for reduced swimming 'efficiency' (Wu, 1971) among sturgeon relative to similarly sized saithe. Differences between interspecific and intraspecific scaling are to be expected given that intraspecific scaling may not accommodate ontogenetic constraints. Interspecific scaling coefficients can also be expected to differ (e.g., scaling across mammalian leg bones versus scaling within bovine leg bones, (Christiansen, 1999). Such complications arise from fitting a bivariate relation to a multivariate problem (Taylor and Thomas, 2014).

A theoretical basis for the observed species-specific differences may be found by extending the theory provided by Gazzola et al. (2014). At very high Reynolds numbers ($Re > 10^3$ to 10^4, as for all fish studied here), and balancing thrust and skin drag for elongated swimming bodies, u is proportional to $TBF\ A_{TBF}$ (Gazzola et al., 2014), where A_{TBF} is the tail beat amplitude. For fish of a given size, when swimming

at high speeds, they maintain an approximately constant length-specific tail beat amplitude (Bainbridge, 1958; Gazzola et al., 2014) which can be defined as $A_{TBF} = al$, where a is some species-specific coefficient; e.g., a = 0.18 for saithe (Gazzola et al., 2014). Given that $u \propto TBF\ a\ l$, and if $TBF \propto l^{-1}$ as indicated by my observations and those of others, then u must be constant. Similarly, at a given speed u, TBF relates to length as $TBF \propto (al)^{-1}$ and this not only provides a mechanical justification for the observed scaling relationship, it also offers an explanation for the differences in the species-specific models; i.e., the species-specific coefficient, a (that scales the constant tail beat amplitude with body length), affects the constant in the scaling relationship accordingly. Until it can be demonstrated that length-specific stroke amplitude (A_{TBF}) is species independent, it is difficult to validate an interspecific relationship. Not only does this advance the scaling between TBF and length, it implies that for a given species, fish swimming speed is independent of length.

Hill's isometric model (1950) is assumed to hold only for efficient movement during "natural swimming behaviour of free-ranging animals in contexts where they are expected to swim efficiently" (Sato et al., 2007). While my studies did not allow the observation of movements unequivocally known to be associated with the above contexts, the predicted relationship was validated. This was achieved by estimating the dominant TBF from the acceleration record using a novel algorithm and discarding unsteady swimming movements. Additionally, I confirmed that for the longest 10% of the continuous steady swimming segments used in the analysis, swimming could be shown to be efficient by calculating the Strouhal number (St), a commonly used index of efficient swimming, $St = A_{TBF}\ TBF/u$, where A_{TBF} = tail beat amplitude and u = swimming speed (Sato et al., 2007; Gazzola et al., 2014). For example, St for saithe was calculated using the estimated swimming speed (Videler and Hess, 1984) with a tail beat amplitude of 0.18 l (Gazzola et al., 2014). For the stable TBF segments the St estimates were between 0.22 and 0.23; close to that expected for saithe during efficient swimming (Kohannim and Iwasaki, 2014). Additionally, it can be shown that dominant TBF is linearly proportional to maximum TBF (Figure 4.8, Table 4.4), which further validates its use as a proxy for efficient swimming.

My results are coherent with the Sato et al. (2007) cross-species model and consistent with the prediction by Hill who equated the work a muscle produced (α *m*) at a given frequency (*TBF*) with the mechanical power required to counteract drag. However, my results are in stark contrast to the theoretical suggestions presented by Bainbridge (1958) that $u \alpha l^{0.39}$ for high Reynolds numbers, by Gray (1968) that $TBF \alpha l^{-0.44}$, and by and Wu (1971) that $TBF \alpha l^{-0.88}$. If swimming speed is proportional to length, with some exponent *c,* then *TBF* scales with l^{c-1} as predicted by Webb (1975). For example, at maximum sustained tail beat frequency, TBF_{max} is proportional to $l^{-0.51}$. Given $u \alpha TBF a l$, this occurs if $u_{MS} \alpha l^{0.49}$, which is close to the predictions by Webb (Pedley, 1977; Peters, 1983). This suggests that the above theoretical models based on muscle power output are insufficient in explaining the underlying mechanism(s) for fish. The most likely reason is the discrepancy between (theoretical) swimming speeds and the swimming modes considered (e.g., critical, maximum, sustained, etc.) and how poorly those modes correspond to the observed dominant swimming mode, which may in fact be the 'efficient' or preferred swimming mode adapted to by a given fish/species. This may help explain why my estimates of average *TBF* are much lower than those predicted by Videler and Hess (1984) and Videler and Wardle (1991); and closer to estimates made for comparable species in the wild, such as Chinese sturgeon (*Acipenser sinensis*, Watanabe et al., 2008), trout (*Oncorhynchus mykiss*, Kawabe et al., 2003b), and sockeye salmon (*Oncorhynchus nerka,* Stasko and Horrall, 1976). Thus, I suggest that "efficient" swimming in fish be defined by the free-swimming fish itself; i.e., the characteristic swimming associated with the steady and dominant *TBF*. Such a definition is testable and it may help advance the science of fishing swimming that has been undergoing refinement for more than six decades.

Calculation of Swimming Speed

Since it is difficult to obtain measurements of swimming speed *in situ*, I used the species-specific prediction models from the literature to estimate swimming speed. However, different models in the literature that scale *TBF* with swimming speed appear incommensurable. For example, while using similar sized white sturgeon (*Acipenser transmontanus*), Long (1995) predicts swimming speeds that are 3 to 4 fold lower than those provided by Cheong et al. (2006). Similarly for saithe; Videler

and Hess (1984) predict almost twice the swimming speed reported by Steinhausen et al. (2005). Therefore, absolute values of estimated swimming speeds, including the estimates I provide here for saithe and sturgeon, must be considered cautiously. Nevertheless, the independence of body length with swimming speed at the dominant *TBF* holds for all speed and *TBF* prediction models found in the literature. I note that for saithe, I used the Videler and Hess model because the observations corresponded well to the theoretical model proposed by Kohannim and Iwasaki (2014) and Lighthill (1960, 1971).

Implications for measuring size-at-age in the wild

I have demonstrated that it is possible to predict size from dominant *TBF* by using species-specific models based on accelerometer tags mounted on free-swimming saithe and shortnose sturgeon of various sizes. While the confidence intervals for each of the models are reasonable, the large prediction intervals may not yet provide a suitable alternative to the conventional methods of estimating size-at-age to infer growth rate. I think that the model coefficients of determination and the prediction intervals, and therefore length prediction certainty, should improve if such studies were repeated over longer periods within more natural environments using a greater range of lengths. Based on the theoretical prediction as outlined above, and demonstrated by empirical data for sturgeon, this scaling exponent is predicted to be -1 since $TBF \propto (al)^{-1}$ and therefore $l \propto (a\ TBF)^{-1}$. In summary, for a given species, size is directly and inversely related to the dominant tail beat frequency, thus allowing the estimation of size from the dominant *TBF* in the lab or in the wild, as shown here from an empirical and theoretical perspective.

Differences that fish experience in the lab vs. field environment (currents, schooling, behaviour) may certainly affect the observations and associated prediction model. Some of my observations may allow me to predict such effects on the prediction model. The experimental set-up leads me to conclude that the effect of currents is expected to be minimal, since for sturgeon, which were exposed to variable currents, the scaling relationship did not seem to be affected. This is not surprising as for most, but not all fish in the ocean, lakes and large rivers the current eddy-field is much larger than the fish. Furthermore, when adding data on *TBF* collected in the

field in a similar species (*Acipenser sinensis*, Watanabe et al., 2008), the prediction model holds and the *TBF* observations support my model. Given the *TBF* observations, my model predicts size-at-time to an accuracy of 4 – 14% compared to their measurements, which certainly suggests confidence in my model. The effect of schooling may have an effect on steady swimming. For example, saithe are a schooling species and the data were collected while fish were spending some of their time swimming in schools or solitary. This difference in swimming behaviour was not apparent in the scaling relationship. Sturgeon were randomly assigned to a swim tank where they were allowed to swim solitary or with conspecifics. Again, when data were pooled by experiment type (solitary vs. communal) no trend appeared. I do not believe that behavioural differences in the wild will have a significant effect on the scaling relationship since, e.g., feeding behaviour and other movement-related behaviour (e.g., spawning, escape etc.) is often exhibited by non-steady and burst acceleration swimming (e.g., Domenici and Blake, 1997). Since the proposed algorithm removes such swimming bouts prior to estimating the dominant tail beat frequency, such behavioural differences should not affect the result.

For the model predictions to prove useful in measuring size-at-time (and eventually growth) a study similar to mine needs to be conducted using fish as they grow to unambiguously demonstrate that within individual variation over time is less than within and among size-class variations. Such a study would determine the utility of the model and using accelerometry to estimate size-at-time (and growth) in the wild as a reasonable alternative to conventional methods such as post-mortem morphometrics that include otolith microstructures. While it is generally accepted that otolith growth is a "running average" of somatic growth (Campana and Neilson, 1985) there are uncertainties in the accuracy of back-calculations of fish size or growth rate from otolith size due to reader bias (Faust et al., 2013; Sardenne et al., 2015) or bias introduced by the way the otolith is cut (Panfili and Ximenes, 1992; Francis and Campana, 2004).

The use of more replicates among size-classes and across a larger size range will likely improve the prediction interval and explained variance by reducing within-class variation that is likely related to individual variability in the short-term

response to tagging-induced stress. Adding additional parameters that scale with length, and (or) by combining the knowledge of the initial size at fish capture along with the theoretical characteristics of growth potential, could further improve the model prediction of size over time by using the prediction from the scaling model in a state-space model. The indirect observations of length from the scaling relationship provides the final element to be combined with an initial measurement of fish length (when tagged) and a prediction from fish growth theory, which may even include additional predictors (such as temperature, Neuheimer and Taggart, 2007) to construct a state space model of fish length at time. Such a model may provide a more reliable time series of length-at-age. For example, an additional parameter could be the maximum velocity (or maximum tail beat frequency) that scales with length as shown in Table 4.4 and Figure 4.8 using 11 species drawn from the literature (Bainbridge, 1958; Videler and Hess, 1984) and maximum *TBF* that is proportional to $l^{-0.51}$. However, it is difficult to observe maximum *TBF* in nature and likely more difficult to determine when maximum *TBF* is reached. Furthermore, when such a model is used to calculate maximum *TBF* for the saithe and the sturgeon, maximum *TBF* was linearly related to dominant *TBF* for saithe with a slope of 2.6 and for sturgeon with a slope of 1.5 (Table 4.4). Therefore, adding this parameter to the scaling model may prove redundant.

Assuming these prediction models can be further validated in nature, and that micro-processing technology of archival accelerometer sensors can employ an *a priori* determined algorithm that continuously (or duty-cycled) calculates size-at-time, then *in situ* estimation of size-at-time and growth rate could be achieved. The algorithm that relates dominant *TBF* to size has the potential of providing a powerful tool in estimating size-at-time in the wild; something yet to be achieved. Since this algorithm is based on sampling a known log-normal *TBF* distribution, which would require ~30 measurements for reliable estimation (Central Limit Theorem), and the dominant *TBF*s among comparable species can be sampled at a low frequency (~ 15Hz), then the accelerometer-tag power consumption would be comparably low.

Chapter 5 MEASURING ABNORMAL ROTATIONAL MOVEMENTS IN FREE-SWIMMING FISH WITH ACCELEROMETERS: IMPLICATIONS FOR QUANTIFYING TAG- AND PARASITE-LOAD

The majority of this chapter is *in press* as:

Broell, F., Burnell, C. and Taggart, C. T. (2016). Measuring abnormal rotational movements in free-swimming fish with accelerometers: implications for quantifying tag- and parasite-load. *J. Exp. Biol.* doi:10.1242/jeb.133033

5.1 Introduction

Quantifying the spatial-temporal distribution of free-ranging animals in the marine environment is problematic due to the paucity of direct observations (Sakamoto et al., 2009; Preston et al., 2010). This can be partially overcome by using a variety of tags that range from conventional tags (e.g., Petersen or Floy tags; Petersen, 1896, McFarlane et al., 1999) to more advanced electronic tags (Cooke et al., 2004; Bograd et al., 2010). Animal-borne archival tags can provide a means to monitor movements of aquatic animals and their environment through *in situ* measurements such as acceleration, temperature and depth. Such data can be used to indirectly quantify variation in behaviour, energetics, and physiology, and to infer how animals interact with each other and their environment (Cooke et al., 2004) for habitat modeling and conservation management (Bograd et al., 2010; Whitney et al., 2010). For example, micro-storage accelerometer tags allow for remote measurements of fine-scale movements and behaviour among free-swimming fish in time and space in controlled mesocosm environments (Chapter 3; Chapter 4; Gleiss et al., 2010; Noda et al., 2014; Wright et al., 2014), as well as in the wild (Kawabe et al., 2003a; Kawabe et al., 2003b; Tsuda et al., 2006; Whitney et al., 2010; Carroll et al., 2014).

The use of accelerometer tags in bio-logging studies has increased due to their commercial availability, data-storage capabilities, and versatility of attachment (Ropert-Coudert and Wilson, 2005; Rutz and Hays, 2009). As with any tagging, external or internal, tag attachments can alter the natural behaviour and physiology of the tagged fish (Ross and McCormick, 1981; Greenstreet and Morgan, 1989; Barrowman and Meyers, 1996; Björnsson et al., 2011; Cooke et al., 2012, Jones et al., 2013). *In situ* capture-recapture or tag-recovery studies using conventional or electronic tags are typically based on the assumption that there is no significant effect of the tag on the fish and that tags are not lost or shed through erratic swimming (Bridger and Booth, 2003). If invalid, the assumption can lead to compromised estimates of the metrics used to estimate population size and distribution as well as activity patterns and energy budgets (Bridger and Booth, 2003; Drenner et al., 2012). This is especially problematic in bio-logging studies where data from a few (typically <10) individuals are collected to make inferences about entire populations (Cooke et al., 2004).

In fisheries applications, the general criterion used to minimize potentially adverse tag effects is the "2% rule" that assumes tag effects are negligible if tag weight is < 2% the body weight of the tagged animal (Winter, 1996), regardless of attachment method. However, tag weight is not the only factor influencing tag impact (Jepsen et al., 2015), and percent weight is regarded by many to be a questionable metric (Brown et al., 2006; Jepsen et al., 2015) because it assumes a 1:1 scaling effect of tag and animal, which is invalid. For some aquatic animals tag weight may have little or no effect, especially in organisms with bladders or lungs that can adjust their buoyancy (Jones et al., 2013). Other factors influencing tag effect include the tag dimensions, volume, buoyancy and attachment position, all of which significantly affect drag (Hoerner, 1965; Jones et al., 2013; Jepsen et al., 2015). Therefore, these variables require consideration to ensure that fish behaviour and movement is unaffected by the tag and attachment designs (Jepsen et al., 2015).

As a behavioural response to tag burden, tag shedding has been reported extensively for various fish species, however, it is rarely quantified in relation to changes in natural behaviour and associated energy expenditure (Barrowman and Meyers, 1996;

Björnsson et al., 2011, Musyl et al., 2011). While direct observations of tag loss and associated swimming behaviour are limited, shortnose sturgeon (*Acipenser brevirostrum*), rainbow trout (*Oncorhynchus mykiss*), and salema (*Sarpa salpa*) fitted with transmitters attached below the dorsal fin have been observed to scour vigorously against tank enclosures leading to external tag loss and skin abrasions (Mellas and Haynes, 1985; Collins et al., 2002; Jadot, 2003). This distinctive and repeated scouring-associated rotational movement (flashing, scraping) in the vertical-lateral plane has also been observed in Atlantic cod (*Gadus morhua*) in order to dislodge parasites (Dr. Jeffrey A. Hutchings, Department of Biology, Dalhousie University, Canada, *personal communication*).

To investigate the effect of external accelerometer tag burden on free swimming Atlantic cod held in a large mesocosm, I quantified the effect of different tag loads (mass) on the swimming behaviour associated with tag shedding, i.e., scouring. I first collected data from a size range of free-swimming Atlantic Cod (*Gadus morhua*) tagged with two different sizes of accelerometer tags. I then developed an automated algorithm to extract the scouring-associated rotational movement from the acceleration time series. I used the extracted scouring events to quantify the amount of time individuals spent scouring, a proxy for energy expenditure and fish size in relation to tag load and time of day, where for the latter there is limited knowledge of swimming behaviour during night-time conditions.

5.2 Materials

5.2.1 Study Animals

Atlantic Cod (n = 22) of total length (l; m) ranging from 0.47 to 0.72 m (average ± SD, 0.61 m ± 0.069) with mass (m; kg) between 0.95 and 3.4 kg (2.0 kg ± 0.66) were collected near Nova Scotia, Canada. Data on the free-swimming fish were collected in a large mesocosm (Dalhousie University) with a diameter of 15.24 m, a depth of 3.54 m at perimeter and 3.91 m at the centre, and a volume 684 m^3 held at 11 °C ± 1.5. Experiments were conducted over 6 trial-days spanning a month. Each individual fish swim trial lasted between 24 and 30 h with a recovery period of three to five days.

5.2.2 Accelerometers

I used two tri-axial accelerometer tag models (Maritime bioLoggers, Halifax, Canada): the cylindrical MBLog PT-1 (2.3 cm diameter, 5.0 cm length, 4.15 cm^2 frontal area, 18.8 g in air, hereafter referred to as the "large" tag) and the rectangular MBLog PT-2 (2.5 cm length, 1.7 cm width, 1.1 cm depth, 1.87 cm^2 frontal area, 6.1 g in air, hereafter referred to as the "small" tag) (Table 5.1). Both tags were set to record tri-axial acceleration at 50 Hz (10-bit resolution) at ± 6 g_o. Drag coefficients for the tags were determined using the characteristic shape and length ratio (Table 5.1) given high Reynolds number flow ($Re > 10^4$) (e.g., White, 1986). For both tags, the ratio between tag and body mass was < 2% (Table 5.1).

Table 5.1 Specifications for tags used in free-swimming trials of Atlantic cod with tag-specific drag coefficient (c_d), sample size (n) and tag load (% body weight).

Model	Shape	Outline dimensions (cm)	Mean weight (g)	Frontal area (cm^2)	Mean Tag load (%) (range)	c_d	n
MBLog PT-1	cylindrical	5.0 x 2.3	18.8	4.15	1.1 (0.57, 2.1)	0.85	22
MBLog PT-2	rectangular	2.5 x 1.7 x 1.1	6.1	1.87	0.42 (0.17, 1.7)	1.05	20

5.2.3 Swim Experiments

Cod were anaesthetized with MS222 (40 mg l^{-1}), measured for l and m and permanently tagged using rectangular Petersen Disc tags to which the accelerometer was attached for swim trials. The Petersen discs were attached using two nickel pins, which ensured that the discs were stable and could not rotate (see Chapter 3 for tag attachment details). Fish were randomly assigned a small or large tag (Figure 5.1) for each swim trial. Fish swam *ad libitum* with no external stimulus save a natural daylight cycle. Following each trial the accelerometer was detached and the animals recovered in a holding tank (2.0 x 2.0 m). At least 22 h of free-swimming data were collected for each individual for a total of 1200 h of data. Data from the same individual carrying the same size tag were combined resulting in n_D = 42 datasets with n_S = 20 from fish carrying small tags and n_L = 22 from fish carrying large tags.

Animal care and sampling protocol for the tagging surgery for this study was approved by Dalhousie University (Permit number 12-049) in accordance with the Canadian Council for Animal Care standards.

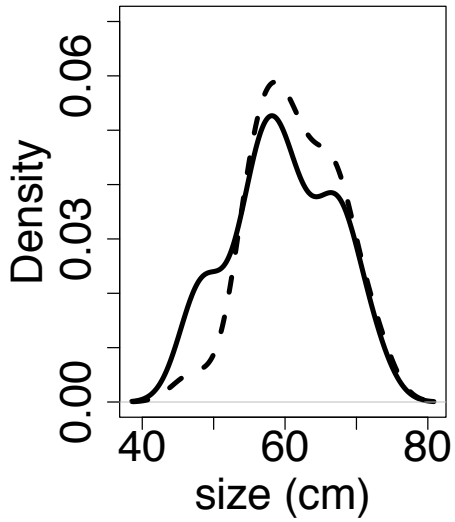

Figure 5.1 Smoothed histograms of size distribution for Atlantic cod for small tag (n_S=29, dashed line) and large tag (n_L=60, sold line)

5.3 Methods

5.3.1 Extracting Scouring Movements

Scouring movements were characterized by a change in orientation of the tag as the animal rotated on its side to scrape its body along a substrate in the water column. Such movements varied in duration ranging from short (~3 s) to long (10 – 60 s). Typically, shorter duration movements were characterized by high-acceleration while longer duration scouring was characterized by lower maximum acceleration during which fish continued to beat their tail (Figure 5.2).

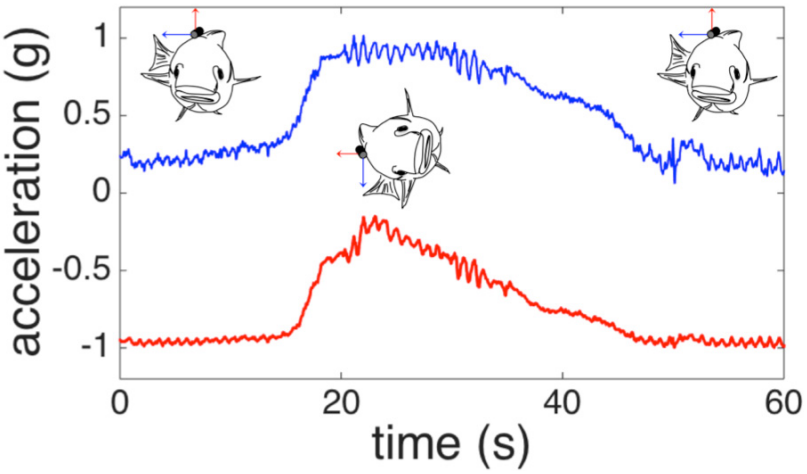

Figure 5.2 Illustration of fish movement and acceleration time series as accelerometer tag rotates during scouring. When the fish is in the upright position, gravitational acceleration is measured in the vertical axis (red). When animal turns laterally, gravitational acceleration is measured in the lateral axis (blue).

To extract such movements, I make use of the fact that gravitational acceleration (g_o) is recorded by the tag (Chapter 2), and when the fish is in its natural vertical (upright) position, gravitational acceleration is recorded in a combination of axes. When the animal rotates laterally (up to 90°), the contribution of g_o to the different axis can be used to measure rotation. For example, if most of g_o is recorded in the vertical (z) axis, during lateral rotation the contribution of g_o to the lateral (x) axis increases until all of g_o is recorded in x; corresponding to a full 90° rotation ("roll", Figure 5.2). This shift in gravitational acceleration can be used to identify scouring movements. To extract this movement, the algorithm was designed to determine the angle in the xz-plane relative to the long-term average of the mean gravity relative to the tag (Figure 5.3). If this angle exceeded the pre-set threshold θ_{Th}, a scouring event was identified. Here, scouring was defined when an animal rotated at least θ_{Th} = 45°. At the centre of the algorithm is a sliding window of length l_W, with an overlap of 5%. Within each window, the cross-over points (t_{ci}) between the static acceleration in the x and z axes (Figure 5.4) using a zero-crossing approach are established (Kedem, 1986; Stein, 2000; Chapter 4). Static acceleration was calculated applying a 2-s moving average to the time series (cf. Shepard et al., 2008a; Wright et al., 2014). Each rotation segment C_i within window W is bracketed by time $tc_{i,1}$ and $tc_{i,2}$. Within each segment, the angle between the acceleration component in the xz-plane and

reference alignment (vertical gravity), θ_{Ci} is calculated. The angle of rotation θ_R within each segment is then calculated by comparing θ_{Ci} with the initial orientation of the tag, θ_{Tag}. The largest rotation angle, $\theta_{R,max}$ is then compared with the threshold value θ_{Th}. If $\theta_{R,max}$ is larger than θ_{Th}, the segment is classified as a scouring movement (e.g., Figure 5.5). The beginning and end of the scouring event is then defined by the first and last roll angle to exceed the threshold; thereby bracketing $\theta_{R,max}$ within the segment. This algorithm allows for variable tag orientation, and sliding window size, and by adjusting the angle threshold parameter, it is also allows for an adjustment to the degree of rotation of interest. By examining the sign of the rotation angle, this algorithm also extracted the directionality of the scouring event, i.e., left or right-lateral side (Figure 5.5).

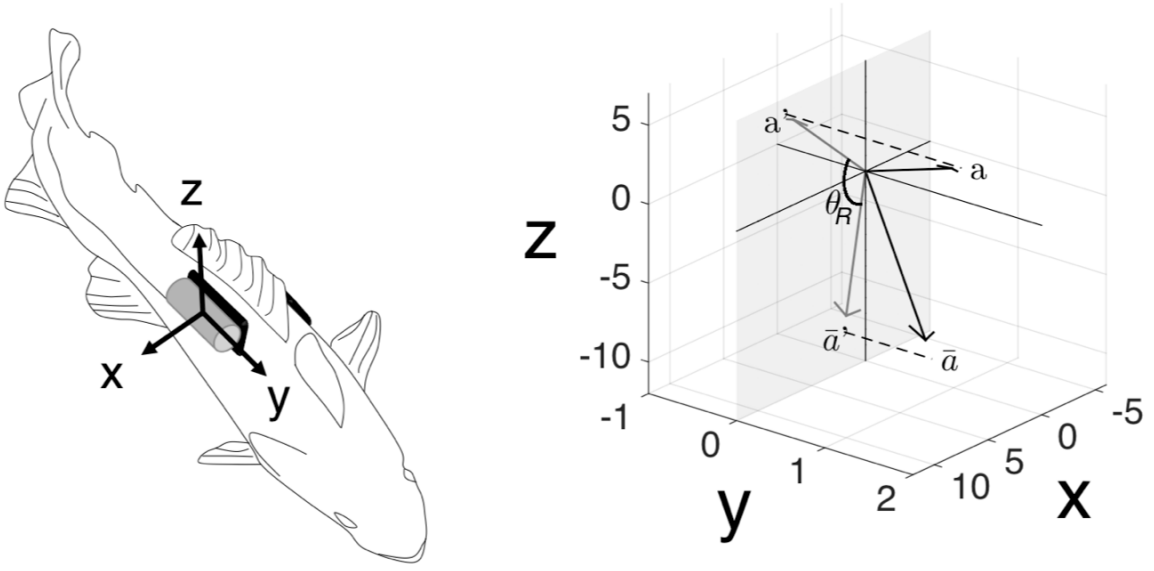

Figure 5.3 Left panel: illustration of acceleration tag as attached to Atlantic cod. Right panel: illustration of angle projection on the *xz* plane where **a** is instantaneous acceleration at time t_i, $\overline{\boldsymbol{a}}$ is the time averaged acceleration vector (i.e., direction of acceleration when fish is upright). In this case, the tag is tilted in the positive *xy*-direction relative to the fish. $\overline{\boldsymbol{a}}'$ is the projection of $\overline{\boldsymbol{a}}$ in the *xz*-plane. Here, the fish has rotated ~120° with $\boldsymbol{a}'$ the projection of **a** in the *xz*-plane. θ_R is the angle between $\boldsymbol{a}'$ and $\overline{\boldsymbol{a}}'$.

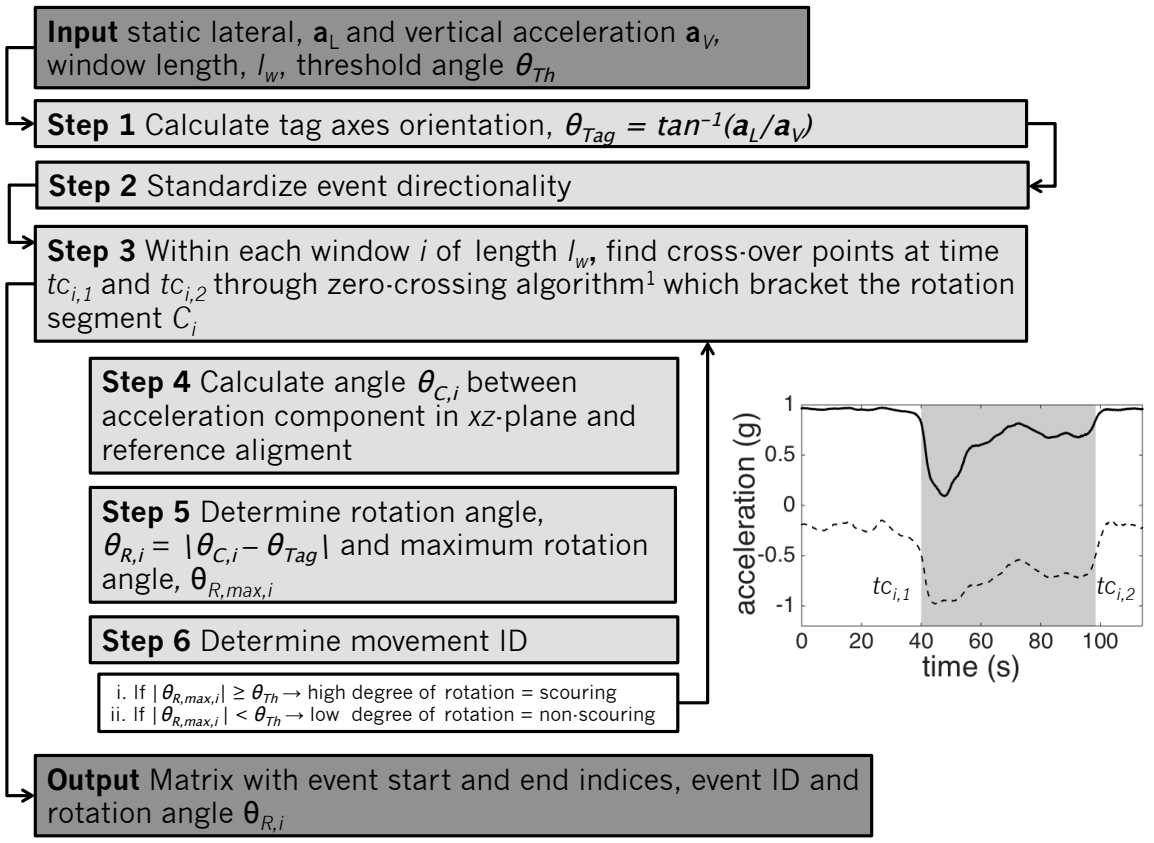

Figure 5.4 Flow chart of the extraction algorithm used to extract scouring movement based on angular rotation in the lateral-vertical (xz) plane. θ_{Tag} is the xz-plane orientation of the sensor on the fish, θ_{Th} is the threshold angle that denote vertical-lateral rotation (here $\theta_{Th} = 45°$). The rotation angles $\theta_{C,i}$ are calculated within cross-over points $tc_{i,1}$ and $tc_{i,2}$, which are found through zero-crossing algorithm (Chapter 4). If the maximum vent rotation angle $\theta_{R,max,i} = |\theta_{C,i} - \theta_{Tag}|$ exceeds θ_{Th}, then scouring movement is identified . The output of the algorithm is a matrix containing start and end indices of events, event ID and the event rotation angle $\theta_{R,i}$.

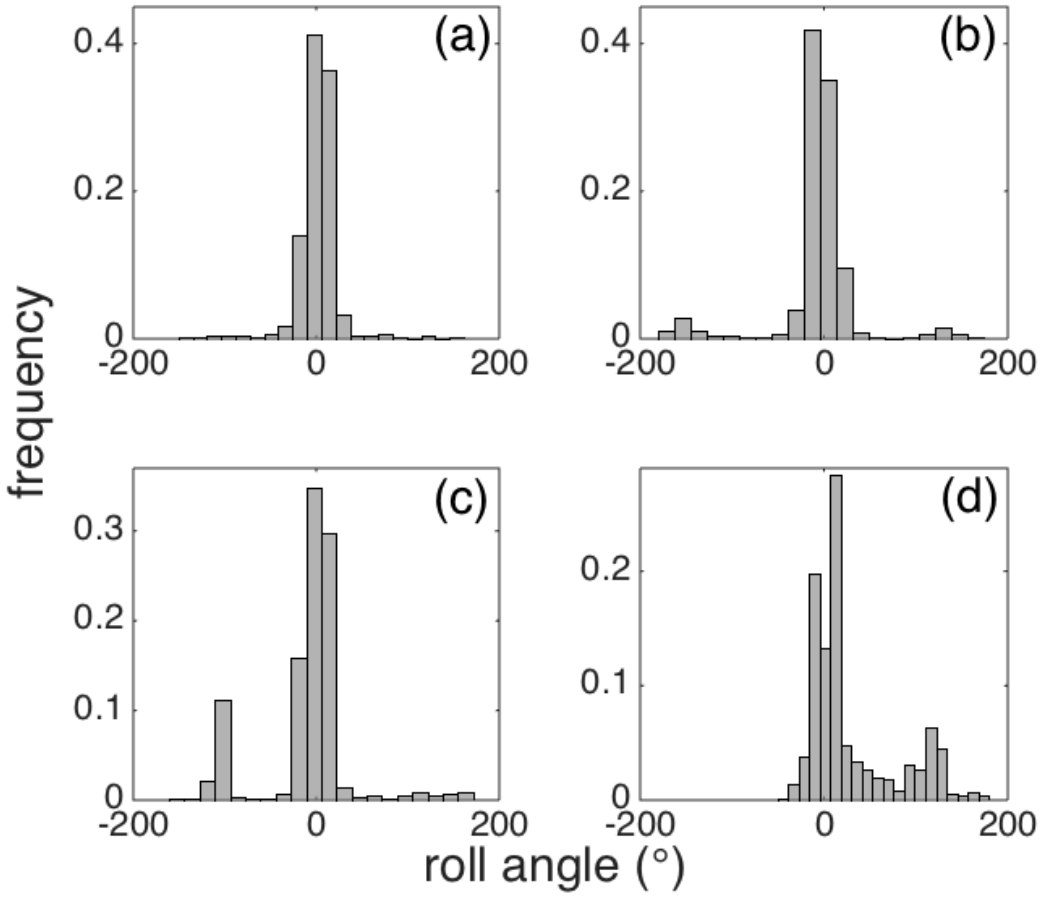

Figure 5.5 Normalized histogram of roll angles within extracted window segments for four different cod showing fish scouring on both lateral sides (a, b), and individuals scouring mostly on the (c) left and (d) right lateral side respectively.

The sensitivity and specificity of the algorithm was determined using a test data set comprised of a random selection of 10% of the experimental data spanning over 1000 positive scouring events where all windows were visually classified. The accuracy, precision, recall or sensitivity, and F-measure were calculated as follows:

$$\text{Accuracy} = (TP + TN)/(TP + FP + TN + FN) \quad \text{Eq 5.1}$$

$$\text{Precision} = TP/(TP+FP) \quad \text{Eq 5.2}$$

$$\text{Recall or Sensitivity} = TP/(TP+FN) \quad \text{Eq 5.3}$$

$$F - measure = (2 \text{ x precision x recall})/(precision + recall) \quad \text{Eq 5.4}$$

where TP, TN, FP, FN signify true positive, true negative, false positive and false negative respectively.

Other detection methods (e.g., wavelet analysis) could not be used since the energy in the frequency spectrum for scouring (~1 Hz) is similar to that of steady-swimming (e.g., tail beat frequency of ~1 Hz; cf. Chapter 4).

5.3.2 Statistical Analysis

All scouring events were analysed using conventional methods (mean-comparison with (non) parametric tests) on the time spent scouring over the entire time series (hereafter referred to as *%TSS*) as a function of animal length, l *(m),* tag type, (s = small, l = large), tag load (% tag mass/body mass) and diurnal pattern (day, night). The energy spent during scouring movements was analyzed as a function of tag type. While energy expenditure could not be calculated exactly using respirometer calibrations (e.g., Wright et al., 2014), the nearly linear relationship between the vectorial sum of dynamic acceleration values, *VeDBA* (Eq 5.5) and oxygen consumption MO_2 in a comparable species (Wright et al., 2014) suggests that *VeDBA* is a valid proxy for energy expenditure (Wilson et al., 2006). *VeDBA* was calculated using the following equation:

$$VeDBA = \sqrt{{A_x}^2 + {A_y}^2 + {A_z}^2} \quad \text{Eq 5.5}$$

where A_x, A_y and A_z are the absolute dynamic acceleration values. Dynamic acceleration was calculated by removing the static component from the acceleration times series after applying a 2-s moving average to the acceleration time series (Shepard et al., 2008a; Wright et al., 2014).

A time series of percent of time spent scouring (±SD) as a function of experimental day for all fish was calculated and differences between day and night scouring were assessed. Directionality of scouring movement was also assessed to determine if

animals spent more time scouring on the right-lateral side, where the accelerometer tags were attached.

Algorithm computations and statistical analyses were performed using R (version 0.98.977, R Foundation for Statistical Computing, Vienna, Austria), and MATLAB R2014b (The MathWorks, Natick, MA, USA). All estimates are provided as the average estimate plus or minus one standard deviation unless otherwise noted.

5.4 Results

5.4.1 Algorithm Efficiency

The identification probability for scouring movements in the test data had an accuracy of 98.7%, a precision of 94.2%, a sensitivity of 92.9%, and an F-measure of 0.936. This demonstrates that the algorithm was highly efficient in detecting and classifying scouring events.

5.4.2 Statistical Analysis

No significant differences for size distributions of fish used for each tag type were determined (Figure 5.1) and this allowed me to compare tag types independently of a fish-size effect.

Time Spent Scouring, TSS

TSS ranged from 0 to 20%. (4.2% ± 3.6) and there was no relationship between *TSS* and tag load (log-linear ordinary least square, OLS, $p > 0.1$, Table 5.2, Figure 5.6). Tag type was not a significant confounding factor (or interaction) when *TSS* was regressed against animal size, and animal size did not affect *TSS* (OLS with interaction, p for all parameters > 0.2, Figure 5.6). *TSS* did not differ between tag type (Figure 5.6, Wilcox Sign Rank Sum test, $p > 0.2$) and *TSS* was significantly higher during day (80%) than during night (20%, Figure 5.7). *TSS* increased significantly from an average of 3% to 8% after 6 experimental days regardless of recovery time between experimental days (Figure 5.8). On average, 70% (69.8 % ± 1.7) of scouring time was on the right-lateral side where the tag was attached.

Table 5.2 Relations between tag effect (tag mass/body mass) and parameters: %time spent scouring (*TSS*), maximum lateral acceleration ($A_{max,x}$), maximum magnitude of acceleration, (MA_{max}), and *VeDBA* a proxy for energy expenditure. Intercept or proportionality constant, slope or exponent is provided if predictor is significantly different from zero with *p*-Value from Ordinary Least Square.

Response	Intercept (SD)	Slope (SD)	*p*-Value	r^2	*n*	Model
TSS			$p = 0.93$	0	42	Log-linear
$A_{max,x}$	0.91 (0.051)	0.27 (0.056)	$p < 0.001$	0.35	42	Log-log
MA_{max}	1.6 (0.052)	0.37 (0.60)	$p < 0.001$	0.49	42	Log-log
VeDBA	0.38 (0.11)	0.79 (0.12)	$p < 0.01$	0.51	42	Log-log

Maximum Acceleration

Lateral maximum acceleration, $A_{max,x}$, ranged from 0.05 to 1.63 g_o (0.37 g_o ± 0.28) and the maximum magnitude of acceleration, MA_{max}, ranged from 0.44 to 2.26 g_o (0.63 g_o ± 0.46). Both parameters were positively related to tag load (log-log Ordinary Least Squares, $r^2 = 0.61$ and 0.70 respectively, Table 5.2, Figure 5.6). $A_{max,x}$ and MA_{max} were significantly higher (Wilcox Sign Rank Sum test, $p > 0.05$, Fig 6.5) for fish tagged with large tags (0.52 g_o ± 0.29, and 0.94 g_o ± 0.43 respectively) than small tags (0.20 g_o ± 0.10, and 0.21 g_o ± 0.28 respectively). Animal size did not affect either parameter (OLS with interaction, $p > 0.05$, Figure 5.6).

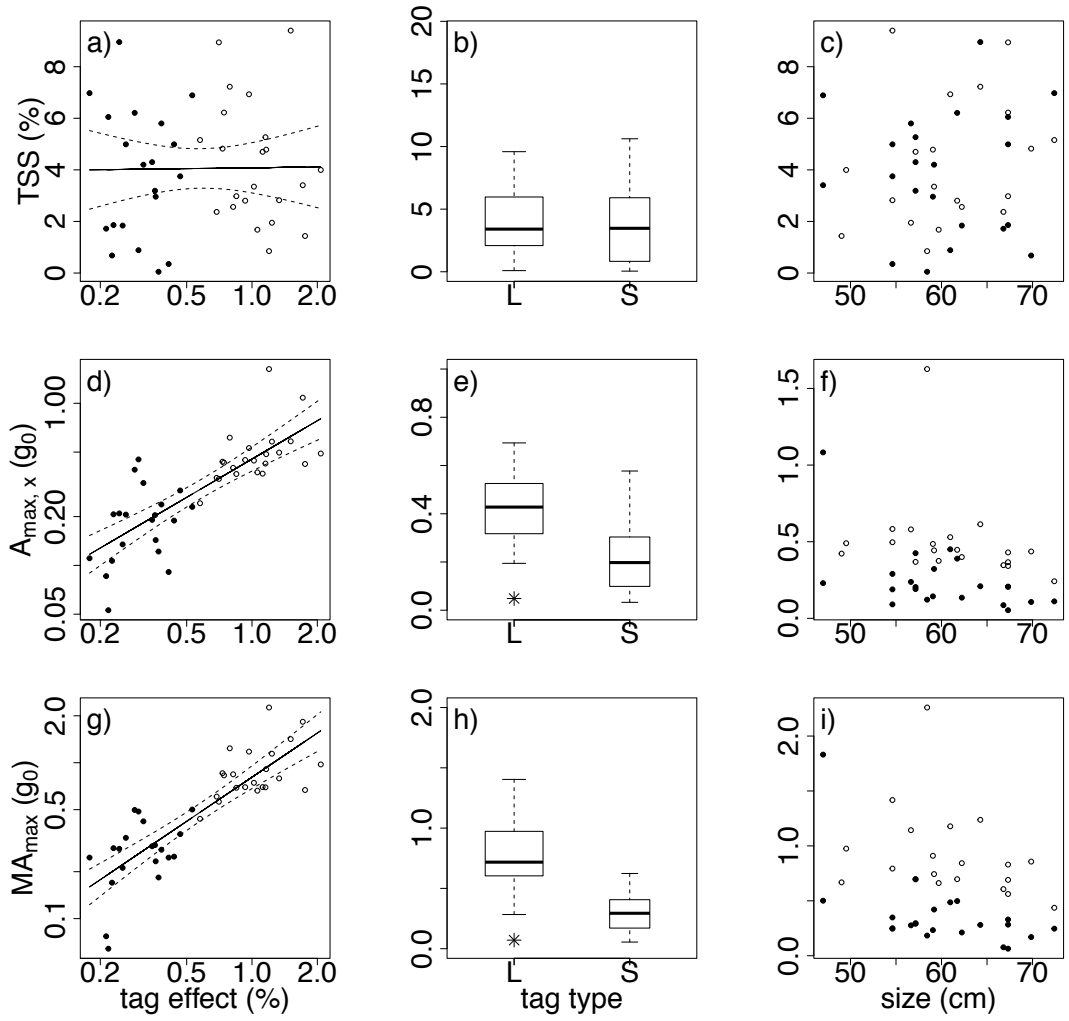

Figure 5.6 % time spent scouring (*TSS*), maximum lateral acceleration ($A_{max,x}$ (g)) and maximum acceleration norm (MA_{max} (g)) as (a), (d), (g) a function of tag effect (expressed as % body weight); (b), (e), (h) Box and whisker plots illustrating differences between tag type (L – large, S – small); and (c), (f), (i) as a function of fish size (cm). In all panels, closed circles = small tag, open circles = large tag. Box and whisker plots illustrating differences, where the box illustrates the inter-quartiles range (IQR), the bar the median, the whiskers are ±1.5 IQR.

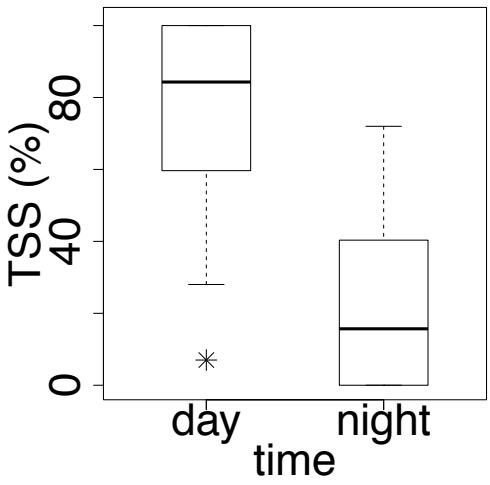

Figure 5.7 Box and whisker plots of time spent scouring, % TSS (%) during daylight vs. nighttime. Box illustrates the inter-quartiles range (IQR), the bar the median and the whiskers are ±1.5 IQR.

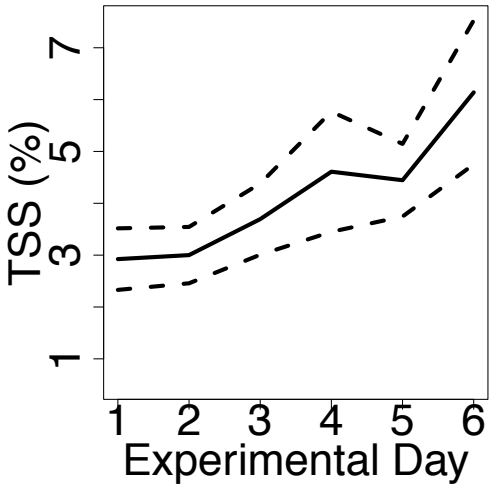

Figure 5.8 Differences in time spent scouring (TSS (%)) over experimental days for all fish. Solid line is average % time spent scouring, dashed lines are 95% standard errors.

Proxy for Energy Expenditure

The proxy for energy expenditure *VeDBA* was positively related to tag load (log-log OLS, $p < 0.001$, $r^2 = 0.51$, Table 5.2, Figure 5.9) and animals tagged with large tags displayed significantly higher *VeDBA* during scouring movements (Figure 5.9). *VeDBA* was independent of fish size. When *VeDBA* was compared within individuals during times when they were tagged with a small vs. large tag, *VeDBA* was higher for fish tagged with large tags in more than 80% of the cases. Of those where *VeDBA* increased, the increase varied amongst individuals with an average of 62% and a range of 26% to 88%, confirming an increase in *VeDBA* with tag load across individuals.

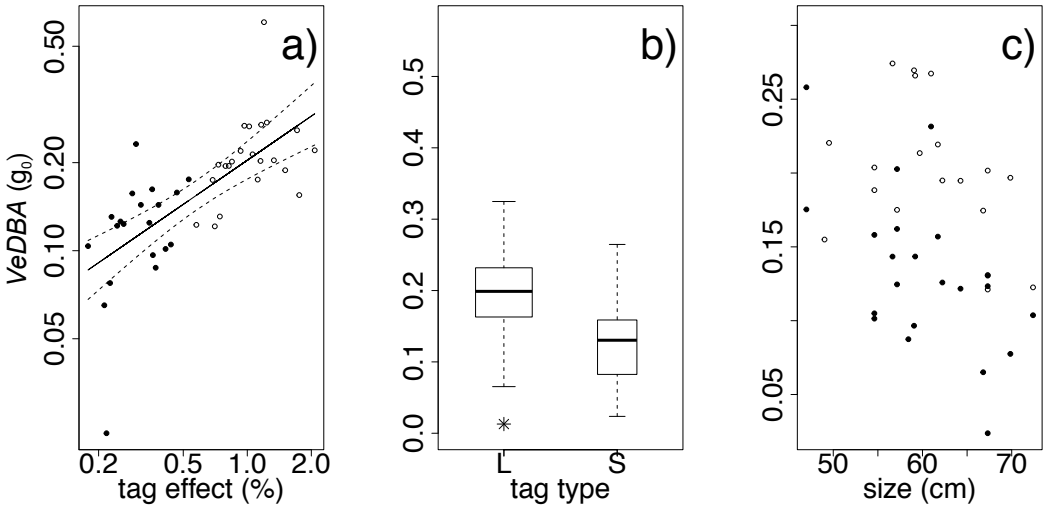

Figure 5.9 *VeDBA* as a proxy for energy expenditure as (a) a function of tag effect (% body mass) (b) box and whisker plots illustrating differences between tag type (L – large, S – small) and (c) as a function of size (cm). In all panels, closed circles = small tag, open circles = large tag.

5.5 Discussion

Based on high-frequency acceleration data, I have developed an algorithm to detect and identify rotational movement in the lateral-vertical plane of fish that is associated with a variety of behaviours and the algorithm has a high efficiency with 98.7% accuracy and 94.2% precision. The efficiency was achieved by a relatively simple algorithm based on the rotation of the three dimensional coordinate system of

the tag given the orientation of the animal. Not only is this algorithm independent of tag attachment and orientation, it also can be easily modified to identify and differentiate various degrees of rotation through the adjustment of the input cut-off threshold. Furthermore, a rotation in a different plane (e.g., forward-vertical or forward-lateral) could easily be implemented to extend the algorithms's applicability to identify various aberrant swimming behaviours among other species; i.e., those deviating from steady continuous swimming (e.g., Chapter 4), such as similar erratic swimming that has also been observed with other behaviour-associated movements as a modal action-pattern in at least 81 fish species (Wyman and Walter-Wyman, 1985). For example, cichlids (*Entroplus* sp.) incorporate scouring as a means of courtship and pair-formation (Wyman and Walter-Wyman, 1985), ludericks (*Girella tricuspidata*) rotate when feeding on seagrass epiphytes (Matthew D. Taylor, New South Wales Department of Primary Industries, NSW AU, *personal communication*), and various salmonids exhibit comparable swimming patterns when building spawning redds (Evans, 1994; Esteve, 2005). Despite the widespread observations of this behaviour, there remains a lack of evidence that explicitly examines rotational swimming among fish species (Wyman and Walter-Wyman, 1985). Therefore, the algorithm not only allows for the identification of a behaviour specific to scouring, it can potentially be applied to acceleration data collected from similar movements associated with parasite load, spawning, courtship or feeding and foraging in the wild.

By changing the threshold angle (θ_{Th}), the algorithm can easily be adjusted to detect and identify different degrees of rotation and therefore the classification of movements associated with various behaviours beyond scouring, such as feeding, courtship, or spawning. Furthermore, the algorithm is robust and input parameters such as the window overlap and window length have little effect in algorithm efficiency (<1%). Since the initial orientation of the tag on the animal (i.e., angle between lateral and vertical axis in the frame of reference of the acceleration sensor) is incorporated in the design of the algorithm, constant tag orientation amongst individuals or even within a single individual is not essential. It is further possible to determine the scouring direction (clockwise or anticlockwise) by using the sign of the rotation angle and thereby delivering even more fine-scale behavioural information.

5.5.1 Usability

Typically, accelerometer measurements do not provide rotational information such as angular velocity and the direction of movement. A gyroscope can directly measure angular velocity and if the initial attitude is known any new attitude achieved through rotational movement can be estimated using the attitude change calculated from the gyroscope measurements (Noda et al., 2013). Therefore, a gyroscope sensor could easily and directly measure rotations in any plane. However, due to battery and tag-size constraints, tags are frequently deployed with a single sensor, and accelerometers are typically preferred over gyroscopes. Accelerometer sensors not only deliver crucial information such as a proxy of energy expenditure (Wilson et al., 2006) and behaviour, they also draw less power than gyroscopes. For example, a sensor chip commonly used in biologging tags (InveSense MPU-9250, InveSense 2015) with a typical operating circuit in the 3-axis gyro mode requires a supply of 3.2 mA, while in the 3-axis accelerometer mode requires 0.45 mA – nearly 7-fold less at the same operating supply voltage. This is especially important for data-logging applications in fish where tag size, which is a direct function of battery size and power consumption, is severely constrained by fish body size. Here, I have shown that rotational movement can be well identified using the tri-axial acceleration signal without the use of a gyroscope sensor and can be of considerable value in studies where only accelerometer tags are deployed.

5.5.2 Tag Effect

Energetic Consequences of Tag load: Chronic and Acute Effects

Reduced swimming performance of tagged fish has been observed in various salmonids (Greenstreet and Morgan, 1989; McCleave and Stred, 1975) and perciformes (Mellas and Haynes, 1985; Ross, 1981). However, < 2% tag load (i.e., tag mass/body mass, Winter, 1996) is often assumed to not significantly affect swimming ability and behaviour. Despite adhering to the 2% tag-load rule I found that all tagged animals spent a significant amount of time scouring – a behaviour often observed in Atlantic cod to dislodge parasites (Dr. Jeffrey A. Hutchings, Department of Biology, Dalhousie University, Canada, *personal communication*). My findings indicate that there may be more fine-scale effects of tag load that have not yet been considered given traditional metrics such as tag retention and survival

(e.g. Ross and McCormick, 1981; Greenstreet and Morgan, 1989; Barrowman and Meyers, 1996; Björnsson et al., 2011; Cooke et al., 2012). Another important point to note is that despite a 'small' tag load of less than 2%, significant tag effects were observed, including some individuals that spent up to 20% of their time scouring. The total time the animals spent scouring was independent of tag load and this indicates that lower tag load does not necessarily result in reduced tag effect. The acute cost and physical damage that is caused by scraping the body to dislodge the tag can damage skin and provide opportunity for secondary infections to occur. Secondary infections can affect animal behaviour and can have energetic consequences, affect growth rate, reproductive performance and survival (Barber et al., 2000).

The chronic cost is the cost to the animal due to energy expenditure associated with added drag as well as tag-load. While individual fish exhibited high variability in scouring behaviour and associated *VeDBA*, generally, fish that carried a tag with a higher tag to body weight ratio exhibited higher lateral and full-body acceleration during such scouring movements, which implies that they used more energy when attempting to dislodge a larger tag. Specifically, *VeDBA* increased 5 fold when tag load (related to body mass) was doubled from 1 to 2%. Subsequently, these exhibited significantly higher maximum lateral acceleration, $A_{max,x}$ and whole body acceleration, MA_{max}. Therefore, the scouring force, $\boldsymbol{F_D}$, exhibited must be higher since $\boldsymbol{F_D} \propto m\ MA_{max}$, where m is fish body mass, and this naturally leads to an increase in energy expenditure (Videler, 1993).

The strategy for allocation of energy is an important contributor to physiological (e.g., oxygen consumption and heart rate) and behavioural (e.g., reproduction, foraging) ecology (Clark et al., 2010) and growth. An increased energy expenditure associated with tag-load reducing response in fish could result in reduced reproductive rates, growth rates or survival.

Tag Load Confounding Factors

For aquatic organisms with the capability to regulate buoyancy through swim bladders (or lungs), the effect of tag load as the weight of the tag and fish in air is

negligible in comparison to the drag coefficient, frontal area, and increased drag (Jones et al., 2013). My results are confounded by other factors beyond just tag weight, given the large difference in tag frontal area (5.14 cm^2 vs. 1.87 cm^2) as well as tag length and shape, which affect the friction drag. Thus, tag load expressed as %body weight does not reflect the true tag load. In an attempt to disentangle mass and other tag effects I separated tag types and examined the effect of tag to fish frontal area ratio (tag frontal area/fish frontal area) within tag type (mass term disappears). While increase in parameters (A_{max}, M_{max}, *VeDBA*) persists within tag type, the amount of explained variation was marginal, indicating that other factors (mass, buoyancy, etc.) are likely involved. Given the strong correlation between tag load expressed as weight and tag load expressed as frontal area (r^2 = 0.9) due to the same aspect ratio, the experimental design did not allow me to disentangle the underlying effects that are responsible for the observed pattern in increased $A_{max,x}$, MA_{max}, and *VeDBA*. However, it remains that the 2% body rule may not be a valid metric given the other variables that affect tag burden (tag buoyancy, shape, friction, etc), and even if the % weight load is small, the effect on the animal due to the confounding factors may be high. Furthermore, the time spent scouring in my study was clearly independent of tag mass or tag frontal area, which in turn, suggests that the observed effect of tag burden is likely attributable to irritation, rather than tag properties, and there is no simple means of assessing irritation.

Additionally, externally attached tags have been shown to influence the hydrodynamics around the fish and can lead to decreased swimming performances and associated energy expenditure given increased frictional drag and flow resistance (Arnold and Holford, 1978; Ross and McCormick, 1981; Mellas and Haynes, 1985; Bridger and Booth, 2003; Jones et al., 2013; Janak et al., 2014). An increase in drag causes a proportional increase in power output, *P,* of the tagged animal, described by

$$P = F_D u \text{ or}$$
$$P \propto c_d u^3 \qquad \text{Eq 5.6}$$

where F_D is the drag force, c_d is the drag coefficient and u is swimming speed (Jones et al., 2013). Therefore, increased drag requires an increase in power output by the animal at constant speed (Jones et al., 2013). For example, for a 0.73 m fish (c_d =

0.01 (Blake, 1983)) swimming at 1 m s^{-1}, a first principle approximation of the drag force,

$$F_D = 0.5\,\rho_d\,u^2\,c_d\,A_{tag} \qquad \text{Eq 5.7}$$

where A_{tag} is the cross-sectional area of the tag and ρ_d the density of the water (1029 kg m^{-3}), reveals that F_D increases from 1.24 N for a fish carrying the small tag ($c_{d,S}$ = 1.05, $A_{tag,S}$ = 0.00027 m^2) to 1.26 N for a fish carrying the large tag ($c_{d,L}$ = 0.85, $A_{tag,L}$ = 0.00038 m^2). This incremental drag increase is nearly independent of fish size, since the difference in theoretical drag from the tag is negligible compared to the drag at different size (m) of fish ($F_{D,0.25m}$ = 0.13 N, $F_{D,0.42m}$ =0.36 N, $F_{D,0.73m}$ = 1.1 N at 1 ms^{-1}). While here, only energetic consequences of tag-load reducing behaviour were investigated, the added drag due to tag load would likely increase the estimated energy expenditure during routine swimming movement and exacerbate the overall energy expenditure. Arnold and Holford (1978) suggest that a tag of similar drag coefficient (c_d = 0.6) only increases total drag by 5 to 7% in Atlantic cod during routine swimming. In their calculations the authors do not observe or quantify scouring movement since experiments were conducted in a flume and not on free-swimming fish. Given that the tags in this study and based on the ratio between tag drag, $d_{tag} = A_{tag}\,c_{d,tag}$, and animal drag $D_{fish} = A_{fish}\,c_{d,fish}$ the increase of drag for a 0.73 m fish would be 12 and 13% for the small and large tag respectively in free-swimming fish. There is little difference between the two tags and both estimates are much higher than in Arnold and Herford (1978) for the same sized fish (1%). Since the cross-sectional areas of the tags used here are 3 to 4.5 times larger and drag coefficients are significantly higher, then the estimated added drag is higher. While this increase may not significantly affect swimming ability (Arnold and Holford, 1978; Cooke, 2003), given my findings that relate to scouring behaviour, tag effect studies that only investigate added tag drag may underestimate overall tag effect.

Given my observations, a decrease in tag load may be able to reduce chronic cost associated with increased energy expenditure during scouring movements and drag. However, acute costs associated with physical damages will likely be constant since they are independent of tag load (even below the 2% body rule). This is a significant result, since generally a decrease in tag load has been assumed to lead to a decrease

in tag effect, but there is no means of decreasing irritation, and this suggests external tagging will always incur a cost.

Diurnal patterns

Cod spent a significantly greater amount of time scouring during the day (80%) than during the night (20 %) and exhibited preferential scouring on the right-lateral side where the tag is attached suggesting that they experience the asymmetry in the tag load. Typically, if a single-sided load is attached to a buoyant normally-upright object (e.g., a submarine) it creates a rolling movement since the weight is not equally distributed and neutral causing an angle of list and/or angle of loll – referred to as the trim or ballasting problem. Since it is only during the day that cod, a visual predator and schooling species, experiences sufficient light for visual referencing of its position (dispersed vs. aggregated; Brodeur and Willson, 1996; Axenrot et al., 2004), I assume that only then do they have a substrate reference for scouring. It is equally possible that it is only during day that the angle of tilt caused by the asymmetrical tag load is apparent to the fish and therefore they try to compensate (Webb, 2002) and/or remove the load. If it is indeed related to the angle of list and/or the asymmetrical load, it becomes essential that tag load (external or internal tags) is mounted symmetrically around the centre of gravity and possibly the centre of buoyancy, though the latter is likely much more difficult to achieve with a physostomous fish.

5.5.3 Implications

Validity of data in the field

Many studies now use implanted tags (Bridger and Booth, 2003; Cooke et al., 2004) due to a variety of advantages such as higher tag retention, reduced biofouling, and reduced added drag that may affect swimming ability, and thus increased survival rates (Bridger and Booth, 2003). However, in certain environments and experimental settings external tags are necessary (Cooke, 2003; Johnson et al., 2015) though they are not always ideal (Methling et al., 2011, Tudorache et al., 2014). This is especially true for Pop-up Satellite tags (PSAT), which have significant effects of added drag to the body (Bridger and Booth, 2003; Methling et al., 2011; Tudorache et al., 2014). Others (e.g., Thorstad et al., 2000; Cooke, 2003) did not observe

adverse short-term effects of tags with a similar tag load for fish, that unlike cod, spend little of their time on the bottom (e.g., salmon, except when spawning) and rolling behaviour was not observed in either species. Similar observations on shortnose sturgeon (Collins et al., 2002) have shown that these animals 'occasionally' scrape the substrate causing eventual tag loss. Other research using similar tags and attachment methods (Chapter 4) on saithe (*P.virens*) did not show a similar behavioural reaction to tag load, but these animals are pelagic species and did not exhibit parasite reducing behaviour as observed in cod. Consequently scouring may be species-specific and more apparent in species associated with a benthic habitat.

Given the results presented here and the significant time allocated by individuals to engage in tag load reducing behaviour, the assumption that the effect of the tag on behaviour and survival of the fish is minimal should be challenged. Especially the assumption that data from tags (especially externally attached tags) represents the normal behavioural repertoire of the tagged animal may be violated in species similar to Atlantic cod.

Effect of missing scouring events

The identification of scouring movements is crucial not only to determine potential tag effects, but also to differentiate such behaviour from routine swimming movements and other behaviours (e.g., feeding, migration etc.). If such movements are overlooked or misidentified, energy and activity budgets and related physiological estimates may be compromised. This is especially crucial given that some algorithms that are designed to identify burst acceleration movements associated with a feeding or escape response (Chapter 3; Noda et al., 2013; Noda et al., 2014) are based on comparing the variance amongst lateral and vertical or forward acceleration within movements. During scouring movements, fish also exhibit burst acceleration characterized by higher variance among the lateral and vertical axis when compared to other behaviours and therefore could easily be misidentified as a feeding or escape response. To ensure the identification of such events it is also crucial to ensure sufficient accelerometer sampling frequency: scouring movements, similar to feeding and escape response in other fish (Chapter

3), can occur over short time scales (< 1s), and if sampling frequency is too low (< 10Hz) such movements may be overlooked or misidentified due to aliasing (Chapter 3). This too could lead to compromised estimates of energy expenditure, but more importantly, a failure to challenge the assumption that the effect of the tag on behaviour and survival of the fish is minimal. Only by examining tagging effects on animal welfare and behaviour can data from such tags be used to make prediction on routine behaviour and movement (McMahon et al., 2012)

Algorithm as parasite indicator with internally attached tags

Demersal fish such as Atlantic cod have been observed to dislodge parasites (Barber et al., 2000; Øines et al. 2006) by scraping their lateral side along the bottom substrate. Documenting the functional significance of scouring with respect to parasite load is particularly important for cod (and salmon) given their increasing economic value in aquaculture production (Lysne et al., 1994) that can be compromised by external parasite infestations (Øines et al., 2006) and thus monitoring such behaviour becomes diagnostic. Infections in cod can induce altered time allocations for foraging and reproduction, reduce swimming performance, increase energy expenditure and change habitat selection, all of which may have implications for anti-predator behaviour, growth and ultimately survival (Barber et al., 2000; Jones and Taggart, 1998). While in this study the externally attached tags elicited a response in cod that is similar to parasite infestation, if accelerometer tags were attached internally and symmetrically they would likely not elicit scouring behaviour and all scouring movements recorded would then relate to parasite infection. Such data could then be used to quantify a response to parasitic infections and the onset of disease. Beyond diagnosing parasitic infections in species such as cod, this would prove especially useful given most fish species loose equilibrium in advanced stages of disease which is exhibited by lateral-vertical rotations due to loss of balance (e.g., whirling). In an aquaculture setting this could help diagnose infected fish, by monitoring parameters studied here such as the percent time spent scouring or loss of equilibrium, and when an individual exceeds a predetermined threshold it could then be removed to help contain the infection. This would be useful given the continuous advancement in miniaturization and low-cost sensor and

telemetry applications that would allow for large-scale direct observations and an *in situ* diagnostic of infection.

Limitations

Dorso-lateral rotations as observed during scouring may also occur during other movement-associated behaviours such as feeding, courtship and spawning. Given the design of the algorithm I provide, it would be difficult to differentiate between different rotational behaviours if they occur in the same movement (*xz*) plane and to the same degree. Fish that were observed in this experiment did not exhibit other rotational behaviours that could confound the classification. For field or aquaculture applications, the algorithm would have to be optimized to account for other burst acceleration movements based on statistical parameters that are capable of differentiation among different behaviours (feeding, escape, scouring).

In this study it was not possible to collect direct measurements of energy expenditure through conventional techniques (e.g., calorimetry, Walsberg and Hoffman, 2005; or oxygen consumption MO_2, Clarke and Johnson, 1999) due to the need to collect data from free-swimming fish. However, given past research, it is reasonable to assume that either the integral of the acceleration vector norm (Bouten et al., 1994; Wang et al., 2005) or dynamic body acceleration, *VeDBA* (Gleiss et al., 2010; Wright et al., 2014) can be used as a proxy for energy expenditure, since both are assumed to be (linearly) proportional to energy expenditure. While this proxy is useful in determining relative changes in energy expenditure it does not allow me to make deductions on 'real' energy expenditure (e.g., as measured by oxygen consumption). While the use of this proxy may be a debatable approach, especially when comparing across individuals, it is reassuring to find that when *VeDBA* is compared within individuals during times when they are tagged with a small vs. large tag, *VeDBA* is higher for fish tagged with large tags in more than 80% of the cases. Of those where *VeDBA* increased, the increase varied amongst individuals with an average increase of 62% and ranges from 26% to 88%, confirming an increase in *VeDBA* with tag load.

5.6 Conclusions

Reduced swimming performance of tagged fish has been observed in various salmonids (Greenstreet and Morgan, 1989; McCleave and Stred, 1975) and perciformes (Mellas and Haynes, 1985; Ross, 1981). However, the effects of tagging are typically not addressed, and, there are few studies that have quantified fine-scale post-tagging behavioural responses in fish. This study has shown that even if relatively small tags (<2% body weight) are used on fish, there are significant effects on behaviour and likely associated energy expenditure. To further quantify the effect of external tags, assessing specific drag of the external tag is important. The results of this study have potential implications for the nature of tag deployments in the wild where external attachment methods are used. Based on the observations here, it may be worth considering additional factors when determining tag load and type especially for demersal fish associated with the benthic environment and species where a history of parasite load reducing behaviour is known.

Chapter 6 POST-RELEASE BEHAVIOUR AND HABITAT USE IN SHORTNOSE STURGEON MEASURED WITH HIGH-FREQUENCY ACCELEROMETER AND POP-UP SATELLITE TAGS

The majority of this chapter is under review in *Animal Biotelemetry* as:

Broell, F., Taylor, A. D., Litvak, M. K. and Taggart, C. T. (*under review*) Post-release behaviour and habitat use in sturgeon measured with high-frequency accelerometer and PSATs. *Anim. Biotel.*

6.1 Introduction

Quantifying the spatial-temporal distribution of free-ranging animals in the marine environment is problematic due to the paucity of direct observation (Cooke et al., 2004; Preston et al., 2010). This can be partially overcome by using a variety of tags ranging from simple physical tags (e.g., Petersen discs, Floy tags, etc., Petersen, 1896, McFarlane et al., 1999) to more advanced electronic tags (Cooke et al., 2004; Bograd et al., 2010). For example, animal-borne micro-storage (archival) tags provide a means to monitor high-resolution movement and behaviour of aquatic animals through *in situ* measurements from a suite of sensors such as temperature, depth or acceleration. Such data can be used to quantify variation in behaviour, energetics, and habitat use and therefore provide objective measurements of how animals interact with each other and their environment (Cooke et al., 2004). Most recently, accelerometer sensors have been used for remote measurements of fine-scale movements among free-swimming fish and the acceleration signals can be used to quantify movement in time and space in controlled mesocosm environments (Gleiss et al., 2010; Noda et al., 2014; Wright et al., 2014), as well as in the wild (Kawabe et al., 2003a,b; Tsuda et al., 2006; Sakamoto et al., 2009; Whitney et al., 2010; Carroll et al., 2014). Typically, *in situ* measurements are collected using implanted archival

tags or pop-up satellite tags (PSAT) that are deployed over weeks to months or even years (Musyl et al., 2011).

Implanted archival tags involve the recovery of fish, whereas PSATs release after some pre-set time, float to the surface and processed data are transmitted to a satellite system without the need to recover the tags. This allows for applications in environments where fish move vast distances in the open ocean and in cases where physical tag retrieval is logistically impossible. Since PSATs typically use the ARGOS satellite system, which constrains data transmission (Fedak et al., 2002), data are binned prior to transmission (Musyl et al., 2011). While raw data are archived on board, they are rarely recovered since it requires tag recovery. For low data-volume sensors such as temperature, depth or light, the associated binned (histogram) data can be informative and provide insights into animal distribution and habitat characteristics (Block et al., 2001; Campana et al., 2011; Armsworthy et al., 2014). However, more complex inertial sensors collect a much higher data volume due to a typically higher sampling frequency that cannot (limited band width) be directly transmitted to the satellite. Consequently, the binned or summarized data provide limited information on the rates of activity and fine-scale variation in the local environment especially for high-resolution sensors such as accelerometers or gyroscopes.

A major challenge with PSAT accelerometer data relates to the PSAT attachment. Such tags generally employ a single-point attachment and release located at the leading end of the tag and tethered to the fish using various anchoring methods to the dorsal musculature (Block et al., 1998; Chaprales et al., 1998; Lutcavage et al., 2001; Prince et al., 2002; Swimmer et al., 2002). While this provides the most reliable tag release (Musyl et al., 2011), the essential PSAT buoyancy (for recovery) causes the tag to flutter in the water column current and (or) as the fish swims in a manner comparable to a handheld balloon in the wind. Such an attachment causes increased drag due to the large cross-sectional area (Methling et al., 2011). The consequence is that the acceleration data are compromised due to the decoupling between animal movement and the fluttering movement and may not correspond to the movement of the animal. For example, it is simple to imagine a scenario where

the tag moves independently of the animal as unbalanced forces cause it to flutter when the fish is swimming. Further, when accelerating, the length of the tether will influence the extent of tag movement in relation to the animal movement. The solution to this problem is a rigid tag mount achieved by a longitudinal two-point attachment similar to methods used for archival accelerometer tags on fish (e.g., Kawabe et al., 2003a,b; Tsuda et al., 2006; Gleiss et al., 2010; Whitney et al., 2010; Noda et al., 2014; Wright et al., 2014; Carroll et al., 2014) and air breathing animals (e.g., penguins, or pinnipeds Payne et al., 2014).

Further to these challenges, the trauma and stress associated with capture, handling and tagging injury or tag placement that impedes body functions and mobility can affect the behaviour of the tagged fish (Bridger and Booth, 2003; Hoolihan et al., 2011). Observed behavioural changes have been related to the physiological and biochemical effects of exhaustive exercise associated with capture and handling (Wells et al., 1986; Skomal and Chase, 2002) along with blood acidosis and high blood lactate levels that have been reported for tuna, sharks, and billfish subjected to capture and handling (Wells and Davie, 1985; Skomal, 2007).

In an attempt to collect high-resolution accelerometer data to determine fish movement as well as post-release behaviour I designed a short-duration PSAT study in an environment where physical tag retrieval was possible (a tidally influenced river) over a short period (days). I first developed a tagging protocol for a secure attachment of a high-resolution accelerometer on a PSAT tag and then investigated short-term behavioural response to tagging and behavioural and locomotion routines in relation to local environmental variables (temperature, light, depth, sea-level). The study animal was the readily available shortnose sturgeon (*Acipenser brevirostrum*) that inhabit the Saint John River and it tributaries. Along the east coast of North America, shortnose sturgeon typically remain in their natal river and estuary (Dadswell, 1979; Kynard, 1997), where they mostly feed on molluscs and large crustaceans without natural predators. In American waters their abundance is less than the minimum estimated for a viable population (Kynard, 1997) mainly due to anthropogenic impacts such as by-catch and poaching, blockage of spawning runs by dams and the regulation of river flows. Thus they are listed as endangered under the

Endangered Species Act 1973 (Kynard, 1997). There is an active recreational (catch-and-release) fishery in Canada regulated by minimum size restrictions, however, direct and post-release mortality and injury have not been quantified. Therefore, a further aim of this study was to assess the suitability of high-resolution accelerometers for evaluating post-catch-and-release behaviour and assessing potential short-term effects of the catch-and-release fishery. For this purpose, I tagged 5 shortnose sturgeon with high-frequency accelerometers mounted on PSATs that recorded environmental variables over a short period of 2 days.

6.2 Materials

6.2.1 Study Site And Animals

The shortnose sturgeon were caught in a recreational fishing competition in the Kennebecasis River, New Brunswick (45.49 N, 65.92 W, Figure 6.1). The River is estuarine with a fjord-like bay that connects it to the St. John River and the Bay of Fundy. The River has very little fresh water flux with only minor inflow (Trites, 1960, Hughes Clark and Parrott, 2001). The fresh water layer is between 5 and 13 m thick depending on the state of the river flow and the tide (Trites, 1960, Hughes Clark and Parrott, 2001) and the water in the Kennebecasis Bay is fairly stagnant although salt water can spill over the sill during a flood tide if the conditions are correct. Therefore, this environment presented an ideal testing ground for the deployment study.

Shortnose sturgeon (n = 5, Table 6.1) of total length (l; m) ranging from 0.83 to 1.09 m (0.96 m ± 0.096) in fork length and 0.94 to 1.21 m (1.06 m ± 0.11) in total length with mass (m; kg) between 4.00 and 12.8 kg (6.55 kg ± 3.68) were caught by rod and reel fishermen involved in the annual October catch-and-release sturgeon fishing derby. Fish were transferred to a holding pen set in the river were they were kept between 6 to 49 hours and each fish was tagged with a PSAT (SeaTag-MOD, Desert Star Systems LLC, USA), upon which I mounted a tri-axial accelerometer (MBLog PT-1, Maritime bioLoggers, Halifax, Canada) and a V9 acoustic transmitter (VEMCO, Amirix, Halifax, Canada). The MBLog PT-1 (50 mm length, 23 mm diameter, 18.8 g in air) and V9 (24 mm length, 5 mm diameter, 3.6 g in air) were glued to the PSAT (27.5 cm length, 2.5 cm diameter at narrowest point, 4 cm in diameter at widest

point, 145 g in air) prior to deployment (Figure 6.2) The PSATs recorded temperature (±0.1°C), depth (±2.15m) and ambient light (75 microLux resolution) at 1 Hz. The accelerometers recorded tri-axial acceleration at 50 Hz (10-bit resolution) at ± 6 g_0. The combined package is hereafter referred to as the 'tag' (167.4 g in air, 1.15 to 3.6 % fish body weight).

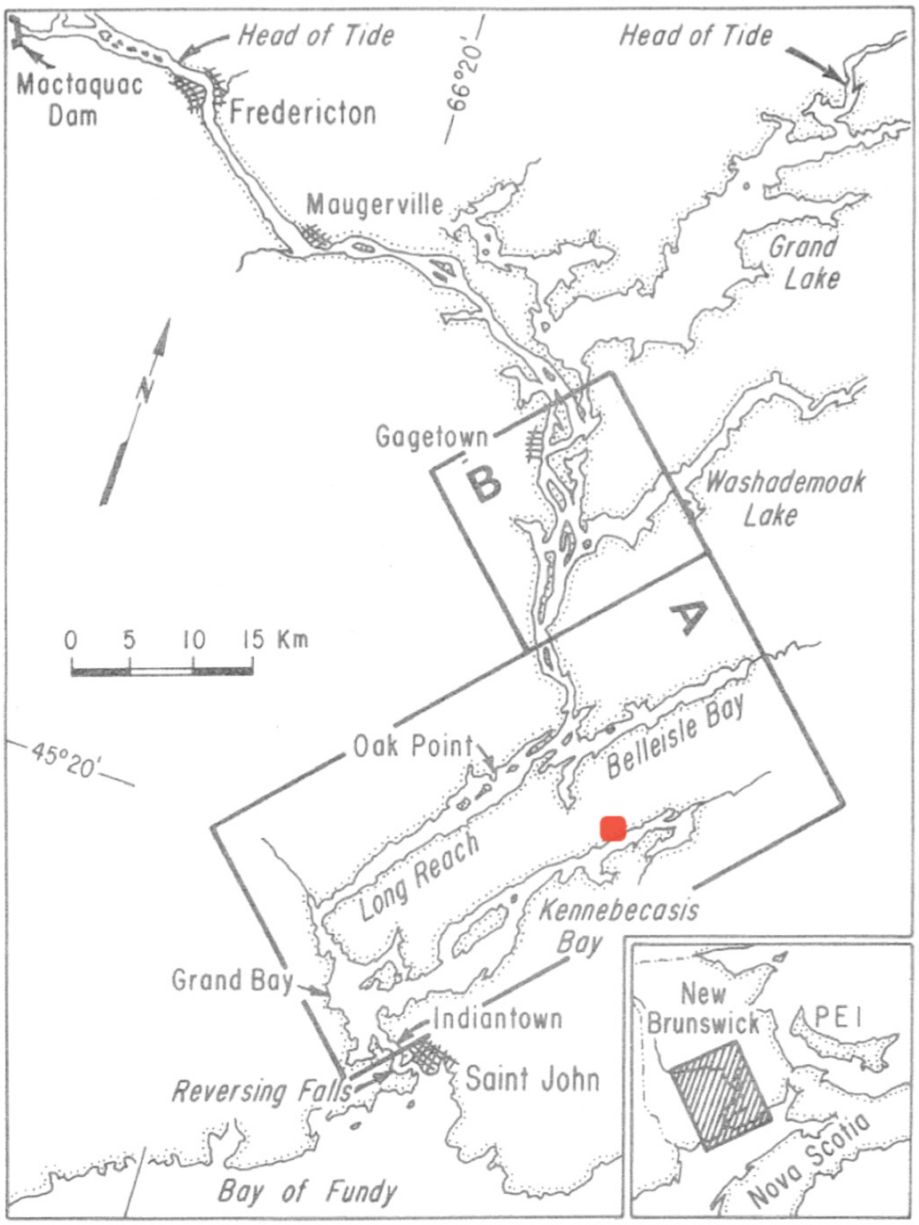

Figure 6.1 Map of study area (adapted from Metcalfe et al., 1976). The solid rectangle A indicates study area in the Kennebecasis River in New Brunswick, Canada; the red marker indicates the release point.

Table 6.1 Data associated with shortnose sturgeon that were caught and tagged in the Kennebacais River, New Brunswick in October 2012. Data includes total length (*TL*, m), fork length (*FL,* m) and mass (kg).

TL (m)	*FL* (m)	mass (kg)	Date tagged	Pop-up date	PSAT recording duration (hh:mm)	Accelerometer recording duration (hh:mm)
1.21	1.09	12.8	10/02/2012	10/04/2012	36:22	44:54
1.12	0.96	6.89	10/02/2012	10/04/2012	35:46	22:26
1.05	0.92	4.04	10/02/2012	10/04/2012	45:46	46:30
0.98	0.90	4.00	10/08/2012	10/10/2012	00:00	09:18
0.94	0.83	5.07	10/08/2012	10/10/2012	00:00	20:42

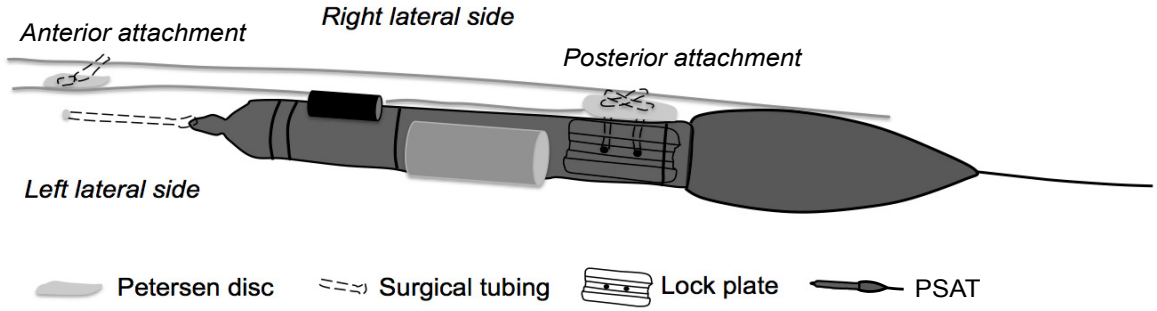

Figure 6.2 Illustration of tag attachment. Pop-up satellite attached to shortnose sturgeon with two dorsal attachment points. Black cylinder represents V9, grey cylinder MBLog PT-1.

6.2.2 Tag Attachment And Release

Rigid tag attachment (Figure 6.2) was achieved by a lock and slide mechanism and two dorsal attachment points: one anterior (toward to the head) and on posterior (toward the dorsal fin). The tag release section, located at the tip of the PSAT, was attached to latex surgical tubing (0. 16 cm ID, 0.32 cm OD, 0.08 cm wall) passed through a single bony scute to the right lateral side of the fish and attached to a Petersen disc (Figure 6.2). The surgical tubing provided sufficient tension to hold the tag in place on the dorsum. The posterior attachment, anterior to the dorsal fin and located ~25 cm from the anterior attachment, consisted of a one-way female slide-lock plate attached to two scutes on the left-lateral side and to a Petersen disc on the right lateral side and connected using surgical tubing. The male slide plate attached to the tag was then slid into the slide-lock plate where it was held in place by the tension created by the surgical tubing anchored anterior to the tag. The PSAT was equipped with an exploding charge release mechanism so it could release in freshwater. Once released from the anterior anchor, the tag slid out of the slide-lock plate, facilitated by the posterior tag buoyancy-package and drag. Since all attachments to the fish were made using dissolvable suture material, the slide-lock plate and Petersen discs were expected to eventually release from the animal.

Once tagged, the fish were released into the river with tags set to pop up after 48 hours. Following their release, the fish were actively tracked from a small vessel using a VEMCO directional hydrophone (VH110) connected to a receiver-decoder (VH100) following the Taylor and Litvak (2015) protocol. This allowed me to determine the location of the tagged fish prior to the scheduled PSAT release time. This proved to be essential given that although all tags did pop-up, no ARGOS transmission for locating the tags were received due to a defect in PSAT manufacture.

Fish care and protocols for fish holding, surgery, and tagging were approved by Mount Allison University (sturgeon, Permit 10-16) in accordance with the Canadian Council for Animal Care standards.

6.3 Methods

A total of 144 hours of acceleration data were obtained from the five tag deployments (Table 6.1). Two PSATs failed to record environmental data and thus only three datasets of temperature, depth and light were available spanning periods of 35 to 45 hours. Several analytical techniques were used to explore post-release behaviour and locomotion, and activity in relation to the ambient environment. To ensure that the rigid attachment did provide reliable accelerometer data, acceleration noise was compared to data obtained from mescocosm studies with the same species (Chapter 4) wherein the tags were firmly attached to the fish.

Swimming activity

Steady swimming (dominant tail beat frequency, *TBF* (Hz)) was extracted using the steady-swimming extraction algorithm (Chapter 4) based on invariant zero-crossing segments (Kedem 1986; Stein, 2000). Absolute swimming speed during steady swimming, u (ms^{-1}) was estimated based on *TBF* and the empirical relation provided by Long (1995) where $u = l\ (0.005 + 0.138\ TBF)$. The relationships between *TBF*, speed and length were then quantified based on prediction models proposed by Hill (1950) and Sato et al. (2007) and in relation to a data collected in a mesocosm study with the same species (Chapter 4).

Orientation

Animal orientation (roll angle - *xz*, θ_R pitch angle - *yz*, θ_P) was calculated using the rotational algorithm outlined in Chapter 5 where the angles were calculated as follows:

$$\theta_R = tan^{-1}\left(\frac{x}{z}\right) - \theta_{xz} \qquad \text{Eq 6.1}$$

$$\theta_P = tan^{-1}\left(\frac{y}{\sqrt{x^2 + z^2}}\right) - \theta_{yz} \qquad \text{Eq 6.2}$$

where θ is the angle of orientation of the tag in the *xz* and *yz* plane (see Chapter 5), x is the static lateral acceleration, y the static forward acceleration and z the static

vertical acceleration. Static acceleration was calculated by applying a 2-s moving average to the time series (see Chapter 5).

Post-release activity

Post-release activity was assessed as a function of *TBF* and high-energy burst acceleration movement, which is a proxy for escape response or abnormal behaviour (Chapter 3). Burst acceleration movement was extracted using the algorithm outlined in Chapter 3, and a proxy for energy expenditure based on *VeDBA* (Wright et al., 2014; Chapter 5, Eq 5.5), was estimated for burst acceleration and for steady-swimming movement.

Behavioural Routine

Behaviour spectra were calculated using the method outlined in Sakamoto et al. (2009) by applying a wavelet analysis (minimum cycle = 0.04 s, maximum cycle = 80 s) with a morlet mother wavelet function (order 10) applied to the lateral acceleration time series at 1 s intervals. The resulting spectra were clustered using a *k*-means algorithm to generate ethograms, which correspond to the percentage of time spent within a distinct behavioural cluster over time (e.g., Whitney et al., 2010; Nakamura et al., 2011; Watanabe et al., 2012; and others).

Relation to environmental variables

Animal behavioural clusters and locomotory activity were assessed in relation to river temperature, depth of fish and ambient light recorded by the PSAT for three fish, and if the length of deployment permitted (>12 hours) to tidal elevation recorded at 1 min intervals at Saint John station 65, 45.251W 66.063N (Environment Canada). Since the time series of dominant *TBF* was unevenly spaced, data were subsampled such that sampling frequency corresponded to 1/60 Hz and the environmental variables were sub-sampled to correspond to the same sampling frequency. A wavelet transformation was used on the dominant *TBF* time series for three individuals (0.83, 0.96, 1.09 m *FL*) to examine lower frequency patterns of activity in relation to behaviour.

Algorithm computations and statistical analyses were performed using R Studio Statistical Computing Software (version 0.98.977, R Foundation for Statistical Computing, Vienna, Austria), MATLAB R2014b (The MathWorks, Natick, MA, USA) and IgorPRO 6.3 (WaveMetrics Inc., USA, Ethographer Package). All estimates are provided as the average estimate plus or minus one standard deviation unless otherwise noted. Details on the various algorithms are found in Chapter 3, 4, and 5.

6.4 Results

Noise levels in the acceleration data were ± 0.01 g_o, and no apparent tag movement (e.g., complete or partial detachment) was observed. These noise levels were similar to data from previous studies on free-swimming sturgeon (Chapter 4).

6.4.1 Tail Beat Frequency And Swimming Speed

Tail beat frequency

Weighted distributions for *TBF* (Figure 6.3) were near log-normal with little variation among sizes and had an average of 1.1 Hz ± 0.47. Size did not have an effect on dominant *TBF* (weighted ordinary least squares, OLS, $p > 0.5$) though the suggestion of a slight increase with size for the larger fish (Figure 6.4) requires interpretative caution given the small sample size. When data were integrated with the mesocosm data for free swimming sturgeon (Chapter 4), *TBF* was a function of length (weighted log-log OLS, $p < 0.01$, $TBF = 1.1\ l^{-1.1}$, $r^2 = 0.74$, $n = 27$, Figure 6.5) with the wild fish falling within the prediction intervals of the mesocosm fish, though significantly lower than predicted for all but the largest two individuals (0.96 and 1.09 m). On average, there were no differences in activity level (dominant *TBF*) between day and night (Figure 6.6) except for the two smallest individuals (Figure 6.6a,b) where day activity was higher and lower than night activity respectively.

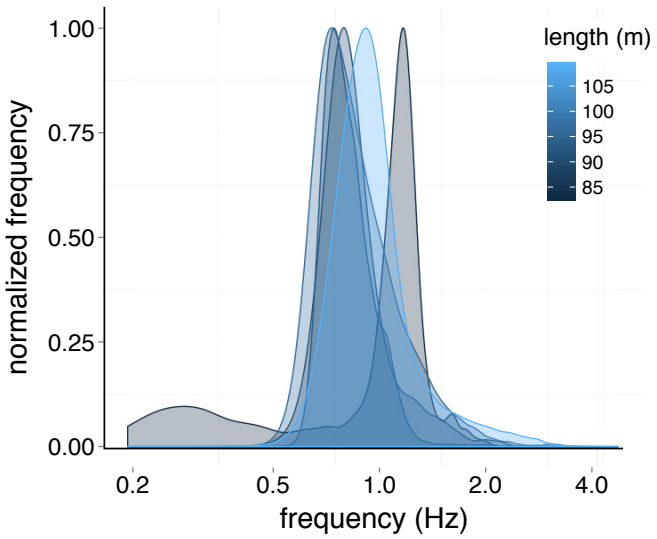

Figure 6.3 Normalized tail beat frequency (*TBF*, Hz) distributions from accelerometer records of shortnose sturgeon (n=5) based on weighted histograms of *TBF* extracted using the zero-crossing algorithm.

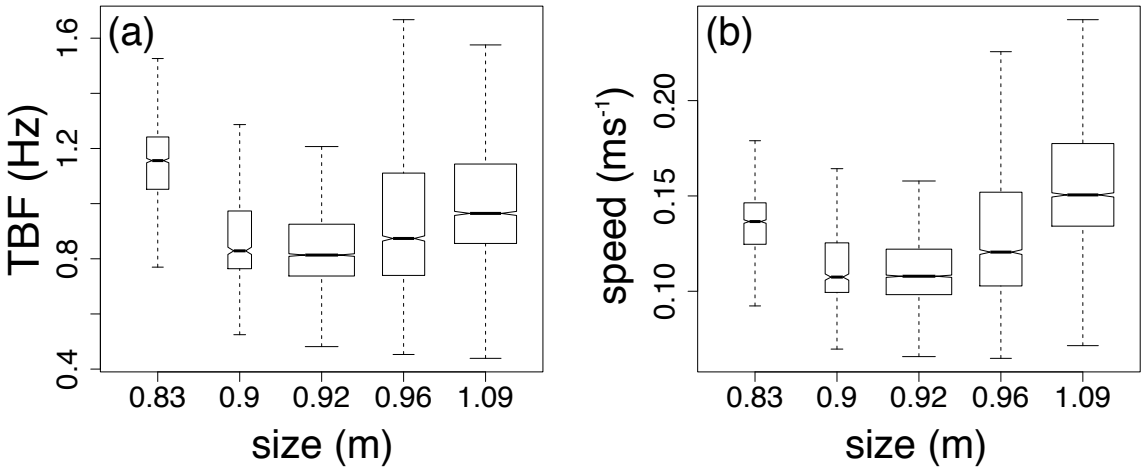

Figure 6.4 Weighted boxplots of (a) dominant tail beat frequency (*TBF*, Hz) and (b) swimming speed as a function of fish size (n = 5) for shortnose sturgeon. Dominant *TBF* was extracted using the zero-crossing algorithm and swim speed was estimated using dominant tail beat frequency and functional relationships in Long (1995).

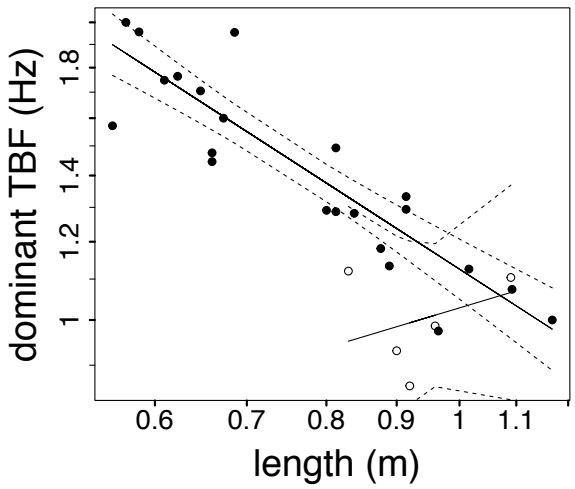

Figure 6.5 Log-log relations between dominant tail beat frequency (*TBF*, Hz) and length (m) for shortnose sturgeon from mesocosm experimental (solid circles, n=22) and field trials (open circles, n = 5) during active swimming. Weighted ordinary least square regressions (solid lines) are bracketed by the 95% confidence intervals (CIs) around the regression (dashed line).

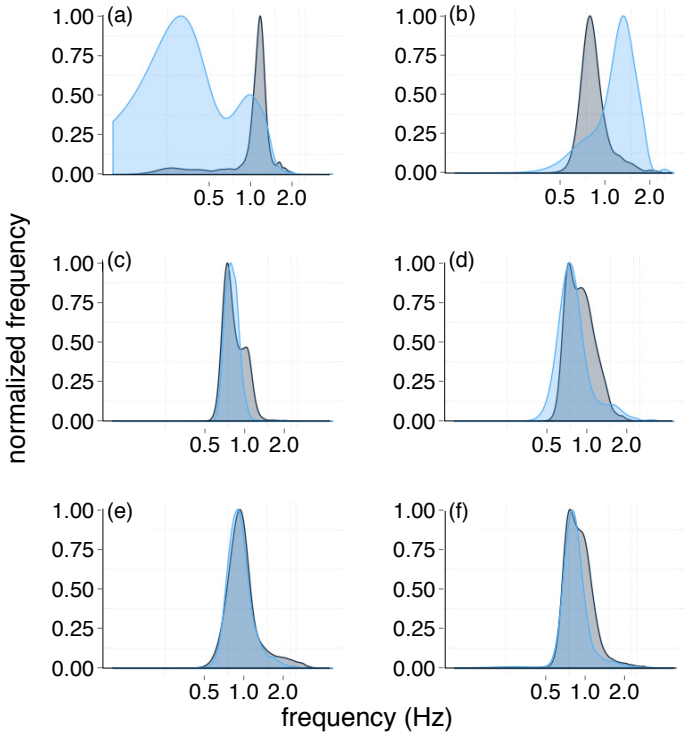

Figure 6.6 Normalized tail beat frequency (*TBF*, Hz) distributions from accelerometer records of shortnose sturgeon (n=5) based on weighted histograms of *TBF* extracted using the zero-crossing algorithm for day (blue) and night (black) for fish of size (a) 0.83 m, (b) 0.90 m, (c) 0.92 m, (d) 0.96 m, (e) 1.09 m and, (f) all fish combined.

Swimming Speed

Average estimated swimming speed for individuals was 0.14 ms^{-1} ± 0.025 (Figure 6.4b). Contrary to predictions (Sato et al., 2007; Chapter 4) size did have a significant effect on average swimming speed during active swimming (weighted OLS, u = -0.04 + 0.18l, p = 0.1, r^2 = 0.48, n = 5), but again, due to the small sample size this relationship should be interpreted with caution. If only the last two hours of data are considered, speed was independent of length (OLS, p = 0.7). When combined with data from the mesocosm studies (Chapter 4) there was no significant relationship between size and speed (log-log weighted OLS, p = 0.2, n = 27).

Animal Orientation

On average, most fish spent a significant proportion of their time (10 - 45%) tilted at pitch (y-z plane) angles greater than 20°, compared to lesser pitch angles (< 10°, ~30% of the time) associated with steady-swimming (Figure 6.7). The body orientation in the x-z plane (roll) was between 5 and 10°, though the smallest individual spent a significant proportion of time (30%) with roll angles exceeding 45° (Figure 6.7a).

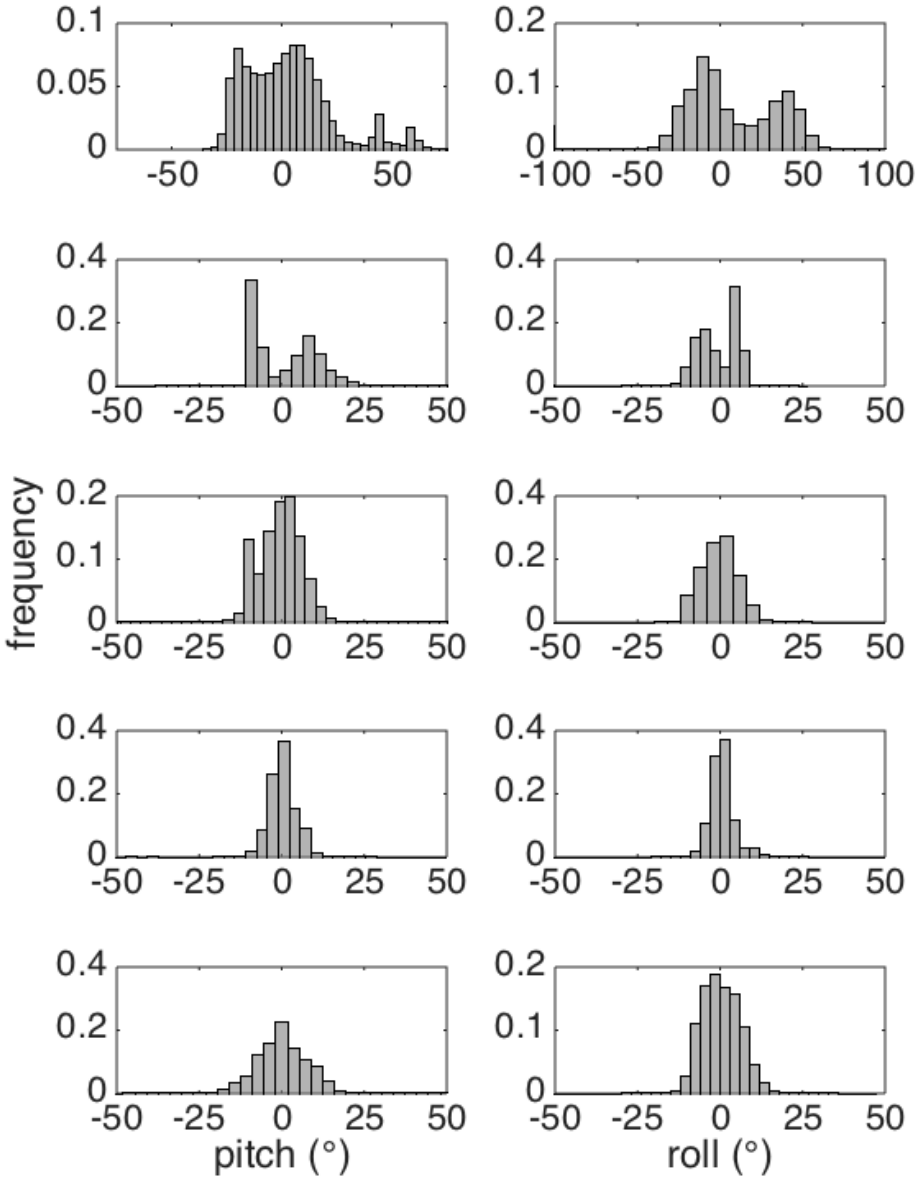

Figure 6.7 Normalized histogram for pitch angle (°) in the *y-z* plane (left panel) and for roll angle (°) in the *x-z* plane for fish of size (a) 0.83 m, (b) 0.90 m, (c) 0.92 m, (d) 0.96 m, (e) 1.09 m. Angles were calculated using rotation algorithm outlined in Eq 6.1 and 6.2.

6.4.2 Post Catch-And-Release Effect

Revisiting all fish, average *TBF* over short intervals following release was highly variable (Figure 6.8). Median *TBF* was low (<1 Hz) during the first few hours (Figure 6.8) for most fish. However, it was apparent that after 7 to 20 hours post release average *TBF* tended to stabilize between 0.5 and 1.5 Hz (Figure 6.8) except for the smallest fish where the average was zero (virtually no swimming) from 12 h post-release to the time of tag release (Figure 6.8a).

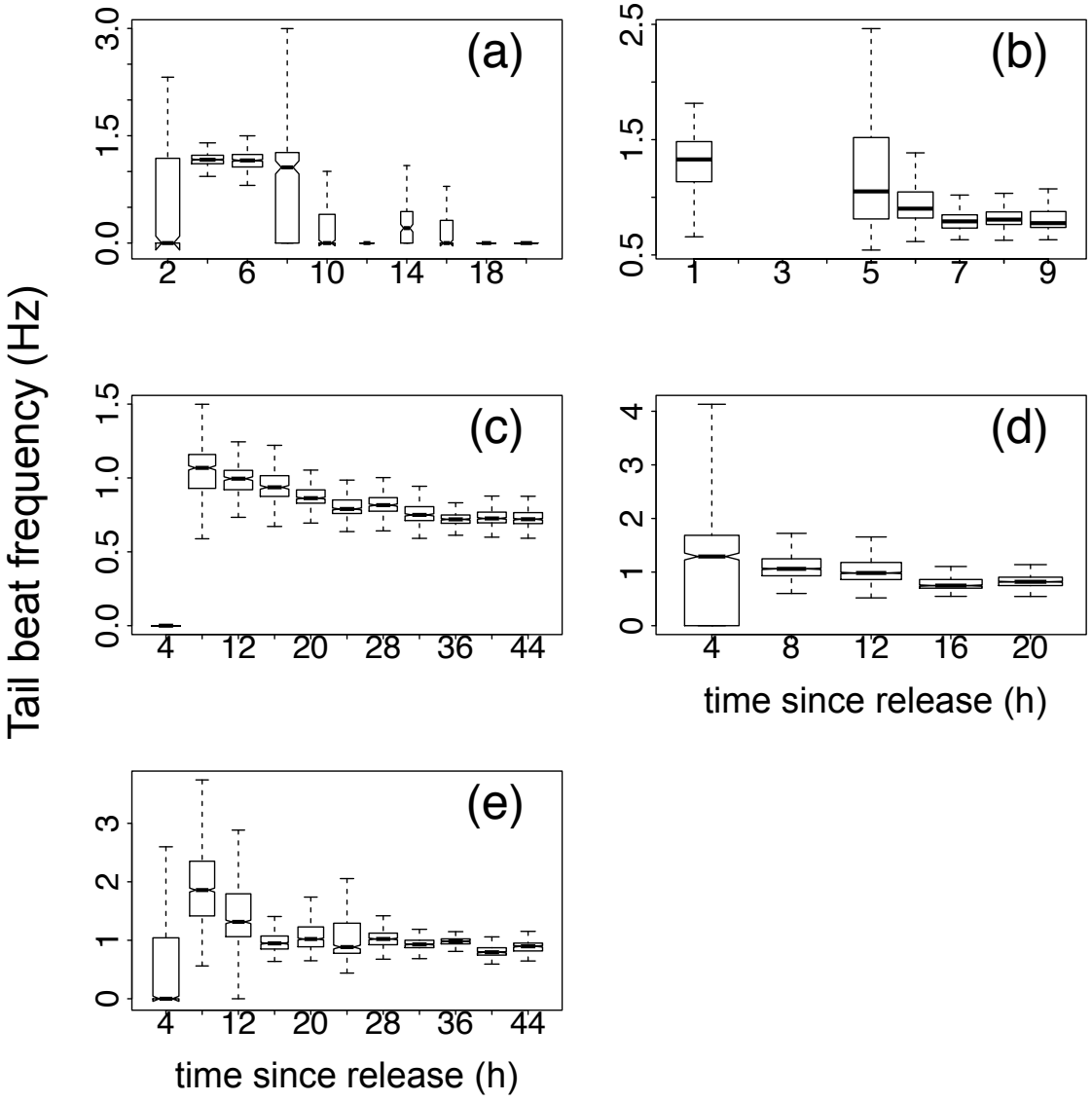

Figure 6.8 Post-tagging dominant tail beat frequency (*TBF*, Hz) for sturgeon of size (a) 0.83 m, (b) 0.90 m, (c) 0.92 m, (d) 0.96 m, (e) 1.09 m

The average *TBF* can however be misleading as demonstrated by examination of the behaviour spectra for each fish (Figure 6.9) where extended resting or recovery periods were apparent for all individuals after deployment and ranged from ~2 (Figure 6.9a, d) to ~4 hours (Figure 6.9b). For each fish the dominant *TBF* was ~1 Hz and interspersed with high-frequency burst acceleration for some. There was no measurable effect of size on recovery period.

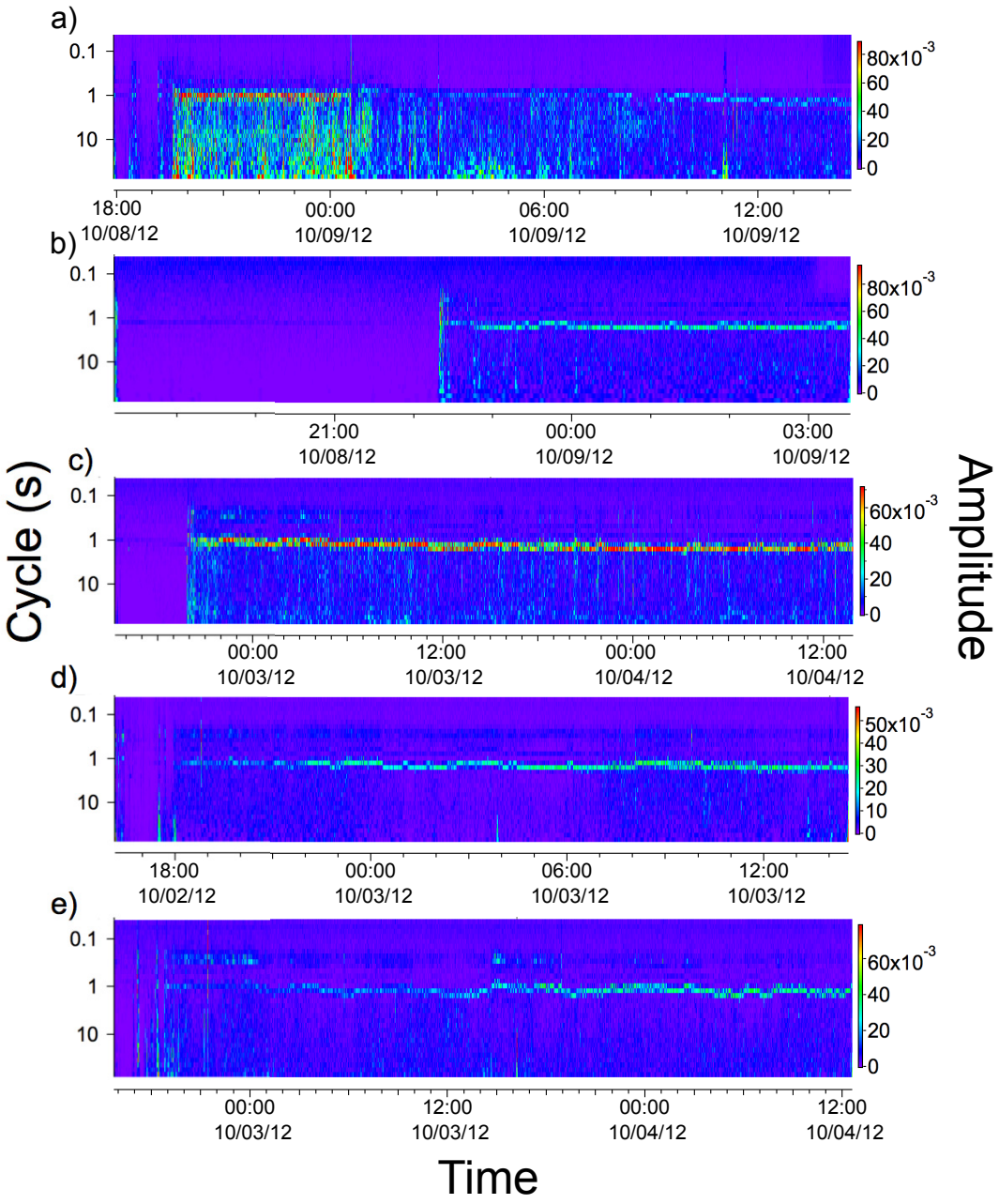

Figure 6.9 Behaviour spectrum calculated using a morelet wavelet transformation based on Sakamoto et al. (2009) approach. (a) 0.83 m, (b) 0.90 m, (c) 0.92 m, (d) 0.96 m, (e) 1.09 m. The tail beat frequency cycles are in seconds and the colour shows the amplitude of the frequency for every second for each fish.

The percent time spent engaged in burst acceleration, which is a proxy for abnormal behaviour and escape response, decreased with deployment time (Figure 6.10). Overall, burst acceleration was low (< 5% per hour) and varied little among individuals, and one fish exhibited higher rates ~6 hours post-release (Figure 6.10b).

While the occurrence of burst acceleration was generally low, *VeDBA* during such events was significantly greater than during steady-swimming (*TBF*) movements ($p < 0.01$) with 2 to 5 fold increases on average (Figure 6.11). For example, for the largest fish (1.09 m) average *VeDBA* during burst acceleration was five times higher than during steady swimming. Although the fish engaged in this behaviour 3% of the total time, this increase represented a 15% increase in its total *VeDBA* and potentially the associated energy budget.

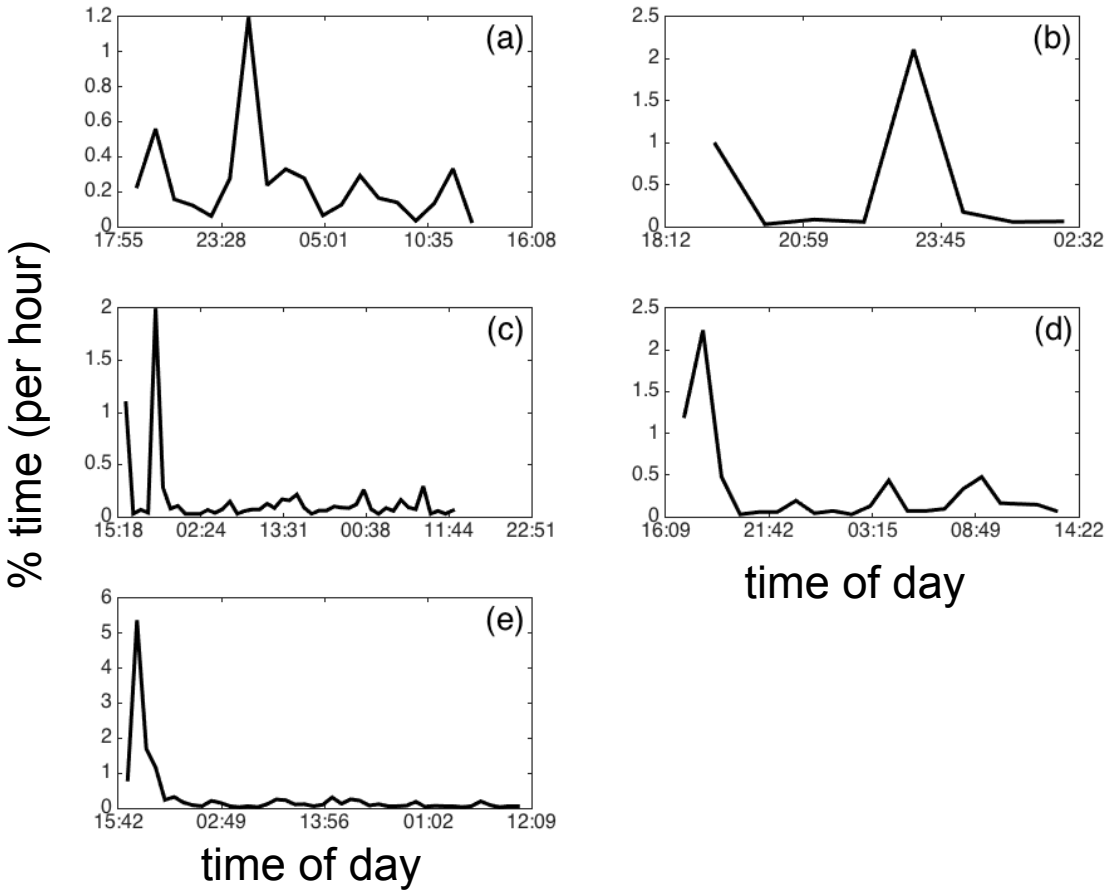

Figure 6.10 Per cent time (per hour) engaging in burst acceleration movements over the deployment period for the 5 sturgeon, (a) 0.83 m, (b) 0.90 m, (c) 0.92 m, (d) 0.96 m, (e) 1.09 m.

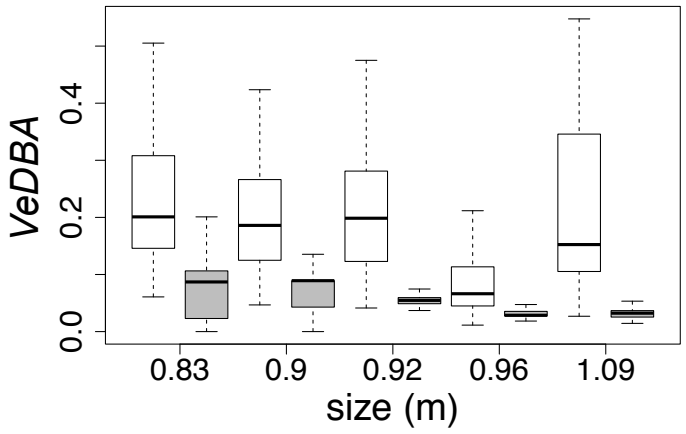

Figure 6.11 Proxy for energy expenditure, *VeDBA* (g) as a function of size (m). Grey boxplots indicate during routine behaviour, white boxplots during burst acceleration movement. *VeDBA* was calculated from burst acceleration movements (Chapter 5, Wright et al., 2014)

The behavioural clustering for the five fish (Figure 6.12) based on the behaviour spectrum in Figure 6.9, shows that the different fish exhibited different behaviours over the deployment period. The smallest (0.83 m) fish (Figure 6.12a) showed a resting period of ~1.5 h followed by 6 h of unsteady-swimming bouts at 1 to 1.5 Hz and low-frequency swaying movements (clusters 1, 2, 3) followed by a 2 h rest period. The 6-h period of unsteady-swimming bouts also coincided with a high roll angle (Figure 6.7) suggesting tag-load removal ('scouring') behaviour. The 0.92 m fish (Figure 6.12c) exhibited three distinct steady-swimming clusters (2, 0, 1) corresponding to 1 to 3 Hz, 1 Hz, and 0.7 Hz "gaits" respectively with activity decreasing over time. Cluster 3 was characterized by high frequency burst acceleration and unsteady swimming, which was dispersed throughout the deployment time when behaviour switched between gaits (Figure 6.12c). The remaining 3 fish (0.90, 0.96, and 1.09 m) exhibited similar behaviour characterized by varying steady-swimming gaits and high frequency burst acceleration, mostly observed shortly after they were released and after the resting and recovery period (Figure 6.12b,d,e). For these fish higher-frequency steady swimming dominated the first 15 hours followed by lower-frequency steady swimming. The two larger fish oscillated between high- and low-frequency gaits with cycle durations of 5-6 hours (Figure 6.12d,e) during their active post-recovery phase.

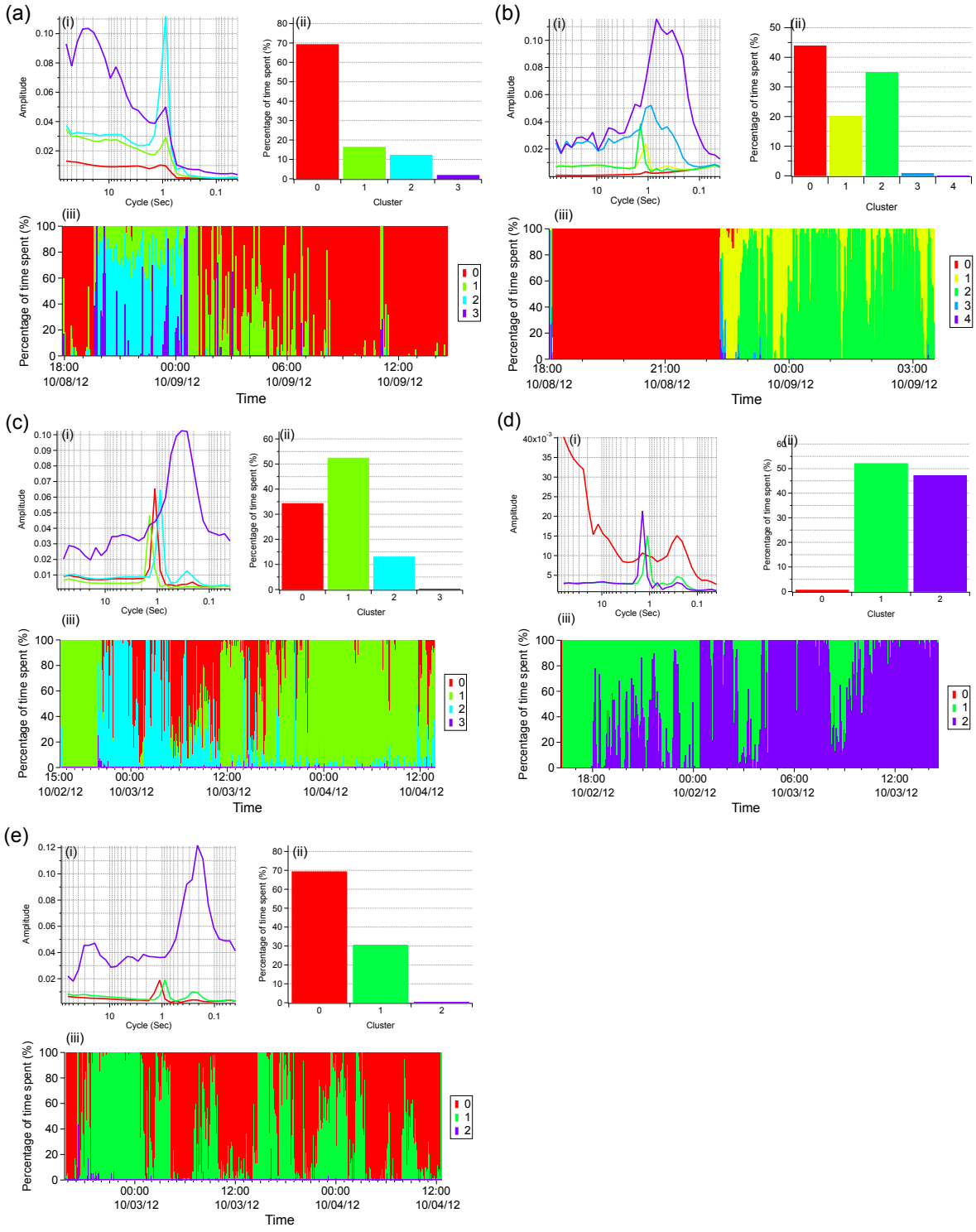

Figure 6.12 Behavioural clustering for the five sturgeon (a to e; smallest to largest respectively) illustrating (i) the four elements of the acceleration ethogram based on the behaviour spectra in Figure 6.9 where the vertical axis represents the amplitude of acceleration, the horizontal axis represents the cycle length of the acceleration, (ii) the percent of time spent in each cluster, (iii) the time series of % time assigned to each cluster over deployment time. Colour coding corresponds to behavioural clusters in (i).

6.4.3 Response To Environmental Variables

There was no clear relation between swimming activity (*TBF*) and depth of the fish and light levels over the deployment period (Figure 6.13). Depth was nearly constant across individuals at ~8 m for the 0.92 and 0.96 m fish, 3 to 5 m for the largest (1.09 m) fish and maximum depth did not exceed 10 m. The two smaller individuals spent their recovery period in shallower waters relative to their active phase (Figure 6.13a, b). Similar to depth, ambient light levels were largely constant around 0.4 V and there was no pattern between daytime and ambient light level, except for one individual (Figure 6.13a), when light level increased markedly around noon though there was no change in the depth of the fish. Water temperatures experienced by the fish were relatively constant at around 15 to 16 °C with some elevation in the afternoon (Figure 6.14)

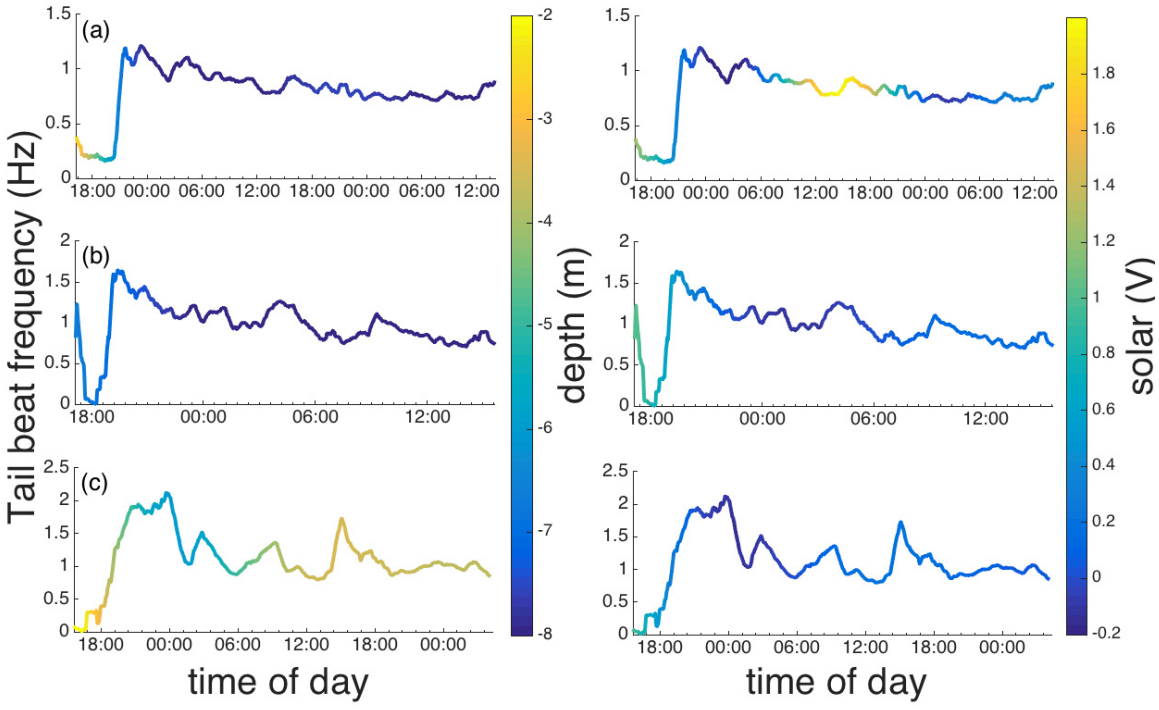

Figure 6.13 Tail beat frequency (*TBF*, Hz) as a function of time and depth (m) and ambient light level (solar V) for three sturgeon (a) 0.92 m, (b) 0.96 m and (c) 1.09 m.

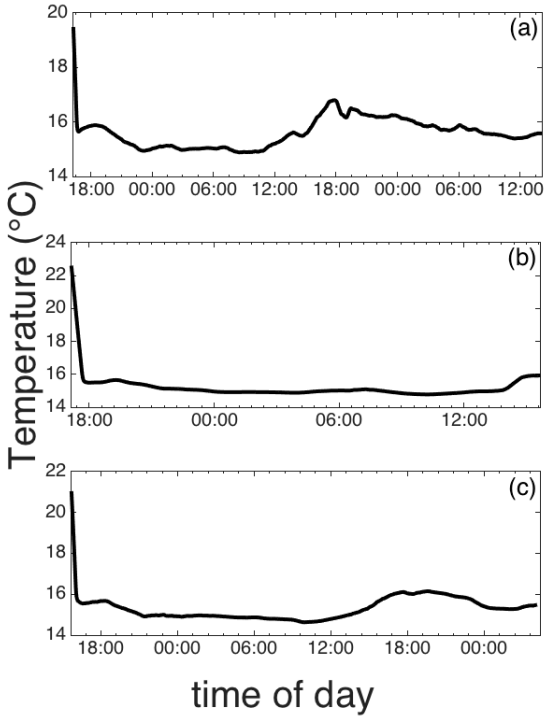

Figure 6.14 Time series of ambient temperature (°C) during deployment for three sturgeon a) 0.92 m, b) 0.96 m and c) 1.09 m.

The response to changes in sea level (i.e., tidal height) are similar amongst individuals: Fish 0.92 m (Figure 6.15b) decreased its activity levels (*TBF*) with high tide, however, the decrease in activity was small (1.2 to 0.9 Hz, and 0.9 to 0.8 Hz). The smallest individual (Figure 6.15a) exhibited higher activity during low tide (20:00 – 02:00), and decreased activity during high tide (02:00 – 08:00). Similar to the clustering analysis, for fish 0.96 m and 1.09 m, a wavelet analysis of *TBF* reveals a significant oscillation pattern in the activity (*TBF*) series corresponding to 4.4 to 5 hours (0.96 m) and 6.1 hours (1.09 m) (Figure 6.16b,c), however, it was not possible to determine if these oscillations relate to changes in sea level (Figure 6.15).

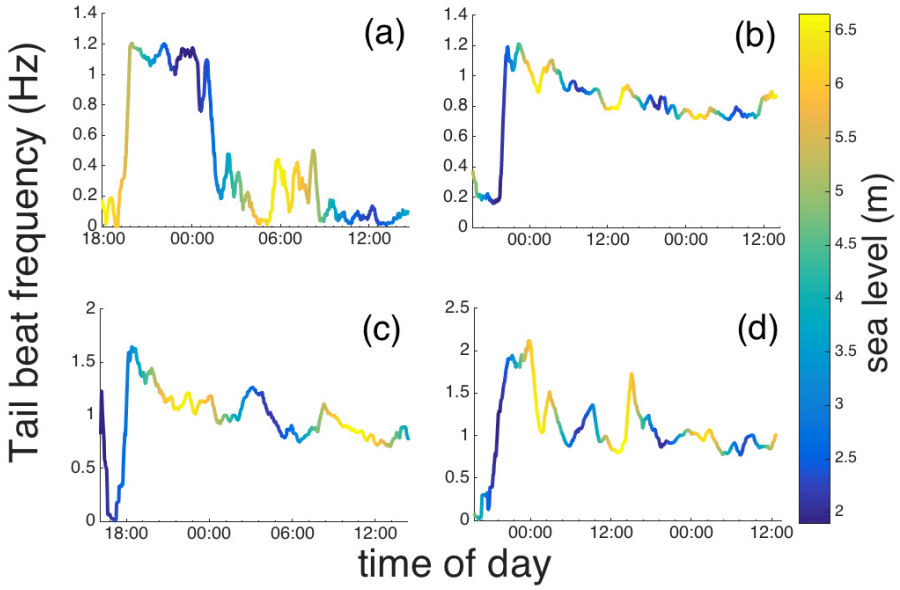

Figure 6.15 Time series of dominant tail beat frequency (*TBF*, Hz) as a function of sea level (m) for four sturgeon, (a) 0.83 m, (b) 0.92 m, (c) 0.96 m, and (d) 1.09 m

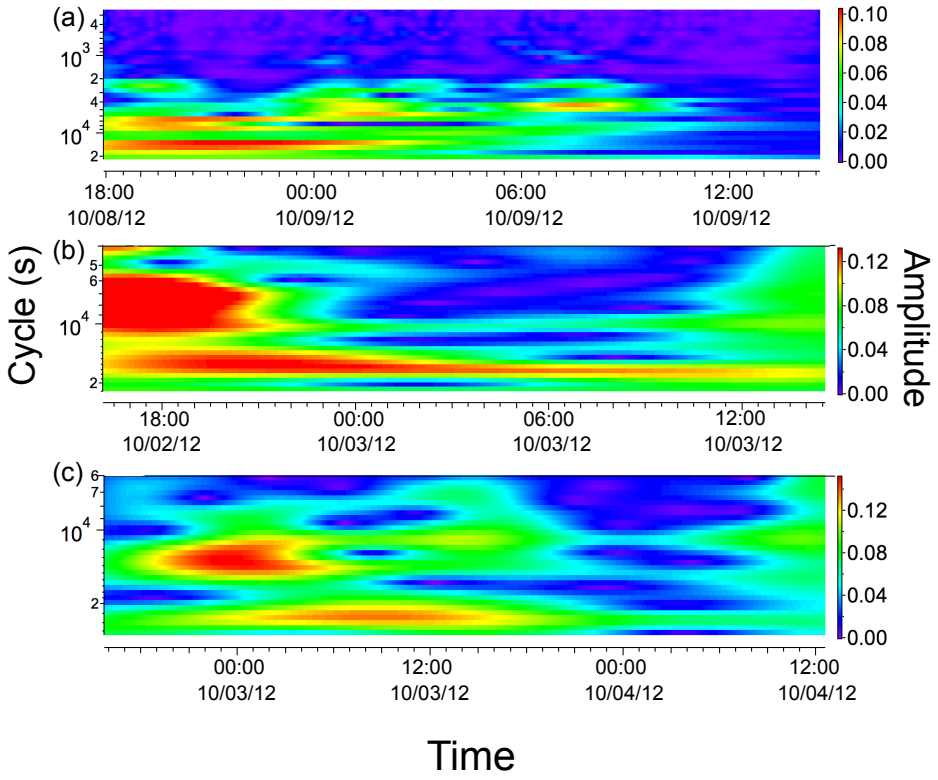

Figure 6.16 Wavelet transformation of dominant *TBF* extracted from the zero-crossing algorithm represented as cycle length (s) as a function of time of day for 3 sturgeon a) 83 cm, b) 96 cm, and c) 109 cm where the colour coding corresponds to the amplitude of the wavelet transform.

6.5 Discussion

I have developed a secure, two-point attachment method for a single-point release PSAT and acceleration tag. I was able to retrieve the tags in the wild using acoustic telemetry and recovered high-frequency (50 Hz) acceleration data for quantifying swimming activity and speed, post-tagging behavioural responses and responses to the ambient environment. Furthermore, I was able to test the biomechanical prediction model between *TBF*, speed and length as proposed by Hill (1950).

Tag attachment

Given that accelerometer noise levels were similar to data collected in a mesocosm study (Chapter 4), I am confident the tag mount was secure. While the tag attachment was specifically designed for sturgeon, it could be easily adjusted for use with other species since Petersen discs have been successfully used for decades (Petersen, 1896, McFarlane et al., 1990). For longer-term studies, this method will likely require modifications since dissolvable sutures were used and the multiple components may be prone to biofouling. One solution could be a cradle that houses the tag and contains a built-in release mechanism. This would provide the secure attachment needed by the acceleration sensor and could reduce tag drag relative to conventional single-point PSAT attachments (Methling et al., 2011).

6.5.1 Post-Release Behaviour

All the tagged sturgeon exhibited extended post-release resting periods (2 - 4 h) characterized by a low *TBF*. This suggests that the fish were holding station on the river bed; perhaps an energy saving strategy (Deslaurier and Kieffer, 2012). Holding station against downstream current can be achieved by flow-refuging (Geist et al., 2005) or by taking advantage of the flattened body morphology by pressing the body and pectoral fins against the substrate as has been observed in flume studies and for various sturgeon species (Adams et al., 1997; Geist et al., 2005; Kieffer and Cooke, 2009). While this has been attributed to be a mechanism for refuge from high flow, it may also function as a compensatory mechanism for recovery from post-release stress. During the recovery phase, fish exhibited short time-scale burst acceleration events characterized by high maximum accelerations of up to 5 g_o. Since sturgeon are

not ambush predators that exhibit typically high-acceleration when feeding (Chapter 3) but feed on molluscs on the river substrate, and have no predators themselves, these movements are likely unrelated to predator-prey interactions. Since these events occur most frequently just post-release, they most likely relate to tagging stress or tag-load reducing behaviour and given the high *VeDBA* and associated energy expenditure, they significantly affect the total energy budget. Increased *VeDBA* during these movements indicated by high roll angles in the smallest individual, likely contributes to additional tag-related energy expenditure. The extended recovery period and increased energy expenditure due to post-release stress likely contributes to increased vulnerability to other stressors, recapture, or death. Given that the fish deployed in the study area were exposed to a very active catch-and-release fishery, as well as recreational boating, the result may reflect a significant decrease in feeding and (or) survival.

Following the recovery period, the activity levels of the sturgeon, measured as *TBF,* remained fairly constant across fish in the 0.5 to 1.5 Hz range suggesting a 'normal' behaviour. Yet, the smallest individual exhibited unsteady swimming activity and station-holding throughout the deployment period. Additionally, this individual displayed movement associated with rolling behaviour during the first 10 hours of deployment (time series of roll angle, not presented here). This suggests a tag-load reducing behaviour similar to the scouring movement in Atlantic Cod (Chapter 5), which has also been observed in shortnose sturgeon in response to tag load (Collins et al., 2002). This too suggests a significant impact of tagging, handling and tag load (> 2%) stresses and questions the health status and long-term survival of the individual and suggests size may be a factor in post-release stress behaviours.

Swimming Speed and Behavioural clusters

The free-swimming wild sturgeon exhibited significantly lower average *TBF* (~ 1 Hz) and associated swimming speeds (< 0.2 ms^{-1} or < 0.2 BLs^{-1}) than are observed in laboratory studies (Webb, 1986; Peake et al., 1997; Wilga and Lauder, 1999; Cheong et al., 2006). The high pitch angles (> 10°) that were observed > 50 % of the time in all fish, may be related to low river-flow speeds of < 1BLs^{-1} when the negatively buoyant fish swim at unsteady rates or to achieve a force-balance when swimming in

the low river current (Wilga and Lauder, 1999). Given that the low swimming speeds were relatively constant over the 2-day deployment, they are likely unrelated to post-release stress behaviour and suggest that in the wild the sturgeon do not typically exhibit high swimming speeds > 1BLs^{-1}. For example, adult lake sturgeon, *Acipenser fulvescens* (1.20 to 1.34 m total length), were observed to swim at 0.3 BLs^{-1} during steady swimming in a still water tank (Long, 1995) and displayed two distinct gaits of locomotion; a 'slow' mode of 0.1 BLs^{-1} and a 'fast' mode of 0.25 BLs^{-1}. I also found evidence of a gait-switching mechanism: for example, the largest individual (1.09 m) spent close to 100% of the time at two gaits, one at 0.83 Hz (0.12 BLs^{-1}) and one at 1.1 Hz (0.16 BLs^{-1}). Chinese sturgeon (*Acipenser sinensis*) equipped with accelerometer tags in a river exhibited low dominant *TBF* and associated swimming speeds (< 1 BLs^{-1}, Watanabe et al., 2008) that are similar to the estimates reported here, and further suggest a discrepancy between free-swimming wild-fish estimates relative to laboratory estimates (e.g., Webb, 1986; Wilga and Lauder, 1999). Most kinematic studies are conducted in flume tanks to simulate dam passage and rarely include swimming at low speeds (e.g., Webb, 1986; Peake et al., 1997; Wilga and Lauder, 1999; Cheong et al., 2006). One potential explanation is that endurance during lower swimming speeds is elevated as suggested by studies on juvenile sturgeon (Delauries and Kieffer, 2012). Recent observations for swordfish also indicate significantly lower swimming speeds in the wild than hypothesized (Marras et al., 2015). I therefore suggest a re-examination of swimming efficiencies in relation to lower speeds in kinematic and energetic studies, since fish in the wild may be adopting speeds much lower than those predicted from flume studies.

6.5.2 Predicting Length With *TBF*

Given the observations from mesocosm studies (Chapter 4), in the wild from Sato et al. (2007) and as predicted from the biomechanical theory proposed by Hill (1950), I predicted that length and swimming speed are independent and that *TBF* is proportional to length^{-1} (Chapter 4). Contrary to the model predictions, observations in this study suggest that dominant *TBF* may be independent of size and that speed may increase with size. This discrepancy could be related to post-release stress due to handling (capture, held in holding tank for >1 day) and tagging, or stress response mechanisms such as station holding on the river substrate or other non-routine

swimming activity. I hypothesize this to be the most likely cause for the discrepancy, since, when I re-assessed the relationships using last two hours of data only (i.e., assumed to be the most 'normal' post-recovery behaviour), *TBF* was closer to the prediction. Further, *TBF* observations from other sturgeon species in the wild (Watanabe et al., 2008) are also close to the predictions. Incidentally, the two fish (0.96 m and 1.09 m) that did exhibit a predicted *TBF* were the largest individuals and they exhibited the least variable *TBF* and highest levels of activity; perhaps indicating better stress-coping ability.

6.5.3 Behavioural Routines

Overall, sturgeon did not exhibit any clear diurnal (i.e., *TBF*) activity pattern likely because they modulated their swimming activity in relation to river flow as suggested for other sturgeon (Geist et al., 2005). On average, all fish exhibited a combination of two or more steady-swimming gaits and for two fish (0.96 m and 1.09 m), these gaits appeared to change every 4-6 h, though the time series is short (~48 h). These behavioural oscillations may be due to a tidally influenced current related to tidal phase, that only has a measurable effect on the Kennebecasis river during the spring tide (Hughes Clark and Parrott, 2001) which coincided with the fish deployment period in the study and was noticeable at the study site (*personal observation*). Using the St John weather buoy to extrapolate timing of high and low tide, however, is difficult, since the lag between the locations (~40 km up river) is unknown and may be significant (> hours). I initially predicted a relationship between activity and tidal flow for sturgeon similar to what has been described for other species (Hunter et al. 2004; Gröger et al., 2007) and therefore expected that fish activity during station holding or upstream movement would be related to some phase of tide. It is possible that the gait change observed for the two largest fish may correspond to an activity response in relation to tidal flow, especially the variation in activity with a near semi-diurnal oscillation (~6 h) as illustrated in Figure 6.15c,d and Figure 6.16b,c. Given the small variability in depth and temperature, these individuals may have been station holding at depth throughout most of the deployment and therefore may have modulated their *TBF* with the tidal flow, however, due to the lag between the time series, it is difficult to relate these observations to the timing of the tide.

All individuals likely spent most of the study period in the upper shallower ranges of the Kennebecasis river, since they all inhabited depth levels < 10 m and Kennebecasis Bay is a fiord-like environment with median depths of ~20 m. This also implies that the individuals did not move far from the release site, confirmed by the tag pop-up locations that were between 2 and 5 km from the release site; similar to observations for other sturgeon (Geist et al., 2005). Differences in depth and light levels among individuals indicate difference in the habitat used or different recovery strategies (relocation from release site vs. recovery by station holding at constant depth close to release site). The two individuals that spent most of their time at constant ambient (low) light likely used habitats closer to the river banks in the upper parts of the river that is dominated by river grasses and marsh banks. Similar observations suggest that sturgeon stay in habitats where velocities would remain relatively low (Geist et al., 2005). Variability in ambient light was only observed in one individual (0.92 m). This fish may have inhabited the streambed where the water is clearer or areas along the riverbanks downstream where marsh-land density is lower.

6.5.4 Summary

Most of the behavioural routines exhibited by the tagged sturgeon were related to post-tagging effects and activities largely characterized by modulations in the swimming gait. While the ethogram analysis was able to allocate the acceleration signal to distinct behavioural clusters, without visual validation of acceleration data, it remains challenging to directly qualify these clusters in relation to behaviour. For example, these gaits may correspond to swimming vs. feeding or searching for food, or different environments such as lower vs. higher river flow.

This study further exemplifies that relating movement and activity to environmental patterns or habitat use is challenging with short duration deployments (days), and this is further exacerbated by the apparent tagging and handling effect on behaviour. Given the short deployment period, it is difficult to quantify the total extent of the recovery (resting + post-release behaviour modification) period for these fish because there are no baseline measurements of high-resolution movement and activity. The post-release resting phase is likely comparable to a ‘shock’ state and it is very likely that it takes more time (hours to days) before behaviour and movement returns to a

'normal' state. If I assume that *TBF* and swimming speed from the mesocosm studies (Chapter 4) as the baseline for this species, then only the two largest individual exhibited *TBF* and swimming speeds similar or close to predictions and therefore could be considered as 'normal' movement and activity. Therefore, making predictions about swimming speed and general activity based on a short tag deployment period (e.g., Marras et al., 2015) can lead to compromised estimates that are affected by post-release stresses.

I expect that behavioural modifications in response to tagging and handling are likely related to the tagging surgery, which was long (~ 15 min), invasive, and without anaesthetics as well as the long holding time (> 1 day). Additionally, tag load may have an effect on animal behaviour (3% for the smallest individual) as indicated by significant scouring movements similar to observations in Atlantic Cod (Chapter 5). It is now commonly acknowledged that devices attached to animals may have adverse effects on their behaviour, as well as individual fitness, and directly or indirectly affect performance (Chapter 5; Ropert-Coudert and Wilson, 2004). While tag attachment delivered nearly noise-free acceleration signals, the significant impact on post-release stress suggests that the surgery and attachment protocols require modification.

For future studies, longer time series of activity (acceleration) using a less invasive attachment method suitable for longer duration studies should allow for the identification of routine behaviours that are not affected by post-tagging stress. Initially, this will require a longer-term tagging trial in a controlled environment. The above results clearly indicate that it is challenging to infer animal behaviour and movement based on a short time series that is exacerbated by post-release stress. In relation to the shortnose sturgeon catch-and-release recreational fishery, the results presented here clearly demonstrate that there are significant short-term (acute) affects on behaviour and potential on longer-term (chronic) effects on survival.

Chapter 7 CONCLUSION

7.1 Summary

Quantifying the spatial-temporal distribution of free-ranging animals in the marine environment has been historically challenging due to the paucity of direct observation (Cooke et al., 2004; Preston et al., 2010) and can be overcome by using a variety of tags ranging from simple physical tags to more advanced electronic tags. Within the suite of biologging techniques, tri-axial accelerometers are especially promising in providing data that can link physiological and ecological processes in the movement context (Nathan et al., 2012). The goal of my research was to determine how this technology can be used to measure a variety of fish behaviours in the framework of locomotion and to monitor species-specific size-at-age in the wild. I also set out to determine the effect of tag load and handling stress and how accelerometers may be able to measure associated behavioural stress response in the lab and in the wild. To achieve this goal, I developed a re-useable micro-accelerometer data logger relevant for fish applications that records and stores tri-axial acceleration data at high (up to 550Hz) sampling frequencies. Based on controlled-environment experiments I then developed a library of automated signal-processing algorithms that relate acceleration signals to rates of activity, locomotion, swimming speed, size and behavioural states in a variety of fish species. Specifically, I was able to extract behavioural states (feeding, escape) relevant to energy budgets as well as states associated with spawning, courtship and parasite dislodging to a high accuracy with a method that is independent of animal size or tag placement, both of which are very difficult to achieve reliably in the field.

Given my objectives,

- I have shown that it is possible to measure fast-start movements that are relevant to energy budgets (feeding, escape) in fish using relative simple species-specific classification techniques.

- I have also shown that it is possible to predict size-at-time in fish with species-specific models that are required given species-specific differences in hydromechanics that affect fish swimming. The large predictive uncertainties of this model may not yet provide a suitable alternative to traditional methods; yet, it shows promise in providing more detailed (*in situ*) information for estimating size-at-time.

- Further, I have demonstrated that technological limitations of the current accelerometer technology with respect to sampling frequency affect classification of behaviours given the time scale of the movement of interest. Low (< 50 Hz) sampling frequency can distort the acceleration signal and can result in important behaviour to be missed or misidentified. Based on these results, high accelerometer sampling frequency (> 50 Hz) is recommended.

- I have shown how accelerometer data can provide a useful method to reveal behavioural modifications in response to external tag load. Fish behaviour can be affected by tagging effects and tag load, which can not be mitigated by decreased tag load and the effect of tag burden is likely attributable to irritation.

- I have also determined how the developed accelerometer analysis techniques can be used to determine how fish change their behaviour and activity in response to tagging and handling and the variation in their surrounding environment. Yet, short-term time series do not allow for the interpretation of behavioural patterns.

The most novel contribution undoubtedly is the development of a scaling relationship between tail beat frequency, speed and length in free-swimming fish, based on accelerometer signal-processing techniques and the theoretical predictions of Hill (1950) and others. These results subsequently can be used to predict size-at-time with prediction uncertainties as low as 18%, thus providing a novel method for estimating length-at-age in the wild that is largely independent of behaviour, unsteady swimming and surrounding current flow. While this may not yet provide a

suitable alternative to the more conventional means of estimating growth rate, the model could be further advanced by incorporating additional parameters or predictors of length (such as temperature; e.g., Neuheimer and Taggart, 2007), and (or) by combining the knowledge of fish size at the time of capture along with the theoretical characteristics of the growth potential with the indirect observations of length from the scaling relationship to construct a model of fish length-at-time. Such a model may provide a more reliable time series of length-at-age and growth than what can be achieved with conventional techniques.

One pattern that emerged throughout my research is that free-swimming fish exhibit much lower swimming speeds (< 0.5 BLs^{-1}) than theorized, which was confirmed by observations from the wild. The most likely explanation is the discrepancy between (theoretical) swimming speeds given the swimming modes considered (e.g., critical, maximum, sustained, etc.; Bainbridge, 1958; Videler and Wardle, 1991) and how poorly those modes correspond to the observed dominant swimming mode, which may in fact be the preferred mode adapted to by a given fish/species. While theoretical swimming modes are efficient from a biomechanical and dynamic theory perspective (i.e., maximizing output), fish may adapt to modes that are efficient from an endurance perspective (i.e., minimizing input) and other less known physiological properties, thereby reducing energy waste. I propose that fish only exhibit swimming speeds predicted by biomechanical efficiency in behaviour-specific instances (e.g., predation on highly mobile prey). If this pattern is confirmed in other species and different environments, it will likely have an impact on ecosystem and fisheries modelling where ~5 BLs^{-1} is a frequently used approximation (Williams et al., 1989; Lucas and Batley, 1996; Krause et al., 1998) that will affect estimates of energy budgets and survival. In the context of scale-effects in animal locomotion (e.g., Pedley, 1977; Peters, 1983), the decoupling between swimming speed and size puts forward a catalogue of research questions concerning size-dependent biomechanical efficiency (at low speeds) and mechanisms that allow fish to school at similar speeds and potentially different sizes (e.g., Krause et al., 1998). Such questions are testable and may help advance the science of fish swimming that has been undergoing refinement for more than six decades.

Throughout this research I was forced to challenge the assumption that movement data collected by accelerometer tags represent the normal behavioural repertoire of the tagged animal given low rates of tag sampling frequency currently deployed as well as the significant behavioural modification caused by tagging and handling stress.

I have demonstrated how sampling frequency constraints of the current technology may lead to aliasing of the acceleration signal and thus compromised estimates of energy expenditure and the classification of behaviour. This leads not only to missing and misidentifying routine behaviours (e.g., feeding) but may also lead to missing tagging and handling related behaviours that occur over short time scales. This will directly result in underestimating tag effect and tag load, and a failure to challenge the assumption that the effect of the tag on behaviour and survival of the fish is minimal.

I have further demonstrated that it is necessary to adjust the sampling frequency based on the time-scale of the movement of interest. Apart from the generally descriptive, and cautionary work of Ropert-Coudert and Wilson (2004) and the metabolic studies of Halsey et al. (2009), this is the first quantitative estimate how measuring behaviour and locomotion in fish (and likely other fast moving animals) is a function of the accelerometer sampling frequency; and that decreased sampling frequency results in decreased event detection and identification probability and thus compromises the ability to detect activities or movements that occur over short time scales. This is predominately relevant in biologging studies where typically, data from a few (<10) individuals are captured to make inferences about entire populations (Cooke et al., 2004).

This and other cases exemplify how technological feasibility and availability can affect scientific results and that, prior to broad-scale application, scientific enquiry requires rigorous testing. One further example where available technology has affected scientific enquiry is the estimation of swimming speed in the wild based on average values of acceleration (Wilson et al., 2013b, 2014). In the search of producing 'fail-proof' methods of estimating swimming speed in salmon in the wild, swimming

velocity was calibrated to average acceleration signals in a flume study (Wilson et al., 2013b) prior to field deployments. This method has significant limitations and only applies if fish exhibit little vertical movement and little vertical acceleration (same depth level), exhibit no movements other than steady-swimming, no sheltering, or flow refuging mechanisms (Liao, 2007 which is common is salmon), schooling, burst acceleration, no instances that require the control of stability (Wilson et al., 2013a; Webb and Weihs, 2015) and tag attachment location and animal size, both of which affect absolute acceleration values, are constant across individuals. At least one or more of these assumptions is unlikely to be valid at all times, and therefore, swimming speeds collected from such calibrations are likely compromised. Further, crucial aspects of low swimming speeds (<1 ms^{-1}) are ignored due to nonlinearities in the prediction model (s) (Wilson et al., 2013a). This is especially problematic since these calibrations are now used in various other studies to explain ecological and physiological processes (e.g., Eliason et al., 2013; Burnett et al., 2014a,b). In this case, the motivation for the calibration was the tag technology itself, which was set to automatically calculate average values of acceleration, instead of the raw acceleration time series. Instead of the technology driving scientific inquiry as exemplified here, new hypotheses should prompt the development of increasingly sophisticated tagging technology. I propose that this is best achieved by a collaborative effort between engineers and researchers as exemplified by rapid advancements in sensor design here and in the past (e.g., Sea Mammal Marine Research Unit, UK; Little Leonardo, Japan and many others).

7.2 Future Of Acceleration Biologging

7.2.1 Data Processing

Increasingly sophisticated tagging technology and continued miniaturization of tags will require new battery technologies, increased memory capacity, signal processing capabilities and advancements in data retrieval. The accumulation of high-volume, complex datasets will advance the development of post-processing analytical techniques, similar to those employed in bioinformatics and computational biology. Data collected from such systems will likely see more integration into applied science and management of stocks, habitats and species.

As demonstrated by my research and that of several others, accelerometer measurements can be calibrated and validated by visual observations of tagged animals in the field or laboratory. Such observations can then be used to train classification or machine-learning algorithms that are then used to classify unobserved behaviours from non-validated data (Nathan et al., 2012) as outlined in Chapters 2, 3 and 5. Processing techniques include a variety of machine-learning algorithms (Nathan et al., 2012) such as linear discriminant analysis, support vector machines, classification and regression trees, random forest and artificial neural networks, many of which are most frequently used for various pattern recognition and classification tasks. This approach uses validated observations that are some fraction of the size of the test dataset to determine cross-validated parameters and help ensure robustness in the algorithm performance. These methods often result in very similar accuracies (80 – 90%, Nathan et al., 2012) and each have specific advantages (theoretical foundation, ease of implementation, results, interpretability etc.) and disadvantages (assumptions, computational effort, interpretability, subjectivity etc.).

One of the main disadvantages with this approach is that outcomes are typically species-specific algorithms that rarely apply across species. For example, the algorithm developed in Chapter 3 to differentiate between feeding and escape in an ambush predator would likely fail to classify similar behaviour in species with different prey and predation strategies (e.g., tuna, sturgeon). Another disadvantage with some of these techniques (e.g., regression trees, random forest) is that in real-data applications, classifiers are often based on absolute, maximum or mean values of acceleration (e.g., Nathan et al. 2012). Such values are significantly affected by tag position on the animal and can be affected by animal size. Therefore, these classifiers and associated algorithms may only provide a limited solution to data across individuals and attachment procedures.

Accelerometer validation steps are not always taken and sometimes behaviour is discerned via visual inspection of the acceleration data without developing a classification system based on validation steps (Nathan et al., 2012). In contrast, such

methods are often based on clustering of acceleration segments (e.g., k-means clustering, Bidder et al., 2014) or its frequency content for sinusoidal locomotion patterns (e.g., Sakamoto et al., 2009). Clustering methods can classify behaviour and locomotion in very simple datasets that exhibit large differences in acceleration signature. However, when I applied this type of clustering (e.g., *k*-means clustering of acceleration segments) to behavioural data in fish (Chapter 3) the method did not achieve significant classification accuracy, and most recent studies (e.g., Noda et al., 2013; Noda et al., 2014) reject clustering in favour of classification trees. I hypothesize that this is mainly caused by a high similarity between different behaviour clusters (e.g., feeding vs. escape) concurrent with high variability within behavioural signals (e.g., feeding). Furthermore, the results in Chapter 6 demonstrate that while clustering the frequency content in acceleration segments (Sakamoto et al., 2009) may differentiate between basic locomotion-related behavioural clusters and routines, not all behaviours can be differentiated by inference (e.g., feeding behaviour) and much is left to speculation.

Accumulating open source accelerometer data-processing libraries and data repositories such as 'Movebank' (movebank.org) may allow researchers to share methods and algorithms that apply within species and outline common features of species-specific algorithms to help in determining which analytical methods are most suited across-species. For example, the burst acceleration extraction algorithm developed to extract fast-start events in sculpin (Chapter 3) has multiple applications and can be used to extract various behavioral routines across fish species.

7.2.2 Technological Advancements

Continuing advances in micro-technology and microcontroller signal processing capabilities will likely result in decreased size and more efficient accelerometer units (battery, storage, micro-processors) that will allow for increasing sampling frequencies, onboard processing, greater storage and longer duration. On-board micro-processing, such as already used in some accelerometer tags, decreases the amount of storage of high-resolution data to be archived or transmitted and could be advanced to the point where algorithms determined *a priori* (e.g., activity detection and identification) constantly calculate key parameters, allocate event IDs as they

occur, and store or transmit the data (see Chapter 2, 3; Føre et al., 2011); thus the *in situ* delivery of activities and behaviour over time. A great advantage of on-board processing is that data-compression would allow for relevant information to be transmitted via satellite or acoustic telemetry and directly provide a solution to challenges in high-volume data retrieval. To advance these systems, tags could further be designed to function as storage and acoustic transmitters that constantly collect, process and store data and transmit all stored information when receivers are nearby. Given technological advancements in miniaturization, tags could further be transformed into mobile listening stations where tags function as data storage, transmitters and receivers simultaneously and such technology is already available (e.g., Hayes et al., 2013; Baker et al., 2014; Lidgard et al., 2014). This would greatly advance data recovery since data could be collected across various individuals that may never pass a receiver.

Especially relevant for fisheries research, management of sustainable fishing pressure and determining effects of size-selective fishing, is the development of a 'smart tag' measuring size-at-age and growth rate. Such a tag could also provide the means to establish the validity of measuring growth in fishes with high-resolution temperature records as suggested by Neuheimer and Taggart (2007). Assuming my prediction models can be further validated in nature, and that micro-processing technology of archival accelerometer sensors can employ an *a priori* determined algorithm that continuously (or duty-cycled) calculates size-at-time, then *in situ* estimation of size-at-time and growth rate could be achieved.

Given that microcontroller capabilities with a small footprint (< 1 cm^2) do not yet allow for advanced signal processing, such smart tags are not yet available. To solve the problem surrounding recovery of high-resolution data in fisheries research in the next few years, I propose another solution: the deployment of high-volume, low-cost (disposable) data loggers in fish populations given an active fishery and considerable tag return rates. For example, in the Pacific Halibut fishery across the US and Canada, there is a 10-15% 3-year tag-return rate (Tim Loher, Research Biologist, International Pacific Halibut Commission, *personal communication*), i.e., 10-15% of the tags that are deployed on halibut are recaptured within three years. For a tag

budget of US$150,000, 200 biologging tags could be deployed ($750/tag from Maritime bioLoggers). Given a 15% return rate and a 20% tag failure rate (i.e., similar to PSAT failure rate, Musyl et al., 2011), 24 tags would be recovered within three years. In contrast, assuming similar tag deployment costs, the same budget would be equivalent to deploying 34 PSAT tags (US$4000/tag Wildlife Computers; $400 ARGOS transmission costs). At a reporting rate of ~80% (Musyl et al., 2011), of which of 90% report prematurely (< 100 days), 24 partial and 3 full PSAT datasets would be recovered. Given that data from PSATs are binned and therefore of limited use (esp., the acceleration data) and data-loggers allow for tagging of much smaller fish species, the advantage of deploying data loggers compared to PSATs in fisheries research should be clear.

Hardware advances will likely revolve around further miniaturization of circuitry and improvements in battery durations. Progress in small-scale energy harvesting may also lead to developments of energy generation sources via harvesting kinetic energy created by the animal itself (e.g., Aktakka et al., 2011; Shafer et al., 2015a) or by the surrounding environment (e.g., Shafer et al., 2015b; Shafer and Morgan, 2015) and may lead to further increases in logging duration of the technology given size constrains. This could also allow the development of longer-term studies without the limitation of battery size and tag size.

I predict that the development and commercialization of rechargeable tags will be crucial in further advancing the field of accelerometry. Such tags would not only enable laboratory studies that are crucial for validating behavioural states with many (> 10) individuals and replicas this would also open the possibility to quantifying tagging and tag attachment effects and how to optimize the use of this technology (e.g., duty cycling, sampling frequency, etc.) given size and battery constraints.

7.3 Potential Applications For Accelerometer Biologging

Data integration into Ocean models

Biologging data such as acceleration, temperature or depth provide a great opportunity for ocean model data assimilation. Especially the integration of acceleration data into ocean models has potential. For example, ocean modeling and assimilation of tag data could be used to determine the most likely fish trajectory by assimilation of tag data time, temperature, depth and acceleration (size-at-time, i.e., growth) plus constraints on swimming velocity using tail beat frequency and size from acceleration records. The ocean model would provide the temperature and flow fields that can be used to determine the 'most likely' trajectories and growth rates based on thermal time through minimizing a cost function over all possible paths based on time and size-varying constraints. These are measures that can be used to determine temperature-dependent growth over time, activity and energy budgets, migration potential and likely spawning migrations. The results could directly impact fishery regulations and management policies that hinge on credible science relevant to sustainable management where there are challenges in obtaining reliable data on stock metrics (number, size, biomass, age, growth, maturity, fecundity, spawning, distribution etc.) and growth is a key as it influences virtually all of these states and rates and with number of individuals it determines not only biomass, but sustainable biomass; i.e., 100 kg biomass of 10 immature fish at 10 cm is not sustainably equivalent to 100 kg biomass of 5 mature fish at 30 cm.

Kinematic and biomechanics research

Fish locomotion is highly complex and even the most simple case during steady-swimming (e.g., Lighthill, 1960; Lighthill, 1971; Triantafyllou et al., 1993) requires highly sophisticated understanding of flow dynamics and fish biomechanics. Accelerometers not only allow remote observations of behaviour but also could be used to provide insights into biomechanics and hydrodynamics of fish swimming that are typically achieved in the laboratory with video observations. For example, such tags could be used in laboratory or field studies to investigate mechanisms of size-dependent schooling and the hydromechanical efficiency of schools (Weihs, 1973;

Breder, 1976; Partridge and Pitcher, 1979; Fish, 1999; Hemelrijk et al., 2015), swimming efficiency at lower speeds, flow refuging (Liao, 2007) or size-dependent kinematics (Domenici and Blake, 1997). Biomechanics and locomotion studies therefore would not be constrained to enclosed study areas and free-swimming fish may then provide insights into realistic locomotion, which is challenging using video cameras and other techniques (e.g., flow visualisation, Liao, 2007). If this is combined with advanced flow visualization techniques it may serve to advance insights into swimming efficiency and associated energy expenditure. The development of re-usable tags with high sampling frequencies (> 500 Hz) will be crucial for such applications.

Tool for Aquaculture

A smart tag could be a useful tool in the offshore monitoring of aquaculture operations and significantly advance sustainable aquaculture. Offshore aquaculture operations require the constant and remote monitoring of growth rate (Chapter 4), disease infection (Chapter 5), and food consumption by the farmed animals (e.g., Chapter 4; Føre et al., 2011), all of which could be achieved through smart acceleration tags. These devices could also be pertinent in establishing new species, different use of established species, and how to rear them (feeding, etc.). For example, my research could lead to the development of a tag capable of determining parasitic infection in demersal fish such as Atlantic cod. Cataloging the functional significance of scouring in relation to parasite reduction is particularly important for cod given their economic value in commercial fisheries and aquaculture production (Lysne et al., 1994). Beyond diagnosing parasitic infections in species such as cod, this would prove especially useful given most fish species loose equilibrium in advanced stages of disease, which is exhibited by lateral-vertical rotations due to loss of balance (e.g., whirling disease). In an aquaculture setting this could help with the *in situ* diagnosis of infected fish by monitoring parameters studied here such as % time spent scouring or loss of equilibrium, and when an individual exceeds a predetermined threshold it could then be removed to help contain the infection or administer treatment. This would especially be useful given continuous advancement in miniaturization and low-cost sensor and telemetry applications that would allow for large-scale direct observations and *in situ* diagnostic of infection.

APPENDIX A

Zero-Crossing Algorithm Evaluation

To verify that the parameter input for the algorithm affect on the estimated *TBF* distribution and associated moments was minimal, I tested the low-pass filter cut-off threshold, the input window length (l_W), the window variability threshold for steady swimming segments (*ThS**) for any effect on the estimated dominant *TBF*.

The effect of the low-pass filter cut-off threshold should be minimal if all frequencies of the range of interest are included and this may be different across species, e.g., 0.5 to 7 Hz for saithe (Hess and Videler, 1984; Steinhaussen et al., 2005). However, the use of the low-pass filter is important and if the cut-off threshold was increased (e.g., 30 Hz) then high-frequency noise would be included in the time series and the extracted dominant *TBF* would be biased. Therefore, the use of a low-pass filter set at the lowest threshold possible to a) ensure that maximum observed steady-swimming frequencies were included and b) high-frequency noise was removed.

Figure A.1 shows the weighted distribution of dominant *TBF* for window length from 1 to 60 s given a constant threshold parameter (*ThS** = 0.05) and a low-pass filter cut-off of 15 Hz. Since estimated median *TBF* was largely independent of window length, input window length did not have a significant effect on the distribution of dominant *TBF* given a constant window variability threshold *ThS**. Further, input window length did not have a measurable effect on the extracted median *TBF* (Figure A.2). However, given the need to resolve low-frequency swimming for large fish (e.g., in saithe ~ 0.5 Hz; Steinhaussen et al., 2005) a species-specific window length that exceeded and resolved the lowest observed frequency (e.g., for saithe, $l_W \geq 2$ s) is recommended. Therefore, I chose a window length of 5 seconds.

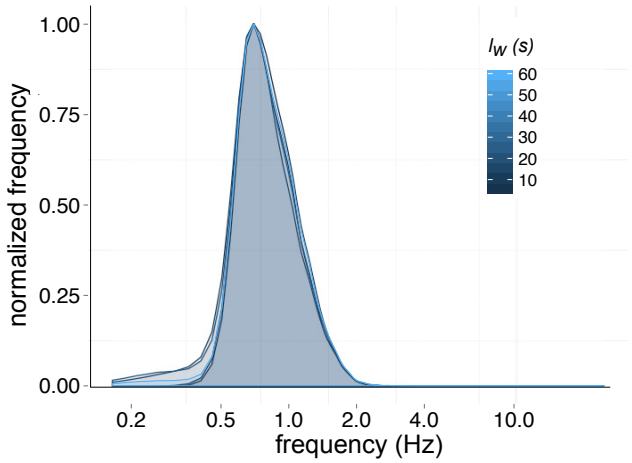

Figure A.1 Normalized tail beat frequency distributions function for input windows, l_W of different lengths from 1 second to 60 seconds.

Figure A.2 shows the estimated median *TBF* as a function of the input threshold value, *ThS**. While *TBF* estimates were all within one standard deviation of each other, estimates of median *TBF* decreased with increasing values of *ThS** to a point where they stabilized at *ThS** = 0.05. Low values of *ThS** impose a very strict rule to the variability within the differenced *Δt's*, i.e., most $(\Delta t_j - \Delta t_{j+1})_{max}$ - $(\Delta t_j - \Delta t_{j+1})_{min}$ variations were considered too high and therefore discarded resulting in the extraction of very short windows. Therefore, I chose a threshold of *ThS** ≥ 0.05.

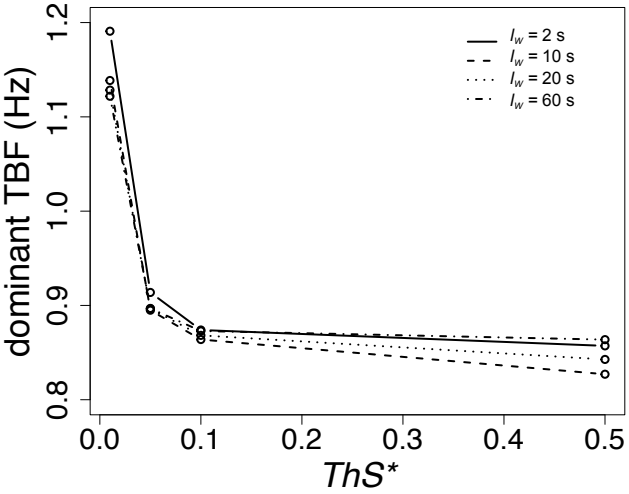

Figure A.2 Estimated median dominant *TBF* (Hz) as a function of window length, l_W and threshold parameter input for window variability to the zero-crossing algorithm for one fish.

Comparison to other peak frequency extraction techniques

Additionally, when the dataset was re-analyzed using other methods (e.g., traditional wavelet analysis, cf. Chapter 6), extracted *TBF* estimates were similar to dominant TBF estimates based on the zero-crossing method, and the scaling relationship between *TBF* and length was confirmed. Yet, for a traditional wavelet analysis, the extraction of peak frequencies can be a non-trivial issue (e.g., Iatsenko et al., 2013) and can be dependent on the chosen mother wavelet and associated scale, the signal amplitude threshold or chosen spectrum entropy all of which can vary across spectra. In comparison to zero-crossing computations, the wavelet approach additionally required greater computational power. Given the robustness of the zero-crossing approach to input parameters and the difference in computational effort between the methods, the zero-crossing provides more potential for incorporation into a on-board processing environment and was therefore used here.

BIBLIOGRAPHY

Aitken, A. C. (1935). On the least squares and linear combinations of observations. *Proc. R. Soc. Edinburgh* **55**, 42-48.

Adams, S. R., Parsons, G. R., Hoover, J. J. and Kilgore, K. J. (1997). Observations of swimming ability in shovelnose sturgeon (*Scaphirhynchus platorynchus). J. Fresw. Ecol.* **12**, 631-633.

Aktakka, E. E., Im, H. and Najafi, K. (2011). Energy scavenging from insect flight. *J. Microm. Microeng.* **21**, 095016.

Armsworthy, S. L., Trzcinski, M. K. and Campana, S. E. (2014). Movements, environmental associations, and presumed spawning locations of Atlantic halibut (*Hippoglossus hippoglossus*) in the northwest Atlantic determined using archival satellite pop-up tags. *Mar. Biol.* 161, 645-656.

Arnold, G. P. and Holdford, B. H. (1978). The physical effects of an acoustics tag on the swimming performance of plaice and cod. *J. Cons. Int. Explor. Mer.* **38**, 189-200.

Axenrot, T., Didrikas, T., Danielsson, C. and Hansson S. (2004). Diel patterns in pelagic fish behaviour and distribution observed from a stationary, bottom-mounted, and upward-facing transducer. *ICES J. Mar. Sci.* **61**, 1100-1104.

Bainbridge, R. (1958) The speed of swimming fish as related to size and to the frequency and amplitude of the tail beat. *J. Exp. Biol* **35**, 109-133.

Bainbridge, R. (1961). Problems of fish locomotion. *Symp. Zool. Soc. Lond.* **5**, 13-32.

Baker, L. L., Jonsen, I. D., Flemming, J. E. M., Lidgard, D. C., Bowen, W. D., Iverson S. J. and Webber, D. M. (2014). Probability of detecting marine predator-prey and species interactions using novel hybrid acoustic transmitter-receiver tags. *PLoS ONE* **9**, e98117.

Barber, I., Hoare, D. and Krause, J. (2000). Effects of parasites on fish behaviour: a review and evolutionary perspective. *Rev. Fish Biol. Fish.* **10**, 131-165.

Barrowman, N. J. and Myers, R. A. (1996). Tag-shedding rates of experiments with multiple tag types. *Biometrics* **52**, 1410-1416.

Bidder, O. R., Campbell, H. A., Gómez-Laich, A., Urgé, P., Walker, J., Cai, Y., Gao, L., Quintana, F. and Wilson, R.P. (2014). Love thy neighbour: automatic animal behavioural classification of acceleration data using the k-nearest neighbour algorithm. *PLoS ONE* **9**, e88609.

Björnsson, B., Karlsson, H., Thorsteinsson, V. and Solmundsson, J. (2011). Should all fish in mark-recapture experiments be double-tagged? Lessons learned from tagging coastal cod (*Gadus morhua*). *ICES J. Mar. Sci.* **68**, 603-610.

Blake, R. W. (1983). *Fish locomotion*. Cambridge University Press: Cambridge

Block, B. A., Dewar, H., Farwell, C. and Prince, E. D. (1998). A new satellite technology for tracking the movements of Atlantic bluefin tuna. *Proc. Natl. Acad. Sci. USA* **95**, 9384-9389.

Block, B. A., Dewar, H., Blackwell, S. B., Williams, T. D., Prince, E. D., Farwell, C. J., Boustany, A., Teo, S. H., Seitz, A., Walli, A. and Fudge, D. (2001). Migratory movements, depth preferences, and thermal biology of Atlantic bluefin tuna. *Science* **293**, 1310-1314.

Bograd, S. J., Block, B. A., Costa, D. P. and Godley, B. J. (2010). Biologging technologies: new tools for conservation. Introduction. *Endang. Species Res.* **10**, 1-7.

Bouten, C. V., Westerterp, K. R., Verduin, M., Janssen, J. D. (1994). Assessment of energy expenditure for physical activity using a triaxial accelerometer. *Med. Sci. Sports Exerc.* **26**, 1516-1523.

Breder, C. M. (1976) Fish schools as operational structures. *Fish. Bull.* **74**, 471-502.

Bridger, C. J. and Booth, R. K. (2003). The effects of biotelemetry transmitter presence and attachment procedures on fish physiology and behaviour. *Rev. Fish. Sci.* **11**, 13-34.

Brodeur, R. D. and Wilson, M. T. (1996). Mesoscale acoustic patterns of juvenile walleye pollock (*Theragra chalcogramma*) in the western Gulf of Alaska. *Can. J. Fish. Aquat. Sci.* **53**, 1951-1963.

Brown, R.S., Geist, D.R., Deters, K.A and Grassell, A. (2006). Effects of surgically implanted acoustic transmitters > 2% of body mass on the swimming performance, survival and growth of juvenile sockeye and Chinook salmon. *J. Fish Bi*ol. **69**, 1626-1638.

Burnett, N. J., Hinch, S. G., Braun, D. C., Casselman, M. T., Middleton, C. T., Wilson, S. M. and Cooke, S. J. (2014a). Burst swimming in areas of high flow; delayed consequences of anaerobiosis in wild adult sockeye salmon. *Physiol. Biochem. Zool: Eol. Evol. Appr.* **87**, 587-598.

Burnett, N. J., Hinch, S. G., Donaldson, M. R., Furey, N. B., Patterson, D. A., Roscoe, D. W. and Cooke, S. J. (2014b). Alterations to dam-spill discharge influence sex-specific activity, behaviour and passage success of migrating adult sockeye salmon. *Ecohydrology* **7**, 1094-1104.

Burnham, K. P. and White, G. C. (2002). Evaluation of some random effects methodology applicable to bird ringing data. *J. Appl. Stat.* **29**, 245-264.

Bushberg, J. T. (2012). *The Essential Physics of Medical Imaging*. Philadelphia: Wolters Kluwer Health/Lippincott Williams & Wilkins.

Campana, S.E. and Neilson, J.D. (1985). Microstructure of fish otoliths. *Can. J. Fish. Aquat. Sci.* **42**, 1014-1032.

Campana, S. (1990). How reliable are growth back-calculations based on otoliths? *Can. J. Fish. Aquat. Sci.* **47**, 2219-2227.

Campana, S. E., Dorey, A., Fowler, M., Joyce, W., Wang, Z. and Wright D. (2011). Migration pathways, behavioural thermoregulation and overwintering grounds of blue sharks in the Northwest Atlantic. *PLoS ONE* **6**, e16854.

Cargnelli, L. M., Grisback, S. J., Packer, D. B., Berrien, P. L., Johnson, D. L. and Morse, W. W. (1999). Pollock, *Pollachius virens*, life history and habitat characteristics. *NOAA Tech. Memo.* NMFS-NE-131

Carroll, G., Slip, D., Jonsen, I. and Harcourt, R. (2014). Supervised accelerometry analysis can identify prey capture by penguins at sea. *J. Exp. Biol.* **217**, 4295-4302.

Cartamil, D. P. and Lowe, C.G. (2004). Diel movement patterns of ocean sunfish *Mola mola* off southern California. *Mar. Ecol. Prog. Ser.* **266**, 245–253.

Chaprales, W., Lutcavage, M., Brill, R., Chase, B. and Skomal, G. (1998). Harpoon method for attaching ultrasonic and 'popup' satellite tags to giant bluefin tuna and large pelagic fishes. *Mar. Technol. Soc. J.* **32**, 104-105.

Chattopadhya, S., Moldovan, R., Yeung, C., and Wu, X. L. (2006). Swimming efficiency of bacterium *Escherichia coli*. *PNAS* **103**, 13712-13717.

Chen, K. Y. and Bassett, D. R. (2005). The technology of accelerometer-based activity monitors: Current and future. *Med. Sci. Sports Exerc.* **37**, S490-S500

Cheng, J.-Y., Pedley, T. J. and Altringham, J. D. (1998). A continuous dynamic beam model for swimming fish. *Phil. Trans. R. Soc. Lond. B* **353**, 981–997.

Cheong, T. S., Kavvas, E. M. L., Andreson, E. E. K. (2006). Evaluation of adult white sturgeon swimming capabilities and applications to fishway design. *Environ. Biol. Fish* **77**, 197-208.

Christiansen, P. (1999). Scaling of the limb long bones to body mass in terrestrial mammals. *J. Morph.* **239**, 167-190

Clark, T. D., Sandblom, E., Hinch, S. G., Patterson, D. A., Frappell, P. B. and Farrell, A. P. (2010). Simultaneous biologging of heart rate and acceleration, and their relationships with energy expenditure of free-swimming sockeye salmon (*Oncorhynchus nerka*). *J. Comp. Physiol. B* **180**, 673-684.

Clarke, A. and Johnston N. M. (1999). Scaling of metabolic rate with body mass and temperature in teleost fish. *J. Anim. Ecol.* **68**, 893-905.

Collins, M. R., Cooke, D. W., Smith, T. I. J., Post, W. C., Russ, D. C. and Walling D. C. (2002). Evaluation of four methods of transmitter attachment on shortnose sturgeon, *Acipenser brevirostrum*. *J. Appl. Icthyol.* **18**, 491-494.

Cooke, S. J. (2003). Externally attached radio transmitters do not affect the parental care behaviour of rock bass. *F. Fish Biol.* **62**, 965-970.

Cooke, S. J., Hinch, S. G., Wikelski, M., Andrews, R. D., Kuchel, L. J., Wolcott, T. G. and Butler, P. J. (2004). Biotelemetry: a mechanistic approach to ecology. *Trends Ecol. Evol.* **19**, 334-343.

Cooke, S. J, Woodley, C. M., Eppard, M. B., Brown, R. S. and Nielsen, J. L. (2012). Advancing the surgical implantation of electronic tags in fish: a gap analysis and research agenda based on a review of trends in intracoelomic tagging effect studies. *Rev. Fish Biol. Fish.* **21**, 127-151.

Dadswell, M. J. (1979). Biology and population characteristics of the shortnose sturgeon, *Acipenser brevirostrum* LeSueur 1818 (Osteichthyes: Acipenseridae), in the Saint John River Estuary, New Brunswick, Canada. *Can. J. Zool.* **57**, 2186–2210.

Deslauriers, D. and Kieffer, J.D. (2012). Swimming performance and behaviour of young-of-the-year shortnose sturgeon (*Acipenser brevirostrum*) under fixed and increased velocity tests. *Can. J. Zool.* **90**, 345–351.

Domenici, P. and Blake, R.W. (1997). The kinematics and performance of fish fast-start swimming. *J. Exp. Biol.* **200**, 1165-1178.

Domenici, P., Standen, E. M. and Levine, R. P. (2004). Escape maneuvers in spiny dogfish. *J. Exp. Biol.* **207**, 2339-2349.

Drenner, S. M., Clark, T. D., Whitney, C. K., Martins, E. G., Cooke, S. J. and Hinch, S. G. (2012). A synthesis of tagging studies examining the behaviour and survival of anadromous salmonids in marine environments. *PLoS ONE.* **7**, e31311.

Eliason, E. J., Wilson, S. M., Farrell, A. P., Cooke, S. J. and Hinch, S. G. (2013). Low cardiac and aerobic scope in a coastal population of sockeye salmon *Oncorhynchus nerka* with a short upriver migration. *J. Fish Biol.* **82**, 2104-2112.

Eschmeyer, P. H. (1959). Survival and retention of tags, and growth of tagged lake trout in a rearing pond. *Prog. Fish Cult.* **21**, 17-21.

Esteve, M. (2005). Observations of spawning behaviour in Salmoninae: *Salmo, Oncorhynchus* and *Salvelinus*. *Rev. Fish Biol. Fish.* **15**, 1-2.

Evans, D. M. (1994). Observations on the spawning behaviour of male and female adult sea trout, *Salmo trutta* L., using radiotelemetry. *Fish. Manage. Ecol.* **1**, 91-105.

Faust, M. D., Breeggemann, J. J., Bahr, S. and Graeb, B.D.S. (2013). Precision and bias of cleithra and sagittal otoliths used to estimate ages of northern pike. *J. Fish. Wild. Manag.* **4**, 332-341.

Fedak, M., Lovell, P., McConnell, B. and Hunter, C. (2002). Overcoming the constraints of long range radio telemetry from animals: getting more useful data from smaller packages. *Integr. Comp. Biol.* **42**, 3-10.

Ferreira, B. P. and Russ, G. R. (1994). Age validation and estimation of growth rate of the coral trout, *Plectropomus leopardus*, (Lacepede 1802) from Lizard Island, Northern Great Barrier Reef. *Fish. Bull.* **92**, 46-57.

Fish, F. E. (1999) Energetics of swimming and flying in formation. *Comm. Theor. Biol.* **5**, 283–304.

Føre, M., Alfredsen, J. A. and Gronningsater, A. (2011). Development of two telemetry based systems for monitoring the feeding behavior of Atlantic salmon (*Salmon salar* L.) in aquaculture sea-cages. *Comp. Electron. Agr.* **76**, 240-251.

Francis, R. I. C. C. and Campana, S. (2004). Inferring age from otolith measurements: a review and a new approach. *Can. J. Fish. Aquat. Sci.* **61**, 1269-1284.

Gazzola, M., Argentina, M., and Mahadevan, L. (2014) Scaling macroscopic aquatic locomotion. *Nature Phys.* **10**, 758–761.

Geist, D. R., Brown, R. S., Cullinan, V., Brink, S. R., Lepla, K., Bates, P. and Chandler, J.A. (2005). Movement, swimming speed, and oxygen consumption of juvenile white sturgeon in response to changing flow, water temperature, and light level in the Snake River, Idaho. *Trans. Am. Fish. Soc.* **134**, 803-816.

Glazier, D. S. (2005). Beyond the '3/4-power law': variation in the intra-and interspecific scaling of metabolic rate in animals. *Bio. Rev* **80**, 611-662.

Gleiss, A. C., Norman, B., Liebsch, N., Francis, C. and Wilson, R. P. (2009). A new prospect for tagging large free-swimming sharks with motion-sensitive data-loggers. *Fish. Res.* **97**, 11-16.

Gleiss, A. C., Dale, J. J., Holland, K. N. and Wilson, R. P. (2010). Accelerating estimates of activity-specific metabolic rate in fish: testing the applicability of acceleration data loggers. *J. Exp. Mar. Biol. Ecol.* **385**, 85-91.

Gleiss, A. C., Norman, B. and Wilson, R. P. (2011). Moved by that sinking feeling: variable diving geometry underlies movement strategies in whale sharks. *Funct. Ecol.* **25**, 595-607.

Goldbogen, J. A., Clambokidis, J., Oleson, E., Potvin, J., Pyenson, N. D., Schoor, G. and Shadwick, R. E. (2011). Mechanics, hydrodynamics and energetics of blue whale lung feeding: efficiency dependence on krill density. *J. Exp. Biol.* **214**, 131-146.

Goolish, E. M. (1991). Aerobic and anaerobic scaling in fish. *Biol Rev.* **66**, 33-36.

Gray, J. (1968). *Animal Locomotion. World Naturalist Series*. London: Weidenfeld and Nicolson

Greenstreet, S. P. R. and Morgan, R. I. G. (1989). The effect of ultrasonic tags on the growth rates of Atlantic salmon, *Salmo salar* L., parr of varying size just prior to smolting. *J. Fish Biol.* **35**, 301-309.

Gröger, J. P., Rountree, R. A., Thygesen, U. H., Jones, D., Martins, D., Xu, Q., Rothschild, B. J. (2007). Geolocation of Atlantic cod (*Gadus morhua*) movements in the Gulf of Maine using tidal information. *Fish. Oceanogr.* **16**, 317-335.

Halsey, L. G., Green, J. A., Wilson, R. P. and Frappell, P. B. (2009). Accelerometery to estimate energy expenditure during activity: best practice with data loggers. *Physiol. Biochem. Zool.* **82**, 396-404

Harper, D. G. and Blake, R.W. (1989). A critical analysis of the use of high-speed film to determine maximum accelerations of fish. *J. Exp. Biol.* **142**, 467-471.

Harper, D.G. and Blake, R.W. (1990). Prey capture and the fast-start performance of rainbow trout *Salmo gairdneri* and northern pike *Esox Lucius*. *J Exp. Biol.* **150**, 321-342.

Hayes, S. A., Teutshel, N. M., Michel, C. J., Champagne, C., Robinson, P. W., Fowlser, M., Yack, T., Mellinger, D. K., Simmons, S., Costa, D. P. and MacFarlane, R. B. (2013). Mobile receivers: releasing the mooring to 'see' where fish go. *Environ. Biol. Fish* **96**, 189-201.

Hemelrijk, C. K., Reid, D. A. P., Hildenbrandt, H. and Padding, J. T. (2015). The increased efficiency of fish swimming in a school. *Fish Fish.* **16**, 511–521.

Hess, F. and Videler, J. J. (1984). Fast continuous swimming of saithe (*Pollachius virens*): a dynamic analysis of bending moments and muscle power. *J. Exp. Biol.* **109**, 229-251.

Hill, A. V. (1950) The dimensions of animals and their muscular dynamics. *Science Progr.* **38**, 209-230.

Hoerner, S. F. (1965) *Fluid-Dynamic Drag: Practical Information on Aerodynamic Drag and Hydrodynamic Resistance*. Hoerner Fluid Dynamics, Midland Park, NJ.

Hoolihan, J. P., Luo, J., Abascal, F. J., Campana, S. E., De Metrio, G., Dewar, H., Domeier, M. L., Howey, L. A., Lutcavage, M. E., Musyl, M. K., Neilson, J. D., Orbesen, E. S., Prince E. D., Rooker, J. R. (2011). Evaluating post-release behaviour modification in large pelagic fish deployed with pop-up satellite archival tags. *ICES J. Mar. Sci.* **68**, 880–889.

Hughes Clark, J. E. and Parrott, R., (2001) *Integration of dense, time-varying water column information with high-resolution swath bathymetric data*. U.S. Hydrographic Conference, Norfolk VA, USA.

Hunter E., Metcalfe J. D., Holford B. H., Arnold G. P. (2004). Geolocation of free-ranging fish on the European continental shelf as determined from environmental variables II. Reconstruction of plaice ground-tracks. *Mar. Biol.* **144**, 787-798.

Iatsenko, D., McClinktock, P. V. E. and Stefanovska (2013). On the extraction of instantaneous frequencies from ridges in time-frequency representations of signal. arXiv:1310.7276.

InveSense (2014). PS-MPU-9250A-01. Retrieved from http://store.invensense.com/datasheets/invensense/MPU9250REV1.0.pdf

Jadot, C. (2003). Comparison of two tagging techniques for *Sarpa salpa:* external attachment and intraperitoneal implantation. *Oceanol. Acta*. **26**, 497-501.

Janak, J., Brown, R., Colotelo, A., Pfugrath, B., Stephenson, J., Deng, Z., Carlson, T. and Seaburg, A. (2014). The effects of neutrally buoyant externally attached transmitters on swimming performance and predator avoidance of juvenile chinook salmon. *Trans. Am. Fish. Soc.* **141**, 1424-1432.

Jensen, J. L. A., Halttunenen, E., Thorstad, E.B., Næsje, T.F. and Rikardsen, A.H. (2010). Does catch-and-release angling alter the migratory behaviour of Atlantic salmon? *Fish. Res.* **106**, 550-554.

Jepsen, N., Thorstad, E. B., Havn, T. and Lucas, M.C. (2015). The use of external electronic tags on fish: an evaluation of tag retention and tagging effects. *Anim. Biotel.* **3**:49.

Johansen, S. D., Coucheron, D. J., Andreassen, M., Karlsen, B. O., Furmanek, T., Jørgensen, T. E., Emblem, Å., Breines, R., Nordeide, J. T., Moum, T., et al. (2009). Large scale sequence analyses of Atlantic cod. *N. Biotechnol.* **25**, 263-271.

Johnson, M. W., Diamond, S. L. and Stunz, G. W. (2015). External attachment of acoustic tags to deep water reef fishes: an alternate approach when internal implantation affects experimental design. *Trans. Am. Fish. Soc.* **144**, 851-859.

Jones, M. and Taggart, C. T. (1998). Distribution of gill parasite (*Lernaeocera branchialis*) infection in Atlantic cod (*Gadus morhua*) and parasite-induced host mortality: inferences from tagging data. *Can. J. Fish. Aquat. Sci.* **55**, 364-375.

Jones, T. T., Van Houtan, K. S., Bostrom, B. L., Ostafichuk, P., Mikkelsen, J., Tezcan, E., Carey, M., Imlach, B. and Seminoff, J. A. (2013). Calculating the ecological impacts of animal-borne instruments on aquatic organisms. *Methods Ecol. Evol.* **4**, 1178-1186.

Kaur, S. (2013). The revolution of the tablet computers and apps: a look at emerging trends. *Consumer Electronics Magazine, IEEE.* **2**, 36-41.

Kawabe, R., Nashimoto, K., Hiraishi, T., Naito, Y. and Sato, K. (2003*a*). A new device for monitoring the activity of freely swimming flatfish, Japanese flounder *Paralichthys olivaceus*. *Fisheries Sci.* **69**, 3-10.

Kawabe, R., Kawano, T., Nakano, N., Yamashita, N., Hiraishi, T. and Naito, Y. (2003*b*). Simultaneous measurement of swimming speed and tail beat activity of free swimming rainbow trout *Oncorhynchus mykiss* using an acceleration data-logger. *Fisheries Sci.* **69**, 959-965.

Kedem, B. (1986) Spectral analysis and discrimination by zero-crossings. *Proc. IEEE* **74**, 1477-1493.

Kern, S. and Koumoutsakos, P. (2006) Simulations of optimized anguilliform swimming. *J.Exp. Biol.* **209**, 4841-4857.

Kieffer, J. and Cooke, S. J. (2009). *Physiologcy and organismal performance of centrachids*. In: centrachids Fishes: Diversity, Biology and Conservations. S.J. Cooke, D.P. Philipp (Eds), Wiley-Blackwell, U.K.

Kohannim, S. and Iwasaki, T. (2014). Analytical insights into optimality and resonance in fish swimming. *J. R. Soc. Interface* **11**, 20131073.

Krause, J., Reeves, P. and Hoare, D. (1998). Positioning behaviour in roach shoals: the role of body length and nutritional state. *Behaviour* **135**, 1031-1039.

Kushner, D. (2011). The making of Arduino. IEEE Spectrum. 26 Oct. 2011.

Kynard, B. (1997). Life history, latitudinal patterns, and status of the shortnose sturgeon, Acipenser brevirostrum. *Env. Biol. Fish*. **48**, 319-334.

Liao, J. C. (2007). A review of fish swimming mechanics and behaviour in altered flows *Phil. Trans. R. Soc. B* **362**, 1973-1993.

Lidgard, D. C., Bowen, W. D., Jonsen, I. D., McConnell, B. J., Lovell, P., Webber, D. M., Stone, T. and Iverson, S.J. (2014). Transmitting species-interaction data from animal-borne transceivers through Service Argos using Bluetooth communication. *Methods Evol. Evol.* **5**, 864-871.

Lighthill, M. J. (1960) Note on the swimming of slender fish. *J. Fluid Mech*. **9**, 305-317.

Lighthill, M. J. (1971). Large-amplitude elongated-body theory of fish locomotion. *Proc. R. Soc. Lond. B* **179**, 125-138.

Long, J. H. (1995). Morphology, mechanics, and locomotion: the relation between the notochord and swimming motions in sturgeon. *Env. Biol. Fish*. **44**, 199-211.

Lowe, C. G. and Goldman, K. J. (2001). Thermal and bioenergetics of elasmobranchs: bridging the gap. *Env. Biol. Fish*. **60**, 251-266.

Lowe, C. G. (2002). Matabolic rates of juvenile scalloped hammerhead sharks (*Sphyrna lewini*). *Mar. Biol.* **139**, 447-453.

Lucas, M. C. and Batley, E. (1996). Seasonal movements and behaviour of adult barbel *Barbus barbus*, a riverine cyprinid fish: implications for river management. *J. Appl. Ecol.* **33**, 1345-1358.

Lutcavage, M., Rhodin, A. G. J., Sandove, S. S. and Conroy, C. R. (2001). Direct carapacial attachment of satellite tags using orthopedic bioabsorbable mini-anchor screws on leatherback turtles in Culebra, Puerto Rico. *Mar. Turtle. Newsl.* **95**, 9-12.

Lysne, D. A., Hemmingsen, W. and Skorping, A. (1994). Distribution of Cryptocotyle spp. metacercariae in the skin of caged Atlantic cod (*Gadus morhua*). *J Fish Biol.* **45**, 352-355.

Marras, S., Noda, T., Steffensen, J. F., Svendsen, M. B. S., Krause, J., Wilson, A. D. M., Kurvers, R. H. J. M., Herbert-Read, J., Boswell, K. M., Domenici, P. (2015). Not so fast: swimming behavior of sailfish during predator–prey interactions using high-speed video and accelerometry *Integr. Comp. Biol.* **55**, 719-727.

McFarlane, G. A., Wydoski, R. S. and Prince, E. D. (1990). Historical review of the development of external tags and marks. *Symp. Am. Fish. Soc.* **7**, 9-29.

McMahon, C. R., Hindell, M. A. and Harcourt, R. G. (2012). Publish or perish: why it's important to publicise how and if, research activities affect animals. *Wildl. Res.* **39**, 375-377.

Mellas, E. J. and Haynes, J. M. (1985). Swimming performance and behavior of rainbow trout (*Salmo gairdneri*) and white perch (*Morone americana*): effects of attaching telemetry transmitters. *Can. J. Fish. Aquat. Sci.* **42**, 488-493.

Metcalfe, C. D., Dadswell, M. J., Gillis, G. F. and Thomas, M. L. H. (1976). Physical, chemical, and biological parameters of the Saint John River Estuary, New Brunswick, Canada. *Fisheries and Marine Service Canada Technical Report* **686**.

Methling, C., Tudorache, C., Skov, P. V. and Steffensen, J. F. (2011). Pop up satellite tags impair swimming performance and energetics of the European eel (*Anguilla anguilla*). *PLoS ONE* **6**, e20797.

Motani, R. (2002). Scaling effects in caudal fin propulsion and the speed of ichthyosaurs. *Nature* **415**, 309-312.

Muramoto, H., Ogawa, M., Suzuki, M. and Naito, Y. (2004). Little Leonardo digital data logger: its past, present and future role in bio-logging science. *Mem. Natl. Ins. Polar Res.* **58**, 196-202.

Murchie, K. J, Cooke, S. J., Danylchuk, A. J. and Suski, C. D. (2010). Estimates of field activity and metabolic rates of bonefish (*Albula vulpes*) in coastal marine habitats using acoustic tri-axial accelerometer transmitters and intermittent-flow respirometry. *J. Exp. Mar. Biol. Ecol.* **396**, 147-155.

Musyl, M. K., Domeier, M. L., Nasby-Lucas, N., Brill, R. W., McNaughton, L. M., Swimmer, J. Y., Lutcavage, M. S., Wilson, S. G., Galuardi, B. and Liddle, J. B. (2011). Performance of pop-up satellite archival tags. *Mar Ecol. Prog. Ser.* **433**, 1-28.

Nakamura, I., Watanabe, Y. Y., Papastamatiou, Y. P., Sato, K., Meyer, C. G. (2011). Yo-yo vertical movements suggest a foraging strategy for tiger sharks *Galeocerdo cuvier*. *Mar. Ecol. Prog. Ser.* **424**, 237-246.

Nathan, R., Spiegel, O., Fortmann-Roe, S., Harel, R., Wikelski, M. and Getz, W. M. (2012). Using tri-axial acceleration data to identify behavioral modes of free-ranging animals: general concepts and tools illustrated for griffon vultures. *J. Exp. Biol.* **215**, 986-996.

Neuheimer, A. B. and Taggart, C. T. (2007) Growing degree-day and fish size-at-age: the overlooked metric. *Can. J. Fish Aquat. Sci.* **64**, 375-385.

Noda, T., Kawabata, Y., Arai, N., Mitamura, H. and Watanabe, S. (2013). Monitoring escape and feeding behaviours of cruiser fish by inertial and magnetic sensors. *PLoS ONE* **8**, e79392.

Noda, T., Kawabata, Y., Arai, N., Mitamura, H., and Watanabe, S. (2014). Animal-mounted gyroscope/accelerometer/magnetometer: in situ measurement of the movement performance of fast-start behaviour in fish. *J. Exp. Mar. Biol. Ecol.* **451**, 55-68

Ogata, K. (1970) *Modern Control Engineering*. Englewood Cliffs, NJ: Prentice-Hall.

Oppenheim, A. V. and Shafer, R. W. (1989). *Discrete-time signal processing*. Englewood Cliffs, NJ: Prentice-Hall, Inc.

O'Toole, A. C., Murchie, K. J., Pullen, C., Hanson, K. C., Suski, C. D., Danylchuk, A. J. and Cooke, S. J. (2010). Locomotory activity and depth distribution of adult great barracuda (*Sphyraena barracuda*) in Bahamian coastal habitats determined using acceleration and pressure biotelemetry transmitters. *Mar. Freshw. Res.* **61**, 1446-1456.

Panfili, J. and Ximenes, M.-C. (1992). Measurements on ground or sectioned otoliths: possibilities of bias. *J. Fish. Biol.* **41**, 201-207.

Pannella, G. (1971). Fish otoliths: daily growth layers and periodical patterns. *Science* **173**, 1124-1127.

Partridge, B. L. and Pitcher, T. J. (1979) Evidence against a hydrodynamic function for fish Schools. *Nature* **279**, 418-419.

Payne, N. L., Gillanders, B. M., Seymour, R. S., Webber, D. M., Snelling, E. P. and Semmens, J. M. (2011). Accelerometry estimates field metabolic rate in giant Australian cuttlefish *Sepia apama* during breeding. *J. Anim. Ecol.* **80**, 422-430.

Payne, N. L., Taylor, M. D., Watanabe, Y. Y., Semmens, J. M. (2014). From physiology to physics: are we recognizing the flexibility of biologging tools? *J. Exp. Biol.* **217**, 317-322.

Peake, S., Beamish, F. W. H., McKinley, R. S., Scruton, D. A., Katopodis, C. (1997). Relating swimming performance of lake sturgeon, *Acipenser fulvescens*, to fishway design. *Can. J. Fish. Aquat. Sci.* **54**, 1361-1366.

Pedley, T. J. (1977). *Scale effects in animal locomotion*. London; New York, N.Y.: Academic Press

Peters, R. H. (1983). *The ecological implications of body size*. Cambridge Cambridgeshire; NY: Cambridge University Press

Petersen, C. G. J. (1896). The yearly immigration of young plaice into the Limfjord from the German Sea. *Rep. Dan. Biol. Stn. Copenhagen.* **6**, 5-30.

Pflug, L. A., Ioup, G. E. and Ioup, J. W. (1993). Sampling requirements and aliasing for higher-order correlations. *J. Acoust. Soc. Am.* **94**, 2159-2172.

Preston, T. J., Chiaradia, A., Caarels, S. A. and Reina, R. D. (2010). Fine scale biologging of an inshore marine animal. *J. Exp. Mar. Bio. Ecol.* **390**, 196-202.

Prince, E. D., Ortiz, M., Venizelos, A. and Rosenthal, D. S. (2002). In- water conventional tagging techniques developed by the Cooperative Tagging Center for large, highly migratory species. In: Lucy JA, Studholme AL (eds) Catch and re- lease in marine recreational fisheries. *Am. Fish. Soc. Symp.* **30**, 155-171.

Robinson, M. P. and Motta P. J. (2002). Patterns of growth and the effects of scale on the feeding kinematics of the nurse shark (*Ginglymostoma cirratum*). *J. Zool. Lond.* **256**, 449-462.

Ropert-Coudert, Y. and Wilson, R. P. (2004). Subjectivity in bio-logging science: do logged data mislead? *Mem. Natl. Ins. Polar Res.* **58**, 23-33.

Ropert-Coudert, Y. and Wilson, R. P. (2005). Trends and perspectives in animal-attached remote sensing. *Front. Ecol. Environ.* **3**, 437-444.

Ross, M. J., and McCormick, J. H. (1981). Effects of external radio transmitters on fish. *Progr. Fish Cult.* **43,** 67–72.

Rounsefell, G. A. and Lawrenec, K. (1945). How to mark fish. *T. Am. Fish. Soc.* **73**, 320-363.

Rutz, C. and Hays, G. C. (2009). New frontiers in biologging science. *Biol. Lett.* **5**, 289-292.

Sabin, W. E. (2008). *Discrete-signal analysis and design*. Hoboke, NJ: Wiley-Interscience.

Sakamoto, K. Q., Sato, K., Ishizuka, M., Watanuki, Y., Takahashi A., Daunt, F. and Wanless, S. (2009). Can ethograms be automatically generated using body acceleration data from free ranging birds? *PLoS ONE* **4**, e5379.

Sardenne, F., Dortel, E., Le Croizier, G., Million, J., Labonne, M., Leroye, B., Bodina, N. and Chassot, E. (2015). Determining the age of tropical tunas in the Indian Ocean from otolith microstructures. *Fish. Res.* **16**, 44-57.

Sastry, S. V. A. R., Sreenu, P. (2012). Applications of nanotechnology in the field of environment. Engineering Education: Innovative Practices and Future Trends (AICERA), *IEEE International Conference* 1-19

Sato, K., Watanuki, Y., Takahashi, A., Miller, P. J. O., Tanaka, H., Kawabe, R., Ponganis, P. J., Handrich, Y., Akamatsu, T., Watanabe, Y. et al. (2007). Stroke frequency, but not swimming speed, is related to body size in free-ranging seabirds, pinnipeds and cetaceans. *Proc. Roy. Soc. B* **274**, 471-477.

Sato, K., Sakamoto, K. Q., Watanuki, Y., Takahashi, A., Katsumata, N., Bost, C.-A. and Weimerskirch, H. (2009). Scaling of soaring seabirds and implications for flight abilities of giant Pterosaurs. *PLoS ONE* **4**, e5400.

Sato, K., Shiomi, K., Watanabe, Y., Watanuki, Y., Takahashi, A. and Ponganis, P. J. (2010). Scaling of swim speed and stroke frequency in geometrically similar penguins: they swim optimally to minimize cost of transport. *Proc. R. Soc. B* **277**, 707-714.

Schindler, D. E., Essington, T. E., Kitchell, J. F., Boggs, C. and Hilborn, R. (2002). Sharks and tunas: Fisheries impacts on predators with contrasting life histories. *Ecol. Appl.* **12**, 735-748

Schreier, P. J. (2005). A note on aliasing in higher order spectra. *6th Australian Communications Theory Workshop 2005. Proceedings,* 184-188

Shafer, M. W., MacCurdy, R., Shipley, J. R., Winkler, D., Guglielmo, C. G. and Garcia, E. (2015a) The case for energy harvesting on wildlife in flight. *Smart Mater. Struct.* **24**, 025031.

Shafer, M. W., Hahn, G. and Morgan, E. (2015b). A hydrostatic pressure-cycle energy harvester. *Proc. SPIE* 9431, *Active and Passive Smart Structures and Integrated Systems* 94310F.

Shafer, M. W. and Morgan, E. (2015). Energy harvesting for marine-wildlife monitoring ASME 2014 *Conf. Smart Mat., Adap. Struct. Int. Sys.* **2**, V002T07A017.

Shepard, E. L. C., Wilson, R. P., Halsey, L.G., Quintana, F., Gómes Laich, A., Gleiss, A.C. et al. (2008a) Derivation of body motion via appropriate smoothing of acceleration data. *Aquat. Biol.* **4**, 235–241.

Shepard, E. L. C., Wilson, R. P., Quintana, F., Laich, A.G., Liebsch, N., Albareda, D.A., Halsey, L.G., Gleiss, A., Morgan, D.T., Myers, A.E. et al. (2008b). Identification of animal movement patterns using tri-axial accelerometry. *Endang. Species Res.* **10**, 47-60.

Skomal, G. B and Chase, B. C. (2002). The physiological effects of angling on post-release survivorship in tunas, sharks, and marlin. In Catch and Release in Marine Recreational Fisheries, 5 – 8 December 1999, Virginia Beach, pp. 135–138. Ed. by J. A. Lucy, and A. L. Studholme. *Am. Fish. Soc. Sci. Symp* 2002.

Skomal, G. B. (2007). Evaluating the physiological and physical consequences of capture on post-release survivorship in large pelagic fishes. *Fish. Manag. Ecol* **14**, 81-89.

Smidt, G. L., Deusinger, R. H., Arora, J. and Albright, J. P. (1977). Automated accelerometry system for gait analysis. *J. Biomech.* **10**, 367-375.

Smircich, M.G. and Kelly, J.T. (2014). Extending the 2% rule: the effect of heavy internal tags on stress physiology, swimming performance, and growth in book trout. *Anim. Biotel.* **2**:16.

Stasko, A. B. and Horrall, R. M. (1976). Method of counting tailbeat of free-swimming fish by ultrasonic telemetry techniques. *J. Fis. Res. Board Can* **33**, 2596-2598.

Stein, J. Y. (2000) *Digital Signal Processing: A computer Science Perspective*. New York, N.Y.: John Wiley & Sons

Steinhausen, M. F., Steffensen, J. F. and Andresen, N. G. (2005). Tail beat frequency as a predictor of swimming speed and oxygen consumption of saithe (*Pollachius virens*) and whiting (*Merlangius merlangus*) during forced swimming. *Mar. Bio.* **148**, 197-204.

Swimmer, Y., Brill, R. and Musyl, M. (2002). Use of pop-up satellite archival tags to quantify mortality in marine turtles incidentally captured in longline fishing gear. *Mar. Turtle Newsl.* **97**, 3-7.

Tanaka, H. and Takagi, Y. (2001). Swimming speeds and buoyancy compensation of migrating adult chum salmon *Oncorhynchus keta* revealed by speed/depth/acceleration data logger. *J. Exp. Biol.* **204**, 3895-3904.

Taylor, G. K. and Thomas, A. L. R. (2014). *Evolutionary biomechanics: selection, phylogeny, and constraint*. Oxford: Oxford University Press.

Taylor, A. D. and Litvak, M. K. (2015). Quantifying a manual triangulation technique for aquatic ultrasonic telemetry, *N AM J Fish Mange.* **35**, 865-70.

Thorstad, E. B., Økland, F. , and Finstad, B. (2000). Effects of telemetry transmitters on swimming performance of adult Atlantic salmon. *J Fish Biol* **57**, 531-535.

Triantafyllou, G. S., Traintafyllou, M. S. and Grosenbaugh, M. A. (1993). Optimal thrust development in oscillating foils with application to fish propulsion. *J. Fluids. Struct.* **7**, 205–224.

Trites, R. W. (1960). An oceanographical and biological reconnaissance of Kennebecasis Bay and the Saint John River Estuary. *J. of Fish. Res. Board Can.* **17**, 377-408.

Toro, E., Herrel, A., Banhooydonck, B. and Irschick D. J. (2003). A biomechanical analysis of intra-and interspecific scaling of jumping and morphology in Caribbean Anolis lizards. *J. Exp. Biol.* **206**, 2641-2652.

Tsuda, Y., Kawabe, R., Tanaka, H., Mitsunaga, Y., Hiraishi, T., Yamamoto, K. and Nashimoto, K. (2006). Monitoring the spawning behavior of chum salmon with an acceleration data logger. *Ecol. Freshw. Fish* **15**, 264-274.

Tudorache, C., Burgerhout, E., Sebastiaan, B., van den Thillart, G. (2014). The effect of drag and attachment site of external tags on swimming eels: experimental quantification and evaluation tool. *PLoS ONE* **9**, e112280.

Urawa, S. (1992). *Trichodina truttae* Mueller 1937 (*Ciliophora Peritrichida*) on juvenile chum salmon (*Oncorhynchus keta*) – pathogenicity and host-parasite interactions. *Fish Pathol.* **27**, 29-37.

van Ginneken, V., Antonissen, E., Müller, U. K., Booms, R., Eding, E., Verreth, J. and van den Thillar G. (2005). Eel migration to the Sargasso: remarkably high swimming efficiency and low energy costs. *J. Exp Biol.* **208**, 1329-1335.

van Leeuwen, J. L., Voesenek C. J. and Müller, U. K. (2015). How body torque and Strouhal number change with swimming speed and developmental stage in larval zebrafish. *J. Roy. Soc. Inter.* **12**, 20150479.

Videler, J. J. and Hess, F. (1984). Fast continuous swimming of two pelagic predators, saithe (*Pollachius virens*) and mackerel (*Scomber scombrus*): a kinematic analysis. *J. Exp. Biol.* **109**, 209-228.

Videler, J. J. and Wardle, C. S. (1991). Fish swimming stride by stride: speed limits and endurance. *Rev. Fish Biol. Fisher.* **1**, 23-40.

Videler, J. J. (1993). *Fish Swimming*. Fish and Fisheries Series 10. Chapman & Hall: London.

Walsberg, G. E., and Hoffman, T. C. M. (2005). Direct calorimetry reveals large errors in respirometric estimates of energy expenditure. *J. Exp. Biol.* **208**, 1035-1043.

Wang, L., Su, S. W., Celler, B. G. and Ambikairajah, E. (2005) Analysis of orientation error of tri-axial accelerometers on the assessment of energy expenditure. *Eng. in Med. Biol. Soc., IEEE-EMBS* 2005

Watanabe, Y. Y., Wei, Q., Yang, D., Chen, X., Du, H., Yang, J., Sato, K., Naito, Y., and Miyazaki, N. (2008). Swimming behaviour in relation to buoyancy in an open swimbladder fish, the Chinese sturgeon. *J. Zool.* **275**, 381-390.

Watanabe, Y. Y., Lydersen, C., Fisk, A. T. and Kovacs, K. M. (2012). The slowest fish: Swim speed and tail-beat frequency of Greenland sharks. *J. Exp. Mar. Biol. Ecol.* **426**, 5-11.

Webb, P. W. (1975). Hydrodynamics and energetics of fish propulsion. *Bull. Fish. Res. Bd. Canada* **190**, 1-159.

Webb, P. W. (1976a). Hydrodynamics: non-scombroid fish. *In* Hoar W, Randall DJ (eds). *Fish Physiology, Vol. 7 Locomotion* NewYork, NY: Academic Press

Webb, P. W. (1976b). The effect of size on the fast-start performance of rainbow trout *Salmo cairdneri*, and a consideration of piscivorous predator-prey interactions. *J. Exp. Biol.* **65**, 157-177.

Webb, P. W. (1978). Fast-start performance and body form in seven species of teleost fish. *J. Exp. Biol.* **74**, 311-326.

Webb, P. W. (1986). Kinematics of lake sturgeon, *Acipenser fulvescens*, at cruising speeds. *Can. J. Zool.* **64**, 2137-2141.

Webb, P. W. (2002). Control of posture, depth, and swimming trajectories of fish. *Integr. Comp. Biol.* **42**, 94-101.

Webb, P. W. and Weihs, D. (2015). Stability versus manoeuvring: challenges for stability during swimming by fishes. *Integr. Comp. Biol.* **55**, 752-764.

Weihs, D. (1973) Hydromechanics of fish schooling. *Nature* **241**, 290-291.

Wells, R. M. G. and Davie. P. S. (1985). Oxygen binding by the blood and hematological effects of capture stress in two big gamefish: mako shark and striped marlin. *Comp. Biochem. Physiol.* **81**, 643-646.

Wells, R. M. G., McIntyre, R. H., Morgan, A. K. and Davie P. S. (1986). Physiological stress responses in big gamefish after capture: observations on plasma chemistry and blood factors. *Comp. Biochem. Physiol.* **84**, 565-571.

Wilga, C. D. and Lauder, G. V. (1999). Locomotion in sturgeon: function of the pectoral fin. *J. Exp. Biol.* **202**, 2413-2432.

Williams, T. L., Grillner, S., Smoljaninov, V. V., Wallén, P., Kashin, S. and Rossignol, S. (1989). Locomotion in lamprey and trout: the relative timing of activation and movement. *J. Exp. Biol.* **143**, 559-566.

Wilson, R., White, C. and Quintana, F. (2006). Moving towards acceleration for estimates of activity- specific metabolic rate in free-living animals: the case of the cormorant. *J. Anim. Ecol.* **75**, 1081-1090.

Wilson R. P., Griffiths I. W., Legg P. A., Friswell M. I., Bidder O. R., Halsey L. G., Lambertucci S. A., Shepard E. L. C. (2013*a*). Turn costs change the value of animal search paths. *Ecol. Lett.* **16**, 1145–50.

Wilson, S. M., Hinch S. G., Eliason, E. J., Farrell, A. P. and Cooke, S. J. (2013*b*). Calibrating acoustic acceleration transmitters for estimating energy use by wild adult Pacific salmon. *Comp. Bioc. Phys. A* **164**, 491-498.

Wilson, S. M., Hinch S. G., Drenner, S. M., Martines, E. G., Furey, N. B., Patterseon, D. A., Welch, D. W. and Cooke, S. J. (2014). Coastal marine and in-river migration behaviour of adult sockeye salmon en route to spawning grounds. *Mar. Ecol. Prog. Ser.* **496**, 71-84.

Winter, J. D. (1996). Advances in underwater biotelemetry. In *Fisheries techniques*, 2nd edition (ed. B. R. Murphy and D. W. Willis), pp. 555-590. Bethesda, MD: American Fisheries Society.

White, F.M. (1986) *Fluid Mechanics*. New York: McGraw-Hill.

Whitney, N. M., Papastamatiou, Y. P., Holland, K. N. and Lowe, C. G. (2007). Use of an acceleration data logger to measure diel activity patterns in captive whitetip reef sharks, *Triaenodon obesus*. *Aquat. Living Resour.* **20**, 299-305.

Whitney N. M., Pratt Jr., H. L., Pratt, T. C. and Carrier, J. C. (2010). Identifying shark mating behavior using three-dimensional acceleration loggers. *Endang. Species Res.* **10**, 71-8

Wright, S., Metcalfe, J. D., Hetherington, S. and Wilson, R. (2014). Estimating activity-specific energy expenditure in teleost fish, using accelerometer loggers. *Mar. Ecol. Prog. Ser.* **496**, 19-32.

Wyman, R. L. and Walters-Wyman, M. F. (1985). Chafing in fishes: occurrence, ontogeny, function and evolution. *Environ. Biol. Fishes.* **12**, 281-289.

Wu, T.Y. (1971) Hydrodynamics of swimming fish and cetaceans. In *Adv. Appl. Math.* **11**, 1–63. New York: Academic.